DYNAMIC CLUSTERING AND SCALING BEHAVIOR OF ACTIVE PARTICLES UNDER CONFINEMENT

by

Matthew D Becton

(Under the Direction of Xianqiao Wang)

ABSTRACT

Active particles, tiny fragments of matter which are driven by external forces, are seeing recent use in scientific fields. With new applications in medicine, and especially for usage within the body, there is an outstanding need to understand how active particles may behave and aggregate in confined fluid systems, such as blood vessels. Presented in this dissertation is a systematic investigation of the dynamic clustering behavior of active particles under confinement, including the effects of both particle density as well as active driving force. A hybrid coarse-grained molecular dynamics scheme is integrated with stochastic rotation dynamics to allow for accurate hydrodynamic interactions, and the diffusion-limited aggregation behavior is studied. Scaling laws based on power relationships define the clustering time as a function of both density of active particles, as well as the applied driving force. There are up to four distinct dynamic regions in terms of clustering as a function of time, dependent on the density of the particles within the system. As driving force increases, aggregation behavior also is accelerated, whereas an increase in density of active particles changes the dynamic procession of the system.

INDEX WORDS: Active Particles, Modeling and Simulation, Aggregation, Confined Fluid

DYNAMIC CLUSTERING AND SCALING BEHAVIOR OF ACTIVE PARTICLES UNDER CONFINEMENT

by

MATTHEW D BECTON

BS, University of Georgia, 2011

MS, University of Georgia, 2015

A Dissertation Submitted to the Graduate Faculty of The University of Georgia in Partial Fulfillment of the Requirements for the Degree

DOCTOR OF PHILOSOPHY

ATHENS, GEORGIA

2021

DYNAMIC CLUSTERING AND SCALING BEHAVIOR OF ACTIVE PARTICLES UNDER CONFINEMENT

by

MATTHEW D BECTON

Major Professor: Xianqiao Wang
Committee: Yiping Zhao
Bingqian Xu
Rodney Averett

Electronic Version Approved:

Ron Walcott
Vice Provost for Graduate Education and Dean of the Graduate School
The University of Georgia
December 2021

DEDICATION

This work is dedicated to the University of Georgia, the City of Athens, and to the decade and a half that I spent there. It has been a great chapter of my life.

ACKNOWLEDGEMENTS

I am deeply grateful to Dr. Xianqiao Wang for having been an incredible Ph.D. advisor to me. From the first months of my work in his lab to the last months of writing, he has been supportive, kind, patient, and generous. He has been with me during my entire graduate career, throughout both Master's and Doctorate, and always allowed me to learn and expand my experiences in many ways. He has provided me the freedom to grow as a scientist; at the same time, he has without exception been available when I sought his advice, for which I am very thankful. I am grateful to Dr. Yiping Zhao for his guidance and for our numerous discussions on data analysis and paper writing. His decades of experience have benefitted me tremendously. I would like to thank my committee members, Dr. Bingqian Xu and Dr. Rodney Averett, for their advice, and for a pleasant final examination. Dr. Mark Trudgen has been a constant source of support and learning; from being graduate students together to helping him with his class. I extend my gratitude to all those who keep the machines running; my research over the years has been supported by the GACRC and its staff. I very sincerely thank Clodagh Phair-Miller and Margaret Sapp for their administrative support, and for helping me out through all my form-filing mistakes. This dissertation would not have been possible without my wife, Victoria, the love of my heart, light of my life, and keeper of my true self.

TABLE OF CONTENTS

LIST OF TABLES

LIST OF FIGURES

1. ACTIVE PARTICLES

1.1. What are Active Particles

The rapid development of novel technologies can be considered as one of the defining aspects of the modern age, especially in the domains of materials and medicine. One of the most versatile tools to arise at the intersection of these fields are particles which can be controlled or otherwise actively operate at the nano- and microscales; to differentiate these from particles which passively react to their environment, we call these ‘active particles’. These active particles can also be termed as nanomotors and micromotors, and the basis of this classification is that the particle be self-propelling. Due to the nature of active particles, they hold great value and potential towards the fields of chemistry and medicine, and as such there have been several reviews on their propulsion and applications. Therefore, this section focuses on recent literature pertaining to the development of active particles, characteristics of systems which contain active particles, the behaviors of mixtures of active and passive particles, and how they interact within free and confined systems.

The interdisciplinary research and development of active (self-propelling) particles, an umbrella term which covers certain types of nanomotors and micromotors, has immeasurable potential for applications in a huge number of areas. Although the term ‘micromotor’ has been around since at least 1988, when the first electrostatic motor smaller than a human hair was developed, in this work the term shall instead refer to propelled particles in fluid, rather than otherwise stationary devices or devices embedded in the walls

of fluid channels, although sometimes very similar motive principles are used [1-5]. Systems containing active particles have been studied extensively in the past two decades, and the vast majority of work has focused on their behavior and applications in a fluid environment, such as chemical mixing or biological studies [6-36]. As a matter of fact, many reviews shining a spotlight on active particles or micromotors have already been written; however, this field is still rapidly growing and requires constant attention [24, 30, 37-51]. The field of active particles is one which is constantly generating new ideas, in much the same way that systems of active particles themselves demonstrate emergent behaviors.

To begin, a general description of what defines active particles is in order. The current commonly used definition of active particles is that they are discrete bits of active matter, that is, matter which can achieve translational, rotational, or vibrational motion due to some driving force beyond the direct mechanical force applied by the surrounding environment, which is the cause of motion in passive matter. To clarify, passive particles are those which only move when directly mechanically acted upon by their surrounding environment, such as by surrounding fluid or solid contact forces. The autonomous or semi-autonomous motion of active particles is the key to their unique abilities, and there are many different methods which have been used to drive these particles, in either a directed or random fashion [52-59]. While there is no definite size limit of active particle definition, this dissertation will focus on those of the micrometer and nanometer scale, as active particles of this size are seeing much attention and application in recent years, across various fields and disciplines. Entities or particles within a fluid such as water will always experience two main types of forces: inertial forces, which cause motion through the fluid

due to the particle's velocity and mass; and viscous forces, which exert drag on the particle due to friction between the fluid and the surface of the particle. A key parameter which indicates the ratio of inertial to viscous forces is the Reynolds number, which is given in Equation 1.1.

$$\boldsymbol{Re = \frac{vl\rho}{\mu} = \frac{vl}{\mu_k}}$$

Equation 1.1

Here, v is the velocity, and l is the characteristic length of the particle. The symbols ρ and μ represent the density and the viscosity of the fluid. The ratio of fluid density to viscosity can be represented as the kinematic viscosity μ_k. Water has a kinematic viscosity of around 0.01 cm^2/s. For a mass on the order of meters moving in water, such as a human, the Reynold's number is around 10,000; this can be considered as a high-Reynolds number system where inertial forces play a strong role, and the fluid flow of this system is considered to be turbulent. A micrometer-sized active particle moving in water, in comparison, has a Reynold's number on the order of 10^{-4} to 10^{-5} and can be considered to be a low-Reynolds number system where viscous forces play the dominant role, and the fluid flow around the swimmer is laminar, Stokes flow. Due to inertial forces becoming vanishingly small at this scale, active particles cannot rely on inertial forces alone to overcome drag, and thus constant, symmetry-breaking methods of propulsion are necessary, whether the active particles are micromotors or microswimmers.

The equations of motion for an incompressible fluid, such as water, are given by the Navier-Stokes equations (Equation 1.2 and Equation 1.3).

$$\frac{\partial \boldsymbol{v}}{\partial \boldsymbol{t}} + (\boldsymbol{v} \cdot \boldsymbol{\nabla})\boldsymbol{v} - \boldsymbol{\mu_k}\boldsymbol{\nabla^2}\boldsymbol{v} + \frac{\mathbf{1}}{\boldsymbol{\rho}}\boldsymbol{\nabla P} = \boldsymbol{F}$$

Equation 1.2

$$\boldsymbol{\nabla} \cdot \boldsymbol{v} = \mathbf{0}$$

Equation 1.3

The Navier-Stokes equations are functions of the fluid viscosity, density, velocity, pressure (P), and applied body force (F). However, at Reynold's numbers $Re \ll 1$, the Navier-Stokes equations for systems of incompressible fluids simplify to the so-called Stokes flow equations, as given by Equation 1.3 and Equation 1.4:

$$\boldsymbol{\mu\nabla^2 v - \nabla P + F}$$

Equation 1.4

Equation 1.4 can be considered to be the case of Equation 1.2 where the inertial (time-dependent) terms vanish at low Reynold's numbers. This differential equation is time-independent, and linear with respect to velocity and pressure. The following discussion and simulations concerning active particles on the micrometer scale will all be considered to be under the Stokes flow dynamics. When active particles are submersed within a fluid, which is very common in the biological and chemical fields, the kinematic reversibility of the fluid within the low-Reynold's number environment that occurs on the micro- and nano-scale of these particles dictates that either an external applied field, or else some method of force-symmetry breaking by using local gradients (chemical or otherwise), are the two broad methods for providing the energy required for the active motion of these devices [45, 53, 55, 56, 60-74]. Additionally, many previous studies on active particles

have been strongly influenced by so-called “natural” active particles, that is, self-propelled bacteria or other types of mobile cells [33, 75-82]. Due to this, these ostensible microswimmers of both organic and inorganic origins have become a broad swathe of the types of active particles being studied today [58, 83-92]. Figure 1.1 demonstrates several different methods of propelling an active particle through fluid, such as chemical bubble catalysis, torque to linear motion, and applied external fields, each of which will be discussed in detail in the following Sections.

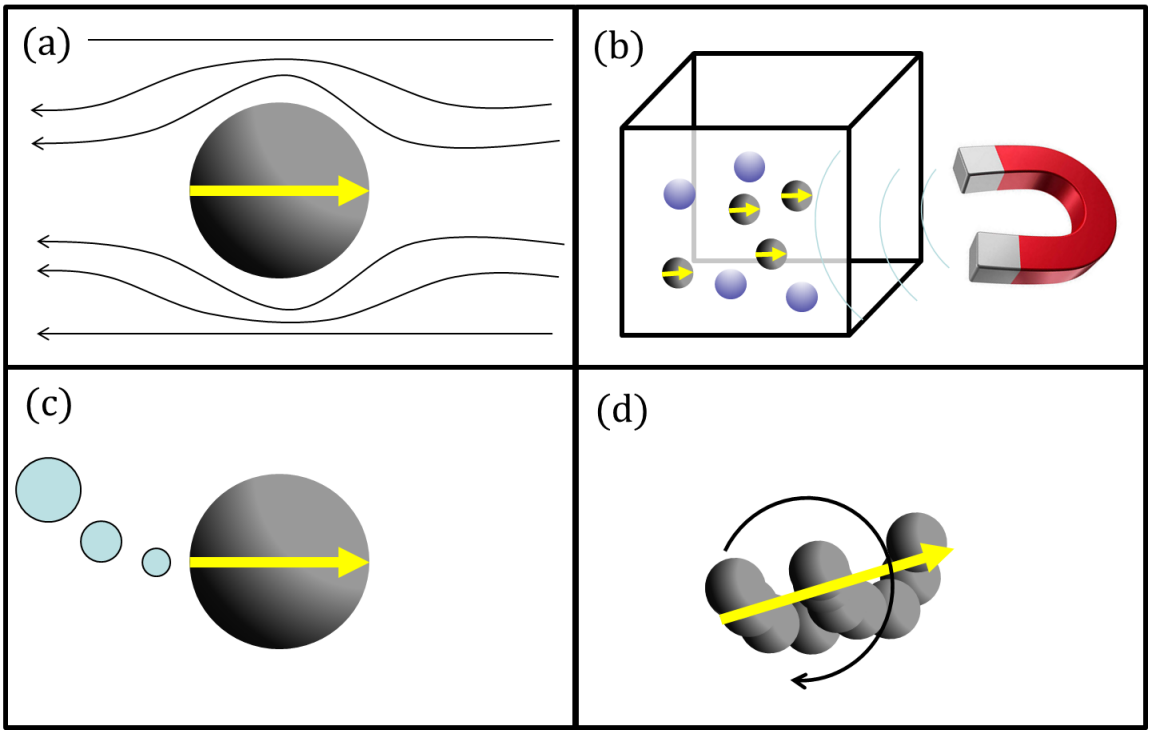

Figure 1.1: Methods of active particle propulsion.

Active particles are driven by an applied body force. (a) An active particle moving through a fluid. (b) Magnetic field effecting motion in active particles, but not passive particles. (c) Chemical fuel is converted to bubble propulsion to drive the active particle. (d) An applied torque causes linear motion.

For clarification purposes, Table 1.1 gives an overview of several different terms common in the field, denoting the parallels between "normal" passive matter and active matter, in several forms and with several ways to describe them. Figure 1.2 shows a hierarchical representation of the relationship between active matter, micromotors, and microswimmers. This figure gives a visual demonstration of how micromotors can be considered as a subset of active matter, and how microswimmers are a specific type of micromotor. Of course, there are many other categories beyond those represented here.

Table 1.1: Terms for different types of passive and active matter.

	Passive	Active
General term for material	Matter	Active Matter
Single micron-sized particle in fluid	Brownian particle	Active Particle / Micromotor / Microswimmer
Many micron-sized particles in fluid	Colloid	Swarm / Active Colloid / Active Fluid
Regular-lattice aggregated particles	Crystal	Active Crystal

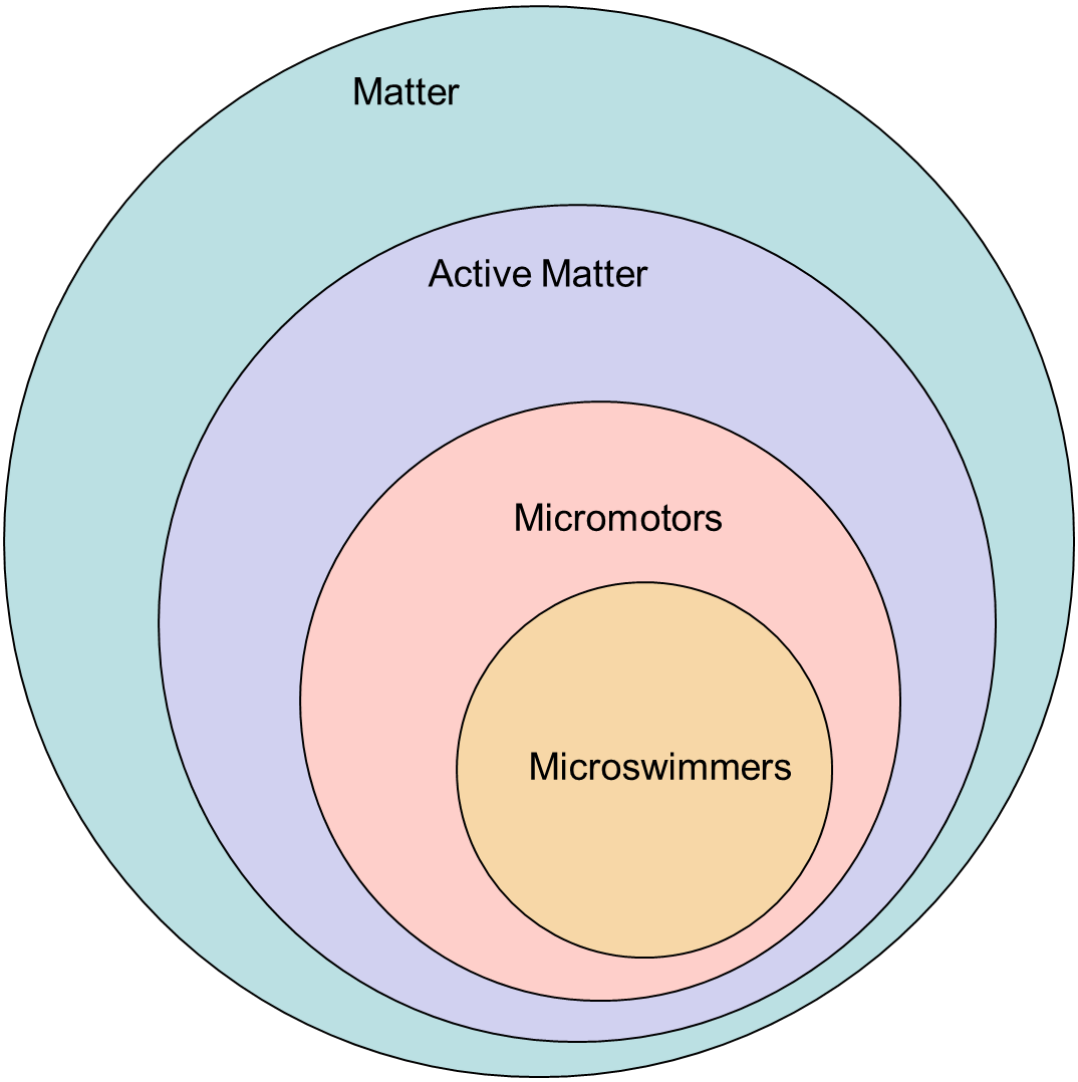

Figure 1.2: Hierarchical representation of different types of active particles.

1.2. Uses of Active Particles

As research and insights into active particles have grown increasingly common, modern applications are varied and multiplex. Modern uses of active particles run quite a wide range; they have been used as agents of catalysis [93], toxin detection [94, 95], cellular marking [96], wastewater treatment [97-104], CO_2 scrubbing [105], chemical and

biological warfare agent neutralization [46, 106-108], 2,4,6-trinitrotoluene (TNT) detection [109], on-the-fly hydrogel polymerization [110], micropatterning [111], and even energy generation [59]. Due to their small size and ability to enact change on scales and within environments which are difficult for standard tools and equipment, scientific interest in active particles has been typically focused within the closely related fields of medicine and chemistry, with an especially large proportion of research being carried out towards applications focused on the delivery and synthesis of various drugs [112-127]. For almost all of the afore-listed applications of active particles, they need to be present in large numbers within the system of interest, and the systems they are in, be it microfluidics devices or even the human body, can be considered as fluid systems with varying degrees of confinement. Due to this standard of use, the focus of this dissertation will be directed toward the collective behavior of microscopic active particles within confined fluid systems, as opposed to single active particles within a bulk system, or other manner of active particles in dry environments or at different length scales.

The tools known as active particles come in a wide variety, with many diverse means of propulsion or activation. The most commonly utilized major methods of driving synthetic active particles are chemical fuel and electromagnetic fields (including those driven by light, as well as electric and magnetic fields). However, this does not mean that only a single method of propulsion can be used to drive a single type of active particle. There are also hybrid types of micromotors which are able to be driven by multiple distinct methods. In March of 2020, a research team led by Escarpa et al. published a paper which describes a method of manufacture for a type of micromotor which can be driven by any of three propulsion methods: chemical catalytic bubble propulsion utilizing Pt or MnO_2

nanoparticles to hydrolyze hydrogen peroxide, light-driven propulsion utilizing quantum dots to provide movement, and magnetic propulsion utilizing embedded Fe_2O_3 nanoparticles to allow for collective motion or capture [70]. These methods can be used independently as well as simultaneously, with the ability to direct and enhance each other. Such a design accurately captures modern scientific ingenuity, allowing for multiple methods to enhance each other in an elegant fashion. However, most active particles mainly rely on a single method of propulsion, for simplicity of manufacture and control. The following is a breakdown of the main methods for driving active particles.

The first generation of micromotors tended to use catalysis of chemicals, most commonly hydrogen peroxide or other similarly toxic fuels [128-131]. This method relies on the generation of bubbles to effect propulsion, with the breakdown of hydrogen peroxide on the catalyst surface creating oxygen bubbles which then drive the micromotor forward. For such chemically-propelled motors, the propulsion velocity is often tied directly to the chemical fuel concentration, while also strongly influenced by the shape of the micromotor and the catalyst used [132]. In recent years, micromotors with linear velocities on the order of 100 micrometers per millisecond (or 10 cm/s) have been observed for H_2O_2 concentrations up to 20% [93, 133-135]. However, chemical catalyst micromotors have two easily recognized and profound limitations; firstly, a certain concentration of fuel must be maintained in the area near the micromotor, which for many applications including medical usage is not feasible; secondly, only the average particle velocity can be controlled through fuel concentration gradients, with little ability to directly control individual micromotor direction. While chemical catalyst micromotors are relatively simple to manufacture and are quite speedy, due to these severe restrictions on usage their

applications can only fall within a certain niche. However, there are many other types of active particles which are not bound by these restrictions.

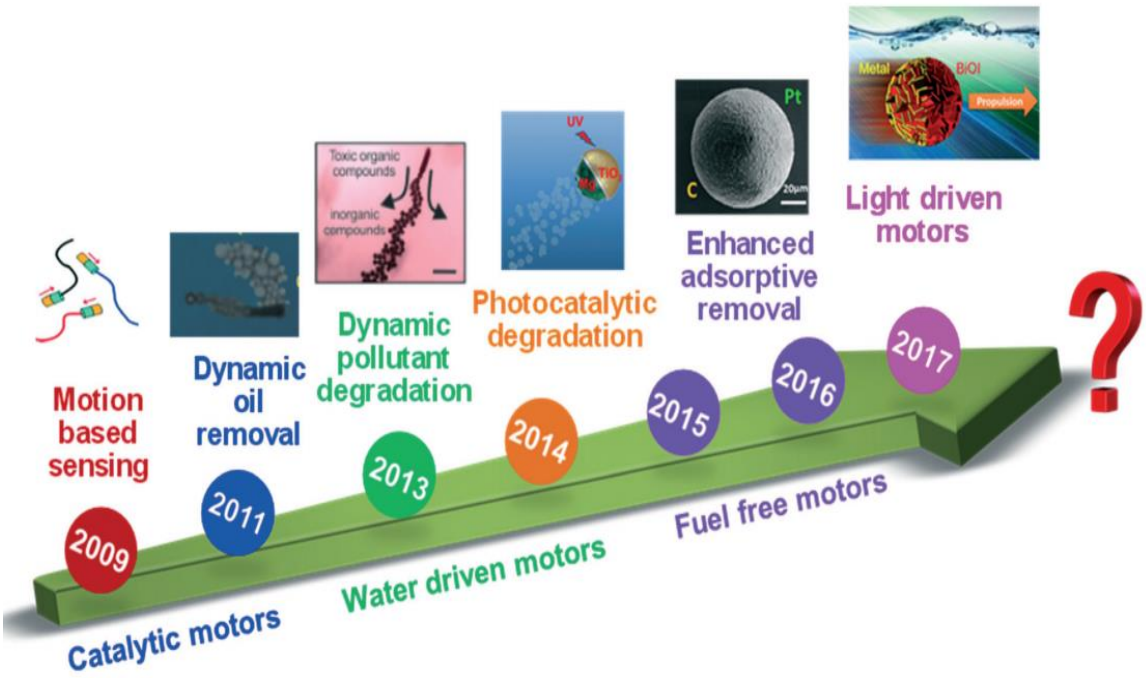

Figure 1.3: Applications of micromotors.

With permission from ref [136].

Micromotors which do not require in-fluid chemicals for reactions are sometimes termed "fuel-free" micromotors (see Figure 1.3) in order to distinguish them from chemical catalyst-driven micromotors. However, the term fuel-free is somewhat of a misnomer, as these active particles do of course require energy for propulsion. The term is often used when discussing light-propelled active particles [137-139]. Regarding the two major limitations discussed above, a type of graphene aerogel micromotor has been reported which uses near infrared light not only as a power source, but also as a method of steering

and directionality control [64]. Such light-driven micromotors can in fact be extremely simple, such as the reported rotary micromotors which are little more than irregularly-shaped sheets of graphene oxide, driven by a specifically conical-shaped laser [140]. It has been demonstrated that depending on controllable factors influencing the particle-fluid interactions, active particles can exhibit either positive or negative phototaxis, moving either towards or away from a light gradient [141]. In a similar manner, electric fields have also been demonstrated to be able to propel fuel-free active particles, as well as the added functionality of allowing them to be used as mobile microelectrodes [142, 143]. In a similar fashion, magnetic iron oxide particles were incorporated into the empty spaces within pine pollen, in order to create magnetic field-driven biohybrid micromotors which can act as biocompatible cargo carriers within the body [144]. Even though non-catalytic micromotors have a stronger case for being used in medical applications, as they do not require the addition of often toxic chemical fuels to the fluid medium, it is only recently that light-driven micromotors have demonstrated the potential to reach such high maximum speeds as have been previously seen only from catalytic motors [145]. In a combination light-based and catalytic bubble-based propulsion method, UV light and metal/TiO_2 have been shown to facilitate water splitting using surrounding water, rather than volatile chemicals such as hydrogen peroxide, as the fuel source for bubble-propelled micromotors [67]. This can be considered to be a hybrid-style active particle propulsion method.

Developing methods to manufacture hybrid-style active particles is currently a growing trend, with the unique properties of each method of propulsion able to compensate for limitations of the other. A paper from early 2020 demonstrates a type of micromotor which uses superlattices of catalytic nanoparticles to allow for chemical fuel-driven

propulsion, while also incorporating magnetic nanoparticles to allow for magnetic field-enabled control of the micromotor direction [146]. A team from France introduced LED-based active particles which use catalytic bubble propulsion as well as induced magnetic field interactions to demonstrate how multiple types of gradient controls, such as pH or ionic gradients, can be used to fine-tune the motion of such active particles [147]. In 2019 a team from China used magnetic fields as a directionality control for Janus micromotors, while the actual propulsive force came from bubbles produced via hydrogen peroxide decomposition [148]. Another study found that light can be used either to enhance or detriment propulsion from catalysis, depending on the structure of the catalytic micromotors [138]. In addition to studies combining electromagnetic fields with catalytic bubble-propelled micromotors, there has also been research into hybrid-style micromotors with alternative propulsion methods. A certain class of micromotor, termed as "microswimmers" as in Figure 1.2, with weak magnetic dipole moments have been shown to display reduced transport due to swimming instabilities, while higher field strengths stabilize the active particles and increases transport efficiency [149].

The term microswimmer refers to active particles which are propelled mechanically in a similar way to living cells. Living cells such as bacteria also can be considered to be active particles, and one of the ways they can move through fluid is via the flagellation of tiny hairs or whips known as cilia. One elegant method of propelling specific cargo is to use the flagella of living cells, such as *Escherichia coli* or sperm cells, as the driving force used in synthetic biohybrid micromotors [76]. One such approach from 2019 demonstrated how marine rotifers could be functionalized in order to dramatically accelerate enzymatic biodegradation of living contaminants such as *E. coli*, or modified in a different fashion to

remove nonliving matter such as heavy metal ions from wastewater [150]. A similar method for the propulsion of fully synthetic devices involves the use of liquid crystals to drive motion, powered by exposure to surfactants in the system in a manner that is reminiscent of yet fundamentally different from chemical fuel-based bubble catalysis [151].

In addition to the wide range of propulsion methods, active particles can also assume a wide variety of shapes, dependent on their manufacture and application. The base case for the study of active particles assumes axisymmetric spheroidal particles [152]. However, results from such a case cannot always be extended to the other commonly seen shapes which active particles may take. Drawing on inspiration from shapes commonly seen in nature, helical active particles rely on their unique shape to translate rotational motion to linear motion, under either AC or DC electric fields [120, 143]. One study from 2019 introduced liquid metal microswimmers which are able to change their shape in an aqueous environment when subjected to alternating magnetic fields in order to achieve propulsion [153]. Even for active particles with a spheroidal geometry, the surface patterning, such as that found on Janus particles, greatly influences the motion of the particle. Anisotropic surface patterning has been found to give rise to linear motion, while active rotation for this type of particle only occurs if the surface is not axisymmetric [154]. Careful study of how individual active particles behave is key to correctly using them for research and commercial applications.

1.3. Collective Motion of Active Particles

The collective behavior of active particles gives rise to many emergent effects when compared with the behavior of a single particle, and can be considered to be more than the summation of individual behavior, due to interactions arising between active particles [155-160]. The presence of other active particles in the fluid can cause complex and never-settling flow patterns which do not follow traditional Brownian or fluid dynamics [17, 161-170]. This can be attributed to the fact that active particles convert some other form of energy to kinetic motion, which changes the equations of state for both the near-field and far-field fluid system [24, 36, 83, 171, 172]. Modelling of the collective motion of active particles can be considered to be quite similar to the modelling of flock of animals, cells, or even robotic drones [173-184]. One of the most influential works in the current field of active matter modelling is the 1995 paper "Novel type of phase-transition in a system of self-driven particles", from Vicsek et al. [185]. This paper gave rise to the oft-cited Vicsek model, which is a commonly-used mathematical model which can mimic experimentally seen collective behavior and swarming [186]. Above a certain individual active particle velocity, the system undergoes a continuous transition from zero net transport to finite net transport arising from spontaneous symmetry breaking of the rotational symmetry within the fluid. Other influential works introduced biologically-mimetic collective motion as the active particles influence other nearby active particles to align their propulsion vector orientations, transitioning from individual random walks (as in singular particle run-and-tumble behavior) to organized collective migration, and showing strong dependence on particle spacing and size [176, 187, 188]. Indeed, it has been shown that, other factors being equal, the average active particle velocity is inversely proportional to the number density of active particles, giving rise to spatial variation in swim speed arising from spatial

variation in particle density; this produces a fluid pressure variation distribution which drives observed reverse-osmotic behavior in some active matter [189]. Other considerations include local and global chemical gradients, for those micromotors which use depletable fuel within their environment [190]. As might be guessed, one externality arising from the usage of an applied field, such as electric or magnetic fields, to drive a number of active particles is that all of the particles are coupled through their interaction with said field. One study tackled this problem by introducing transchiral helical micromotors, using the different chirality to enable decoupled motion between populations of active particles, as well as being able to set the translation direction as a function of rotating magnetic field frequency [191]. These devices can be tuned such that each device shape is only activated by a certain band of frequencies, allowing for simultaneous yet disparate control over multiple populations in the same system. These are some of the many interesting behaviors and challenges which set the study of active matter apart from similarly composed passive systems. Due to the added degrees of freedom for active particles over passive ones, the increase in complexity can lead to so-called emergent behavior, meaning that oftentimes for collective systems of active particles, it is necessary for experiments or large-scale simulation to be carried out in order to investigate the systems of interest.

The collective behavior of active particles gives rise to many emergent effects when compared with the behavior of a single particle, and can be considered to be more than the summation of individual behavior, due to interactions arising between active particles [155-160]. It has been shown that a mixture of active and passive colloidal particles can lead to clustering and phase separation, forming chains or clusters of particles [192]. Active

colloids operate by dissipating energy at the level of the active particles in order to cause motion with no equilibrium equivalent, leading to clustering when dissipation is low and collective motion when dissipation is high [193]. The tendency of colloids to aggregate can have many different implications.

1.4. Diffusion-Limited Colloidal Aggregation

To appreciate the influence of active particles on their fluid systems, a brief discussion on similarly scaled passive systems will be presented. A solution of many passive particles of the micrometer scale is termed as a colloid [194-196]. Colloidal systems are typically defined as kinetically stable, meaning that the dispersed phase will eventually separate from the continuous one in which it is suspended [197]. Depending on the individual particle properties, as well as the dispersion fluid, colloids can aggregate, flocculate, or remain discrete within the fluid environment. Due to the fluid inertia and small length scales, most mathematical models for the base fluid on these scales use the Navier-Stokes equations of state for fluids, assuming incompressibility, and Neo-Hookean or rigid body material for the solid particles; the associated approximations included in these assumptions are favorably validated with experiments [198-201]. The presence of passive colloidal particles, although not driven as active particles are, still causes certain viscoelastic effects in the fluid depending on density and a number of other factors, such as fluid flow [202-206]. Diffusion-limited colloidal aggregation (DLCA) refers to the aggregation of particles which is limited only by their diffusion and subsequent collision; that is, if two particles collide, they will certainly stick together [207]. Another form of aggregation is rate-limited colloidal aggregation (RLCA), where whether two particles

stick together after collision is a function of their velocity and interaction potential. For simplification purposes, this work and all simulation and theory within it will refer only to DLCA except where explicitly noted.

One of the most often-used approximations for the interactions of colloidal particles in fluid is called DLVO theory, named after Boris Derjaguin, Lev Landau, Evert Verwey, and Theodoor Overbeek. This theory quantitatively describes the aggregation behavior of aqueous dispersions, and as such is very useful for the modeling of colloidal interactions, which generally present long-range repulsion and short-range attraction between dispersed particulates [208-210]. DLVO describes the force between two spheres interacting through a combination of Lennard-Jones and doubly-screened electrostatic interactions, and with a certain amount of modification can also be used to describe nonspherical particles [211]. Due to the doubly-screened electrostatic interactions felt by the particles, aggregation behavior is strongly dependent on the screening potential / chemical makeup of the suspending fluid, with the polar solvent water being the most commonly used [212]. It has been shown that this type of colloidal aggregation theory can also describe general crystal formation, which can not only nucleate through stochastic association of atoms, but can also proceed through assembly of building blocks such as amorphous precursors or nanocrystalline fragments [208]. Further expanding on traditional colloidal theory, a microrheology work from 2020 demonstrates that a bath of colloidal spheres causes particles which actively move through it to have a larger friction coefficient to particle size ratio than expected from traditional Stokes law behavior [213]. This indicates that colloidal indications must be considered for any active particle moving through such a system. Similarly, much knowledge of the nonlinear fluid properties of colloids is collected through

"active rheology" studies, where a Brownian particle is actively moved through a complex fluid in order to infer the fluid properties from observing the particle motion [202, 214-216]. Such studies are intricately tied to study of active particles, as the motion of such a particle is directly comparable to self-propelled active particles or micromotors [217, 218]. The field of colloidal aggregation is far from fully developed; the many variables and huge range of parameter space contribute to extreme complexity in this seemingly simple field. In fact, one of the most recent developments is the application of machine learning to study the aggregation of colloids, in an attempt to make better predictions about how clustering evolves within colloidal systems [219]. Due to the importance of DLVO theory, Section 2.4 provides the governing equations from DLVO theory used for the simulations in this Dissertation.

1.5. Active Particle Colloidal Aggregation

For passive systems, colloidal behavior is typically exhibited by particles on the micrometer order of magnitude, where Brownian motion dominates [2, 220]. As such, collective behavior of active particles on this scale is often analyzed by the particle deviation from typical Brownian motion (such as by using mean squared displacement methods), to easily distinguish them from passive colloidal particles, and they can be likewise termed as active Brownian particles [221-228]. In recent years, many different models have been proposed for certain types of active particle suspensions. One study focused on active liquid crystals, in order to investigate instability phenomena observed in the laboratory [229]. A 2020 work devised a model for a system of magnetic spinning active particles, and demonstrated the potential for dynamic transitions between liquid and

crystalline states at the air-water interface, highlighting how a remote excitation field can be used for tunable reconfiguration and transport of cargo particles [230]. An even more general work investigated the dynamics of one- and two-particle colloidal systems under confinement, highlighting that active particles introduce multiplicative noise into stochastic descriptions of particle positions, leading to very different behavior on a fundamental level between active colloidal particles in a passive fluid as compared with passive colloidal particles in an actively fluctuating fluid [231]. This helps to highlight the difference between a passive fluid which is in motion due to driving forces on the system, and a fluid which is influenced by active particles within it, which can also be termed as an active fluid. A study from 2017 demonstrated that a mixture of passive and chemically active particles can induce self-sustained convective motion [232].

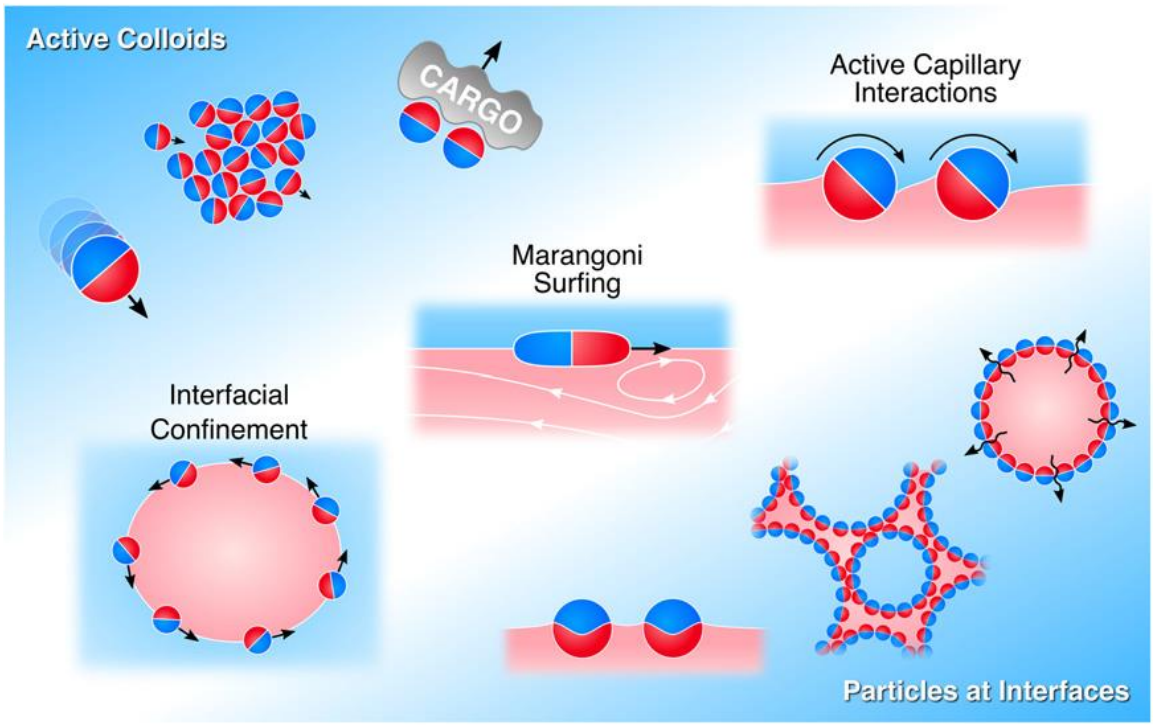

Figure 1.4: Behaviors of active colloidal particles.

With permission from ref [233].

In the same manner that passive micron-sized particles in solution can be termed as a colloid, the terms “active colloid”, “active fluid”, or “active suspension” have been used to describe fluid systems with a relatively dense concentration of active particles [30, 33, 42, 44, 47, 91, 233-249]. The entire field of active matter includes a much wider range of materials containing active agents, and covers a very wide range of length scales, and is beyond the scope of the current work [38, 92, 172, 250-252]. Table 1.1 defines various types of active matter discussed in this work, along with their passive counterparts. For all of these various types of active matter, there are different pertinent qualities to consider, as well as different applicable methods of modeling and describing these types of active matter. Figure 1.4 demonstrates different behaviors and applications of active colloids in particular, such as their ability to carry cargo, tendency to aggregate near interfaces, and their conduct of propulsion and clustering.

Active colloids demonstrate many intriguing properties when compared with both their passive counterparts as well as singular active particles, including anomalous diffusion, turbulence, and thermomechanical properties [16, 17, 189, 253-256]. The most obvious difference between an active colloid and a collection of similarly-sized passive particles is of course the individual propulsion of particles beyond the direct force which the fluid environment exerts, which causes the term “equilibrium” to be inapplicable, as work is continuously being done by the active particles within the fluid [85, 257-264]. Active colloids operate by dissipating energy at the level of the active particles in order to

cause motion with no equilibrium equivalent, leading to clustering when dissipation is low and collective motion when dissipation is high [193].

One of the most sought-after applications of active particles is the ability to carry cargo; Figure 1.5(a) demonstrates how a swarm of active particles can be used to transport individualized cargo containers without the added step of ligand binding [265]. Figure 1.5(b) demonstrates how, in the same system setup, fluid velocity as well as the number density of the active particles both play key roles in whether the particles in an active colloidal system aggregate or disperse [266]. Figure 1.5(c) gives images of experimental validation of the aforementioned DLVO aggregation reliance on the screening capability of the fluid [212]. Active particle shape and volume fraction are changed in Figure 1.5(d) to demonstrate how these parameters influence the aggregation of active particles [267]. Once the particles in a dispersed active colloid aggregate, the proximity of the active particles can give rise to a new set of behaviors as well. As demonstrated in Figure 1.5, certain systems of active particles can give rise to aggregations of the active particles into amorphous or crystalline structures. In these systems, the larger collections of active particles may behave as a single, larger active structure; this type of structure has also been called by the term “active crystal” [13, 268-273]. This type of aggregate active structure opens up a variety of new applications and behaviors when compared with disperse solutions or active fluids. Recent studies have demonstrated that this type of aggregation is very controllable: light, electrical and magnetic fields, or chemical species can be used to dynamically change whether or not the active particles assemble together, and can induce so-called “swarming” behavior [138, 265, 274-277]. When the swarms become rigidly locked together under an external stimulus, this has been termed as “directed self-

assembly" [278-281]. Bacterial swarms can also be considered as this type of active matter, and much like synthetic active matter, have the potential to be driven into organized states by the dissipation of energy [282].

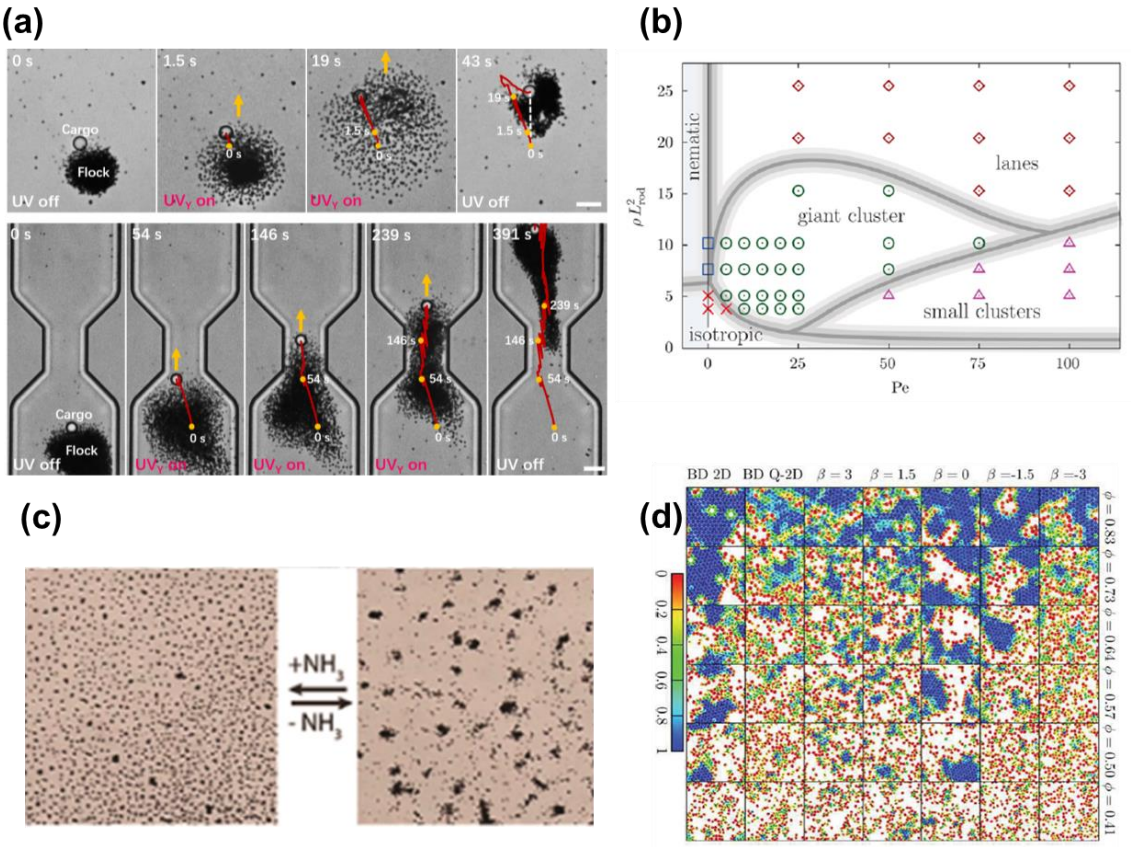

Figure 1.5: Collective behaviors of active particles.

(a)Active particles can be used to drive a passive cargo with permission from ref [265]. (b) The system flow as well as the density of the active particles both play key roles in how active particles congregate together, with permission from ref [266]. (c)Due to the nature of colloidal particles in an aqueous system, ions within the water can dynamically change clustering behavior, with permission from ref [212]. (d) Active particle shape and volume

fraction, as well as system confinement parameters, can have significant influence on the aggregation of active particles within the systems, with permission from ref [267].

A key parameter of active colloidal systems in terms of determining behavior is the density of the active particles within the fluid system in question [261, 283, 284]. It has been shown that the propulsion motility of the active particles plays a significant role, with slower active particles showing a greater tendency to cluster together, while more rapidly moving particles are likely to remain unbound, that is, the colloidal aggregation factor can in fact be tuned by active particle propulsion [266]. This can lead to so-called phase separation of the active particles within the fluid [31, 285-293]. The physical parameters of the fluid wherein the active particles reside also heavily contributes to the system behavior, as the viscosity and diffusivity of the fluid determines how much work is needed to drive the particles through the fluid at a rate surpassing that of simple passive diffusion, while shear forces and turbulence can induce separation or migration of the active particles [236, 278, 294-299]. Recent research on microswimmers has shown that clustering of these active colloidal particles is heavily dependent on the convection of the fluid, and such clustering can be suppressed by changing the geometry of the fluid system [300, 301].

When passive particles are also included in the active particle system, the system can reflect the behavior of active particle systems or passive particle suspensions, based on parameters such as species concentration or fluid properties such as the Reynolds number or Peclet number [242, 302]. Such active-passive particle mixtures have been termed as a type of "complex fluids", although this term is relatively broad and general in scope [303]. As mentioned previously, the field of microrheology, the study of flow on the micrometer

scale, often uses a single driven particle through a suspension of passive particles as a method of determining the properties of the passive suspension; this has been termed "active microrheology" [18, 40, 269, 304-310]. The inclusion of active particles induces enhanced diffusion to the passive particles, as active particles interact with the passive particles [311]. Interestingly, the complex interaction between active and passive particles has been shown to have the ability to give rise to complex biomimetic "predator-prey" interactions and motion, in a system containing diffusiophoretic attractive microparticles (prey) and diffusiophoretic repulsive microparticles (predator) [312, 313]. A similar study demonstrated how pairwise interacting active particles can generate long-range currents on passive particles, sustaining such currents even without an external driving factor as is necessary in conventional passive fluids [314]. The activity difference between active and passive particles of similar sizes can also lead to either homogeneous mixing or activity-based separation, dependent on the difference in energy dissipation between the active and passive particles [315]. To give another factor of complexity to the behavior of active matter, the geometry or confinement of the system is also a very influential factor, as previously demonstrated by the differences in 2D, quasi-2D, and 3D systems displayed in Figure 1.5(d).

1.6. Active Particles Under Confinement

The local and general environment of an active particle system plays a large role on the given behavior. Passive colloidal particles tend to settle along boundaries, with relative wall-to-fluid velocity and surface corrugation as determinants of whether these particles are pinned (static) or depinned (kinetic) with respect to the boundary in question

[316]. When an active swimmer is near a surface or boundary, it displays markedly different motion when compared with the bulk system, as confining walls tend to have a repulsive effect on active particles, and can exhibit elastic or inelastic properties based on a number of factors [29, 240, 317-319]. It has been shown that active particles may also produce ordered or semi-ordered layers near boundaries, due to hydrodynamic trapping [320]. A number of recent studies on active matter have focused on particles which are confined to a plane or thin slab, so-called 2D or semi-2D confinement; this approach allows for investigation of fluid interfaces, which are of great interest in several fields of application [86, 233, 266, 273, 315, 321-330]. Due to the low Reynolds number of most fluid systems at the micrometer scale, the confined Stokes flow is often modeled as a Hele-Shaw confinement, wherein two flat plates bound a small gap containing Stokes flow liquid; such a model is useful for real confinement cases such as the interface of two fluids where active agents are confined at the interface [151, 300, 331-333]. Another method of real confinement has been realized in a study from 2019, which demonstrates how electric field lines can be used as a way to confine electrically polarizable Janus particle-based micromotors in a contactless and dynamic manner [32]. Of course, 2D or slab confinement is only one of the many types of fluid confinement.

Tubular and more complex confinement of active fluids is very useful for modeling behavior in microfluidic or biological systems [334-337]. It has been demonstrated that complex boundaries or confinements can induce aggregation of active particles, while a dense concentration of microswimmers within a confined environment can give rise to spontaneous rotational flow as well as myriad other dynamical states [337-341]. Due to shear forces driving particles away from the center of a channel, and wall repulsion forces

driving particles away from walls, the precise arrangement and flow tendency of a system is highly dependent on the complex balance of forces, allowing for controllable tunability, heavily prized in microchannel sorting technologies [342]. The addition of propulsion forces from active particles only adds to the complexity of such behavior, which has given rise to many recent studies investigating such behavior [34, 39, 192, 221, 324, 343, 344]. A study from 2020 clearly demonstrates that for active Brownian particles in a wide-channel plane Poiseuille flow, the steady-state concentration profile of microswimmers across the channel is a direct function of the Peclet number, and that such microswimmers migrate towards the channel walls at high-shear, and towards the center of the channel at low shear [295]. The Peclet number Pe is given by Equation 1.5, where D is the mass diffusivity rate of species within the fluid:

$$\boldsymbol{Pe = Re * \frac{\mu}{\rho * D}}$$

Equation 1.5

At the low Reynold's numbers which occur for the active particle systems described in this text, the diffusion coefficient D for spherical particles is given by the Stokes-Einstein equation (Equation 1.6):

$$\boldsymbol{D = \frac{k_B T}{6\pi\mu R}}$$

Equation 1.6

Here, k_B is Boltzmann's constant, T is the system temperature, and R is the radius of the spherical particle. The diffusion coefficient is one of the most important parameters for defining a colloidal particle in fluid, and it is a direct function of the temperature of the

system, the dynamic viscosity of the fluid, and the size of the particle in question. As many active particle systems occur in laminar fluid flow with colloidal sized particles, this quantity can be used as a basis of motion for passive (non-active) particles in order to discern the effects of active motion[345].

Work on magnetic active swimmers demonstrates that population splitting across channels can be induced by a transverse magnetic field, implying future use of strong fields to preferentially direct such active particles [346]. Mathematical models have indicated that for fluids containing dispersed active particles, the individual and collective motion of the particles cause large variation in density at scales smaller than the mean free paths of the particles, whereas Fickian diffusion at larger length scales causes uniform fluid density [347]. The combination of shear flow and active particle propulsion leads to cycloidal trajectories, due to the competing forces on the particles [348]. The effects of the fluid medium play a key part in how active particles move, and in a similar fashion, the presence of active particles grants new behaviors to the fluid as a whole. Mathematical models have been used to show that active fluid demonstrates increased wetting and capillary actions, approximately proportional to the activity factor, and such active fluids show an increased capability for spontaneous imbibition into porous media [349]. Under confinement, micromotors have been shown to strongly affect one another, as the increased proximity induces single-file behavior for those traveling in the same direction, while nearby micromotors traveling in different directions tend to reorient and align with each other; at high particle densities, turbulence-like aggregates form as multibody interactions become complex [32]. Hydrodynamic fields acting between active particles, as well as between active particles and boundary walls, are crucial for determining the overall collective

motion of the system, as well as being a key component along with volume fraction to determine if the active particles aggregate [267]. The wide variety of behaviors arising from the complex interplay of factors in confined active particle systems allows for a huge amount of potential applications for these multifaceted devices. Active particles within a confined fluid system show strong anisotropy as well as spatial dependence of various properties including motor velocity, orientation, and diffusion, due to the particular properties of the confining geometry [132]. This has profound effects on active particle applications within microfluidic or even cellular environments.

Active particles have shown themselves to be some of the most versatile tools to arise at the forefront of modern materials science, especially due to their ability to actively operate and enact changes in fluids at the nano- and microscales. Magnetically-controlled active particles, such as those made of iron oxide, have shown great promise in drug delivery as well as the removal of blockages from blood vessels within the body [144, 350, 351]. For these purposes, active particles are generally present in large numbers, and the systems they are in, be it microfluidics devices or the human body, can be considered to be confined fluid systems; a recent experiment studied flow patterns of a 22% volume fraction suspension of micron-sized hard polystyrene spheres inside of a microcapillary [352]. However, depending on several factors such as driving force and particle density, active particles within the body may have the potential to aggregate and cluster together, and this process needs further study to understand potential risks [112, 353].

Recent research has demonstrated that the directed assembly of colloidal dispersions can be used to synthesize a wide range of functional materials in a controlled fashion [278, 354, 355]. While passive colloids also can self-assemble, colloidal systems

composed of active particles demonstrate an enhanced ability to self-assemble, due to the driven nature of the particles [280, 356]. This type of active aggregation has been shown to create dynamic clusters which change over time, through work done by both the fluid velocity as well as individual active particle motion, in order to overcome the long-range repulsion common in colloidal systems [250, 357]. The aggregation of active colloidal particles has been shown to occur naturally in systems with colloidal volume fractions of $3\% - 50\%$ [358]. Active particles can demonstrate enhanced diffusion of a fluid system, with increasing active particle density leading to a greater effective diffusion coefficient [329]. The aggregation of active particles can be notably complex; behavior mimicking that of living cell aggregates has been shown to develop as active colloids self-organize into clusters [313]. Active particle microswimmers in particular have been shown to display motility-induced clustering as well as phase separation in a quasi-2D environment [359]. Under weak confinement, autophoretic active particles demonstrate both clustering and dispersion modes, dependent on the driving force and interparticle interactions [333]. In many cases, the presence of geometrical confinement grants far different dynamics to active particles as compared to the more widely modeled unbounded case, highlighting the importance of considering explicit confinement when modeling non-bulk systems [240, 360]. The presence of physical or other manner of confinement has a profound effect on the behavior of active particles, as the existence of a boundary introduces complexity to the motion of the driven motors, leading to phase separation, boundary clustering, and other emergent behavior [361-364]. Confinement can also be used as a tool to predict and control the behavior of active particles such as micromotors [365]. Thus, the behavior of active particles on the micrometer scale, especially within confined systems, is a system which is

currently worth study, to add to the rapidly growing set of literature of computational methods for modeling active matter [37]. Active colloidal particle aggregation has been shown in previous literature to be heavily dependent on the size and surface properties of the particles [366, 367]. In addition, the application of external electric or magnetic fields can also drive the aggregation process [278, 368]. However, there remains a lack of research towards the confined collective behavior of active colloids, specifically covering a range of volume fractions and driving forces, especially as it relates to their aggregation [42, 369, 370]. This is one of the open problems which I aim to tackle with the research within this Dissertation.

1.7. Experimental Observations

The applications of active particles are boundless, with new uses being realized constantly. When discussing modern research into active particles, one of the first things to consider is what the application of the particle will be. Active particles contained within a fluid will, by their very motion, add a certain amount of kinetic energy to the fluid around them. Due to this, one of the most basic uses of active particles is to increase the effective diffusion of both themselves, and the fluid system that they are a part of. Within the field of active matter, much attention is given to how the active particles change or enhance the local and global fluid flow. In addition to the active particles propelling themselves around, there has also been research into using freely suspended active particles, powered by light, which are able to pump fluid towards desired point sources, based on active particle density and light source intensity [137, 139]. A work from 2019 demonstrates how hydrogel-encapsulated catalysts can be used as actively propelled micromotors in order to enhance

chemical flow and diffusion of catalysts in microreactors [130]. However, this is only the very beginning of the potential uses of active particles. Figure 1.3 shows a schematic view of how micromotors have developed in the past two decades, not only in their propulsion methods, but also in the various methods of utilization.

Arising from concerns over unprecedented post-industrial levels of pollution, the treatment of wastewater is a common goal of many teams currently researching micromotors [101, 136, 371-377]. Chemically powered micromotors which use H_2O_2 as fuel have been shown to be able to efficiently catalyze methylene blue, as well as capture oil droplets from wastewater, with the body of the micromotors being developed from the airborne contaminant carbon soot, in an ingenious method of "using waste to clean waste" [378]. A work from 2020 has further demonstrated that not only can visible light be used to power micromotors which use catalysis for wastewater treatment, but that the iron oxide nanoparticles incorporated into them are suitable for using magnetic retrieval for easy recycling, in a similar composition to hybrid-powered micromotors discussed in Section II [379]. A similar study showed that magnetically driven BiOBr-based micromotors can use solar power to degrade organic pollutants, with the activity of the micromotors not only enhancing diffusion but also stirring the liquid to enhance diffusion [71]. Work has also been done on developing micromotors for the removal of heavy metal ions using various side-chain functional groups on tubular structures, with bubble-driven Ni/Pt catalysts for propulsion [380]. It has been shown that the fluid mixing induced by active particle action can greatly increase the chance of contact between reactive oxygen species on a micromotor with pollutants, enhancing wastewater treatment by up to 3.5 times when compared with unpropelled counterparts [93, 381]. One report from 2019 demonstrates

micromotors which can simultaneously sense, remove, and recycle metal ions in wastewater, using a composite polycaprolactone/Mg propulsion system [382]. Inorganic pollutants such as heavy metal ions are not the only concern with wastewater, however. Micromotors have been developed which can actively capture and remove antibiotics from water [119]. Metallodielectric Janus particle micromotors have been shown to be able to trap, transport, and selectively electroporate bacteria under both continuous alternating current as well as pulsed signal conditions in order to help combat biological waste products [142]. The use of graphene as the outer body of micromotors has proven to not only benefit from the mechanical stability of this material, but has also demonstrated antibacterial properties against *Escherichia coli* and *Staphylococcus* cultures [383]. Similarly, a large amount of research on active particles has focused on how they can be used in the biological and medical fields.

As seen previously with chemical mixing, micromotors can be used to enhance mixing efficiency; in the medical field this can allow for faster testing with much smaller samples than would be needed otherwise [384]. A paper from 2020 demonstrates the usage of micromotors in enhancing the efficiency of C-reactive protein immunoassays for determining sepsis in preterm infants, allowing the usage of much smaller samples than needed for conventional immunoassays [384]. The ability of micromotors to demonstrate enhance diffusion over passive agents has been used in order to enhance the retention of cargo within the intestines, allowing for better deep-tissue imaging via photoacoustic computed tomography [385]. However, the applications of active particles in medical research is not limited to only this. One research team has proposed the idea of generalized, nonfunctionalized micromotor surfaces for label-free dynamic loading, transport, and

release of commercially available functionalized beads, which can be used for immunosensing or DNA binding tests with a major goal of reducing intermediate fluid handling steps such as buffer exchange or washing which are commonly used in current practices [386]. One study expanded upon this idea with the loading of iron and selenium into magnesium-based micromotors, which can operate within gastrointestinal fluids, for the purpose of combating anemia, and demonstrated positive results in a mouse model [387]. As evidenced by Figure 1.6, there has also been significant research into the use of magnetically-driven active particles as a method disrupt blood clots within deep veins, bypassing the need for surgery in some cases [351, 388]. These methods of using the mechanical power of micromotors all demonstrate some of the unique ways which they can enhance current medical technology, as well as develop it further.

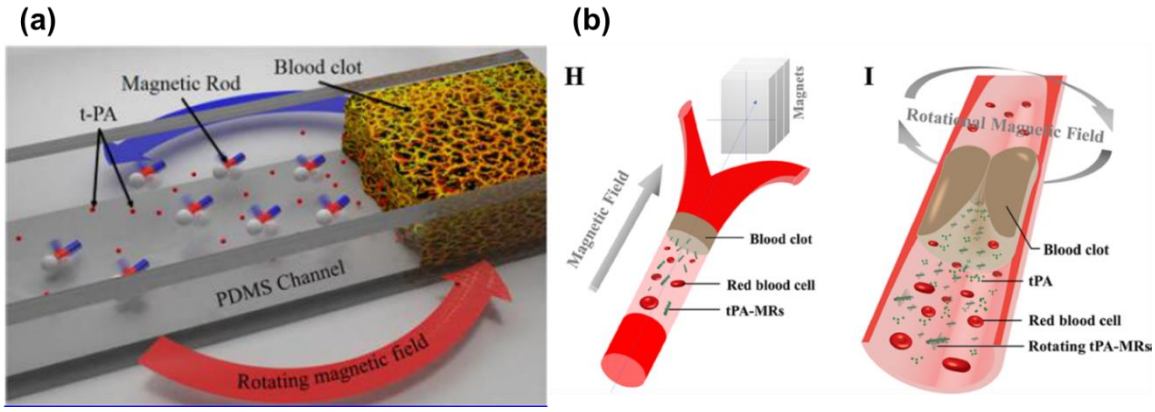

Figure 1.6: Using active particles to destroy blood clots.

(a) With permission from ref [388], (b) ref [351].

There has also been recent research which has moved beyond the concept of singular micromotors moving through a fluid. A lab at the University of California San Diego has used micromotor-style catalysis propulsion using magnesium to generate H_2 bubbles and drive microneedles from a dermal patch to enhance payload delivery; such a technique can be considered an alternative application of active particle technology, and helps to show how technology development is not always linear [389]. Beyond the usage of distinct, separate individual active particles, it has been shown that active colloidal crystal clusters can be useful as well, with the ability to be tuned to have a specific size or with the inclusion of catalysts or magnetic elements, in order to use as dynamic bar-coding to facilitate detection processes ideal for biomedical applications [96]. In addition to having the active particles use their driving force to perform mechanical or chemical tasks, the enhanced diffusion is also remarkable for the use of marking and detection applications. Specially coated micromotors have demonstrated ten times the light reflection of simple gold particles, in addition to being controllable via magnetic fields, offering great suitability as theranostic imaging tools [390]. Jellyfish-shaped micromotors have been used for the detection of DNA in solution, using the driving catalase on the micromotor limbs to also trigger displacement-based release [134]. Such bioinspired designs are a commonly seen starting point for current research using active particles. Several innovative methods of creating synthetic active particles involve using existing cells as the base, due to their motive capability and biocompatibility. A study from 2020 demonstrates the potential of asymmetrically immobilizing urease onto existing platelet cells, thereby creating a type of Janus micromotor with high biocompatibility, which can then be loaded with anticancer or antibiotic drugs for a variety of biomedical applications [121]. A novel approach for

biocompatible micromotors uses the outer membrane of red blood cells as the framework for platinum catalyst-powered micromotors, incorporating the strength and flexibility of a cell into a controllable active particle [391]. Helical magnetic micromotors inspired by the flagellar motion of *E. coli* have been put forward as cellular microcarriers to be used for cell seeding and cultivation, allowing for the dynamic assembly of complex cellular structures [120].

Based on the astounding amount of research within the past few years, the field of active particle research is rapidly expanding, especially in biological and medical fields of study. However, there is a distinct lack of information on the clustering behavior of colloidal active particles in confined environments such as blood vessels and capillaries; it is the purpose of this Dissertation to use the theoretical and simulational techniques which will be explained in Chapter 2 in order to carry out a systematic investigation of this matter. The simulations which I carried out will be defined and explained in Chapter 3, reported and analyzed in Chapter 4, and then clustering behavior scaling laws based on the density and applied driving force of the simulated active particles will be given in Chapter 5. Chapter 6 is a short overview of the work, overall conclusions of the field based on the literature study and research, and potential directions for future research utilizing the simulational framework presented here.

2. ACTIVE PARTICLE THEORY

2.1. Theory of Active Particles

The potential and realized usages of active particles are varied and complex, as is their behavior in such fluid systems. To begin discussion on the behavior of active particles in a fluid environment, the behavior of a single active particle must first be studied. The performance of a single active particle in a fluid system lays the initial groundwork for modeling and understanding more complex systems [162, 392, 393]. Figure 2.1 gives some of the most important characteristics of active particles in a fluid system, and helps to elucidate what properties should be considered when discussing their behavior, and what influences that behavior. As mentioned in Chapter 1, at low Reynold's numbers active particles must break time-reversal symmetry in order to enact motion, and systems containing active particles cannot be considered to be in equilibrium, due to the energy which active particles add to the system by definition. Active particles on the order of a micrometer, or even nanometer, can be considered as a special kind of Brownian particle, and as such the influence of Brownian motion is very strong in these systems. However, rather than having their motion completely dictated by heat and the random collision of the surrounding fluid, active Brownian particles instead rely on the extraction of energy in some manner as discussed above in order to drive their motion. It has been shown through mathematical modeling that the damping factor of the surrounding fluid is a critical parameter which strongly influences whether the dominant motion of such a particle is random-collision (Brownian) dominated or self-driving (active) force dominated; the

Brownian force is a function of the fluid medium, while the self-driving force corresponds to the induced potential of the active particle [394, 395]. It is the active force which is most often the subject of study in the field of active particles.

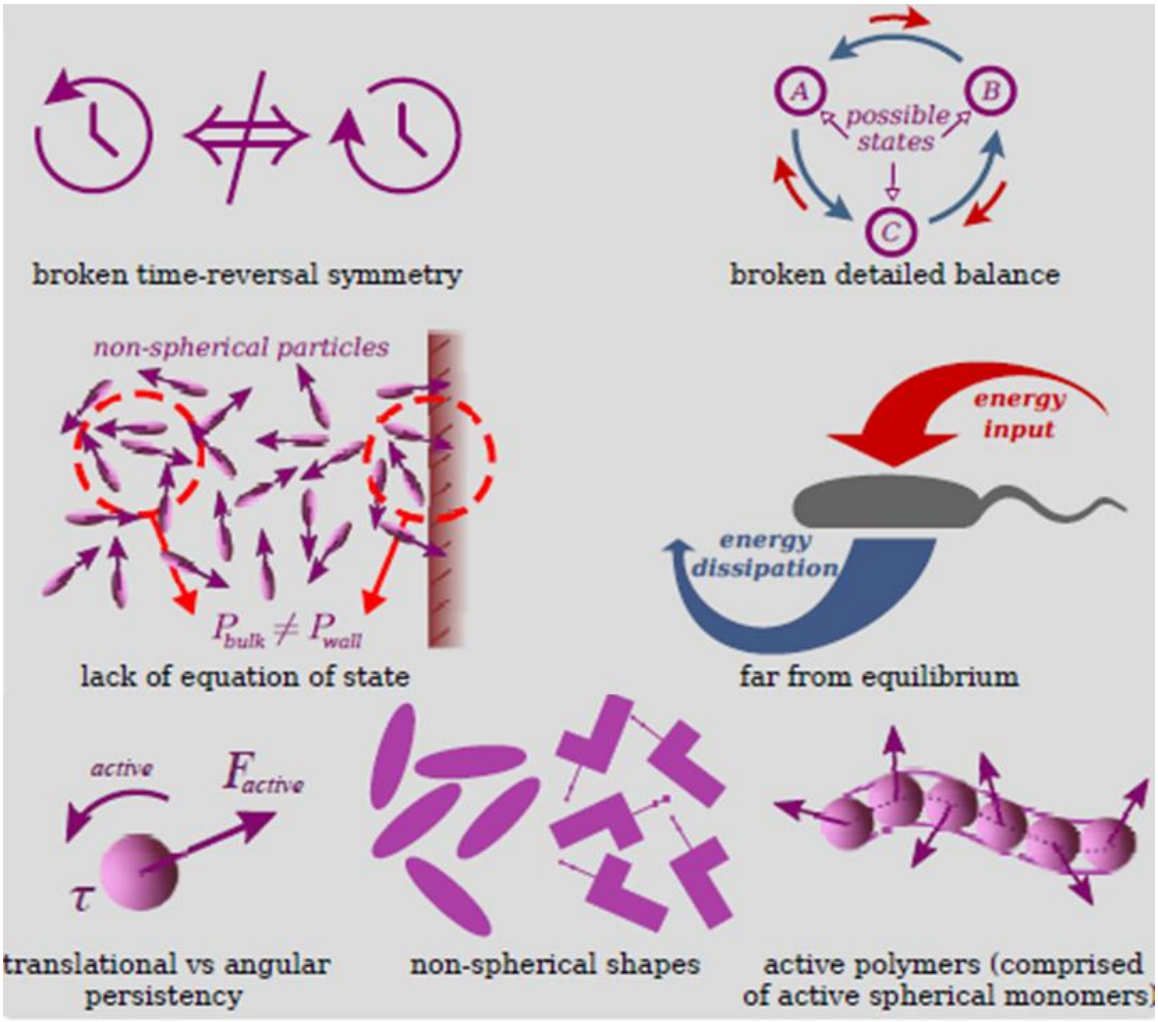

Figure 2.1: Properties of active particles.

With permission from ref [37].

The propulsion method of an active particle strongly influences its behavior; it can be understood that microswimmers have a different propulsion mechanism than catalytic

or magnetically driven particles, and the geometry must be taken into consideration as well, for it has been observed that linear tube or nematic micromotors have markedly different kinematics in fluid when compared with spherical particles or amorphous cells [8, 25, 168, 310, 383, 396-402]. It has also been shown that L-shaped particles on the micrometer scale can demonstrate coupling between translational and rotational motion, and L-shaped micromotors have been experimentally observed to exhibit circling trajectories which differ greatly from typical spherical or rod-shaped micromotors [403]. One specific type of motive behavior, termed "run-and-tumble" motion, was first observed in natural active particles such as bacteria or microalgae. These particles can be considered to be driven by flagellar motion, and often exhibit intermittent motion between high-motility "run" periods broken by low-motility "tumble" periods [404]. In fact, a study on the photosynthetic model organism cyanobacterium *Synechocystis* demonstrated that light intensity had a profound effect on the ratio between time spent in the run versus tumble states, as well as collective positive phototaxis, which persisted for up to an hour after cessation of the light source [405]. One study from 2019 demonstrated that magnetotactic bacterium demonstrated complex behavior influenced not only by magnetic field lines but also by the chemical gradient of oxygen within the environment, influencing the natural run-and-tumble behavior of the cells [406]. Such run-and-tumble behavior was first characterized by observing living cells, but has also been observed in a number of synthetic active particles as well. In a specific case, chemical propulsion of rod or tube-like micromotors has been experimentally shown to lead to this run-and-tumble behavior, as opposed to the relatively constant motion exhibited by field-driven or spherical catalyst micromotors [101, 331]. These types of active particles exhibit periods of relatively linear directed motion

interspersed with periods of random tumbling behavior, in a similar manner as the aforementioned bacteria.

Chemical propulsion, magnetic/optical field propulsion, and swimmer-based propulsion all generate differently shaped flow fields around each active particle, giving rise to differences in active fluid behavior at both the individual and bulk scales [340]. The hydrodynamics surrounding active particles is thus a good place to begin a discussion of the motion of the particles. The basis of motion for active particles within a fluid can be considered to be the particle-fluid hydrodynamic interactions. It is on this foundation of hydrodynamic interactions that the propulsive force (in most cases), drag force, and all other forces, act and effect motion within the fluid. Hydrodynamic descriptions also set the basis further, for the active particle behavior near walls, in channels, and even determine their collective behavior, as inter-particle interactions must all be mediated through the surrounding fluid, whether through direct mechanical force or field effects [37]. The addition of active particles to a fluid also has profound indications on the behavior of the fluid, making fluid-active particle influence a two-way function [407]. The scaling of the effective diffusion coefficient of a fluid system has been shown to be non-monotonic with respect to the driving force of the active particle, with these flow-field effects being demonstrated in the motion of biological active particles such as motile phytoplankton or other microorganisms [343]. Such self-propelled particles have velocity distributions which indicate individual particle-based turbulence, even in the absence of bulk fluid turbulence, leading to further complexities for the description of fluid flow when active matter is involved [408]. System-wide field forces must also be considered. On larger scales, the influence of gravity on active matter flows becomes nontrivial; although many

simulational studies on active particles at the micrometer scale neglect gravitational forces, this is not always the case [395, 409, 410]. Active particles are affected by all of the same forces as similar passive particle systems, but the addition of propulsive forces adds another layer of complexity. A study from 2019 demonstrated that asymmetrical metallic patches on spherical colloidal particles can allow for alternating current electric fields to tune the shape of individual particle trajectories, such as causing the active particles to achieve 3D helical pathways in order to navigate complex environments more efficiently than is possible with random or linear trajectories [411]. Obviously, care must be taken not to overly simplify or generalize complex active particle systems, as the mode of propulsion and geometry of the particle heavily contribute to the single-particle behavior, and also the collective behavior of many active particles in a fluid system [16, 70, 412]. The simulations performed in this work consider the active particles to be spherical and driven by a generalized non-chemical motive force, for simplicity.

2.2. Simulational Work

Due to the complexity of active particle systems, there has been much research done via simulation in order to observe emergent behaviors not able to be captured by theory alone. It has been shown that, while passive colloids can self-assemble, colloidal systems composed of active particles can demonstrate an enhanced ability to self-assemble, due to the driven nature of the particles [356]. This type of active aggregation has been shown to create dynamic clusters which change over time, through work done by both the fluid velocity as well as individual active particle motion, in order to overcome the long-range repulsion common in colloidal systems [250].

Lone active particles within a bulk fluid can move freely, due to the low particle densities; however, at high particle densities active particles have been shown to be able to form turbulence-like aggregates or serpentine chains [32]. The aggregation of active colloidal particles has been shown to occur naturally in systems with chemical signaling between active particles, for colloidal volume fractions of $3\% - 50\%$ [358]. At higher particle densities, the term active fluid is more appropriate that active colloid, as the fluid itself will attain a glassy state due to crowding effects and jamming of the dense active particles [413]. Due to this, the simulations within this work will study systems with an active particle density of $5\% - 30\%$, as this range allows for rapid aggregation without major hindrance from the steric effects seen at higher active particle densities.

Some simulational work has focused on the shape effect of active particles. In a parallel to the way different individual behaviors of active particles arise based on their geometry, the collective behavior of active particles in a fluid system is strongly influenced by the active particle shape, with rod-shaped motors demonstrating very different dynamics as compared to colloidal spheres or Janus particles [359]. Shape-encoded programmed dynamic assembly of active particles has also been demonstrated as a method of creating heterogenous complex devices with larger degrees of freedom as compared to monolithic micromachines [354]. A 2019 study on active Brownian particles used molecular dynamics to establish how active particles can demonstrate enhanced diffusion of the fluid system, with increasing active particle density leading to a greater effective diffusion coefficient [329]. Collective motion of cells presents a good natural model to study in order to better understand active particle behaviors, with prior results indicating that dynamic behavior arising from such collective motion spans across a wide range of length and time scales

[51, 414]. Recent work from 2021 has shown via several simulations and models that active particles increase mixing at small scales, while actually inhibiting transport across larger length scales; this active particle coupling between activity and flow can lead to nontrivial effects on mixing and transport [415]. Figure 2.2 gives a generalized overview of the different models used for the various categories of active matter. Due to the complexity of the systems in question, some of the most important steps for setting up a simulation of active matter is the choice of coarse-graining, as length and time scales are too long for first-principles or fully atomistic simulations, as well as the choice of implicit or explicit solvent, due to the large contributions and emergent effects of the fluid system which the active particles may be embedded in.

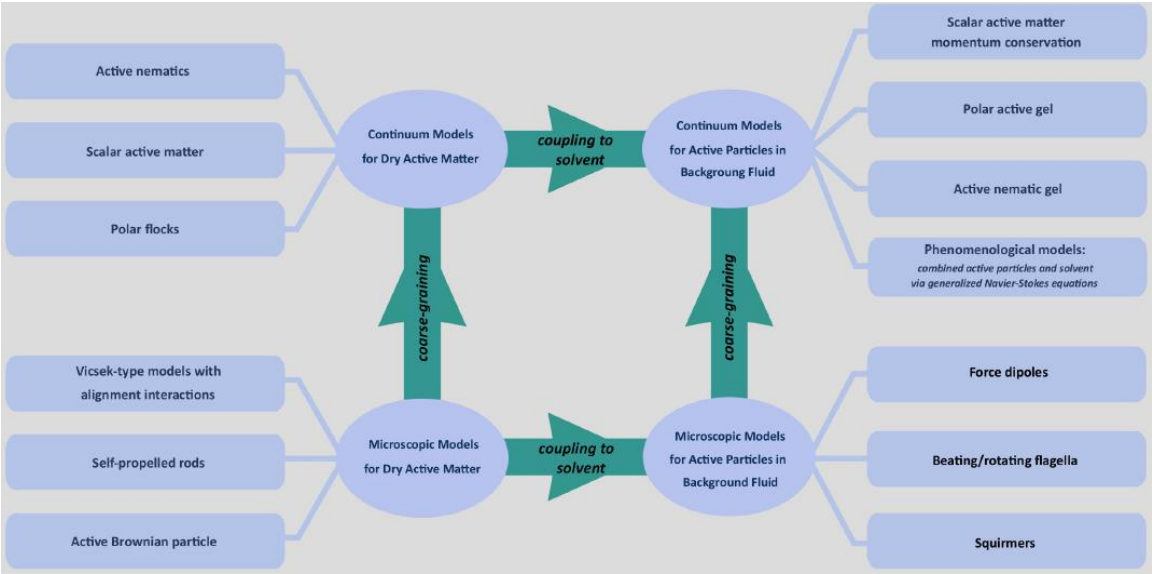

Figure 2.2: Computational models for active matter

With permission from ref [37].

2.3. Fluids and Solvents

There is a tremendous difference in scale for both length and kinematic time between colloidal particles and solvent particles; for example, a typical colloid particle (1 μm diameter) occupies a volume comparable to that of 10^3 water molecules. Thus, coarse graining of the solvent is necessary in order to reasonably reach significant scales of time and size for the simulated system. In this work, we use stochastic rotation dynamics (SRD), also called multiparticle collision dynamics, in order to create a fluid system that is computationally efficient, hydrodynamically accurate, and can handle thermal noise[416]. For this work, the coarse-graining length scale is chosen to be smaller than that of the mesoscopic colloidal particles, but much larger than the natural length scales of the solvent molecules (in this case, water). By obeying local momentum conservation, the following methods reproduce Navier-Stokes hydrodynamics (Equation 1.2 and Equation 1.3) at larger length scales.

SRD is a dynamic mesoscopic coarse graining technique which has been previously used to capture the behavior of passive and active colloidal particles under low Reynolds numbers (Equation 1.1) and low to moderate Peclet numbers (Equation 1.5) [141, 417, 418]. SRD was developed for cases when fluid dynamics are important, but the detailed chemical properties can be neglected. Compared to DPD, where transport coefficients and effective viscosities can vary by up to 50%, SRD values are generally within 1% of experimental results. The lattice Boltzmann method for solvent particles can be more efficient than SRD, but is also far less accurate in regimes where thermal fluctuations are needed (such as the effect of Brownian motion). Brownian dynamics can be more efficient

than SRD, but less accurate if inertia and full hydrodynamics are necessary. The fluid-representative solvent is composed of point masses, and SRD draws from both Monte Carlo and lattice methods with no numerical instabilities. It can also be easily coupled with MD simulations. The SRD method maintains synchronous, discrete-time dynamics with continuous velocities and local multiparticle collisions used to efficiently describe the dynamics of the solvent, while colloidal particles are coupled to the solvent through explicit interaction potentials[417].

In SRD, the solvent is represented by a large number of point-like particles of mass $1\, m_s$ (an explanation of units is given below). These are termed the fluid particles; however, they are not merely composite particles or clusters made up of aggregates of water molecules. The particles can be considered as a convenient computational device to allow coarse graining of the fluid properties. SRD works as follows: In the first step, the streaming step, the positions and velocities of the fluid particles are calculated directly by integrating Newton's equations of motion, as seen in Equation 2.1:

$$\boldsymbol{x_i \rightarrow x_i + v_i}$$

Equation 2.1

Here, x_i is the position of particle i, and v_i is the velocity. The forces on the fluid particles can be generated by external forces such as the system walls or colloidal beads, but there are no direct forces between fluid particles, and the lack of such pairwise calculations contributes to the high efficiency of the method. After the streaming step, the second step of the algorithm, the collision step, simulates the collisions between fluid particles. The system is partitioned into cubic cells of length $1\, \sigma$. The velocities of all fluid

particles are rotated by rotation vector $\hat{\omega}$ relative to the center of mass velocity V of their respective cell separate cell, as given in Equation 2.2.

$$\boldsymbol{v_i \rightarrow V + \hat{\omega}[v_i - V]}$$

Equation 2.2

This step is where momentum is transferred between the fluid particles. The rotation procedure can thus be viewed as a coarse graining of particle collisions over time and space. Because mass, momentum, and energy are conserved locally, accurate Navier-Stokes (as given in Equation 1.2, Equation 1.3, and Equation 1.4) hydrodynamic effects can be captured, including that of thermal noise. The method of SRD coarse-graining of a fluid thus allows for easy control of viscosity and coupling properties and can demonstrate phase segregation and reactive hydrodynamics from complex solutes.

2.4. DLVO Theory

Depending on the individual particle properties, as well as the dispersion fluid, colloids can aggregate, flocculate, or remain discrete within the fluid environment. Due to the fluid inertia and small length scales, most mathematical models for the base fluid on these scales use the Navier-Stokes equations of state for fluids, assuming incompressibility, and Neo-Hookean or rigid body material for the solid particles; the associated approximations included in these assumptions are favorably validated with experiments [198-201]. DLVO theory, named after Boris Derjaguin, Lev Landau, Evert Verwey, and Theodoor Overbeek, quantitatively describes the aggregation behavior of aqueous

dispersions, and as such is very useful for the modeling of colloidal interactions, which generally present long-range repulsion and short-range attraction between dispersed particulates [208-210]. The general form of the DLVO interaction potential is a summation of electrostatic (Equation 2.3) and van der Waals (Equation 2.4) forces.

$$\boldsymbol{U_{Coul} = \pi\epsilon_r\epsilon_0\left[\frac{4k_BT}{q}tanh\left(\frac{q\Psi_0}{4k_BT}\right)\right]^2\frac{d^2}{r}\exp(-\kappa[r-d])}$$

Equation 2.3

For the Coulombic interaction, ϵ_r is the electric permittivity of the fluid, ϵ_0 is the vacuum permittivity, q is the particle charge, Ψ_0 denotes the effective surface potential of the colloid, and κ is the inverse Debye screening length. The Debye screening length is a measure of how quickly loose ions within the solvent attenuate particle surface charge as a function of the distance; this leads to the often seen "double-layer" screening seen for charged particles in solvents such as water. The van der Waals component of the DLVO interaction is given by Equation 2.4:

$$\boldsymbol{U_{vdW} = -\frac{A_H}{12}\left[\frac{d^2}{r^2-d^2}+\frac{d^2}{r^2}+2\,ln\left(\frac{r^2-d^2}{r^2}\right)\right]}$$

Equation 2.4

Here, for the van der Waals interaction, A_H is the Hamaker constant, d is the bead diameter, and r is the distance between the colloidal bead centers. DLVO describes the force between two spheres interacting through a combination of Lennard-Jones and doubly-screened electrostatic interactions, and with a certain amount of modification can also be used to describe nonspherical particles [211]. Due to the doubly-screened

electrostatic interactions felt by the particles, aggregation behavior of charged particles is strongly dependent on the screening potential / chemical makeup of the suspending fluid, with the polar solvent water being the most commonly used [212]. Thus, in this work, DLVO-based interaction potentials are used for colloid-colloid interactions, along with the aforementioned stochastic rotation dynamics method of modeling the solvent.

2.5. Coarse Graining

This work studies specifically the common scheme of diffusion-limited colloidal aggregation; that is, when two colloidal particles are close enough, they will certainly form a cluster together[207, 419]. This progression is inherently a non-equilibrium kinetic process. The CGMD colloid-colloid interaction potential uses the DLVO potential developed for colloidal interactions[420]:

$$\boldsymbol{U = U_{vdW} + U_{Coul} + U_{Hertz}}$$

Equation 2.5

Equation 2.5 gives the summation of forces acting between colloidal particles. Here, the total potential energy between two colloidal particles is the summation of a van der Waals (attractive) force, given by Equation 2.4; a Coulombic (screened electrostatic) force, given by Equation 2.5, and a Hertz (hard repulsive contact) force.

The Derjaguin-Landau-Verwey-Overbeek interaction is suitable for use when coupling CGMD with SRD, and has been proven to give accurate hydrodynamic interactions for colloidal systems of Peclet number smaller than 20 [421]. To model steric

repulsion between colloidal particles, and prevent overlap or penetration of the beads, a Hertz contact force is included, as given by Equation 2.6:

$$\boldsymbol{U_{Hertz} = K(d - r)^{\frac{5}{2}}, \qquad r < d}$$

Equation 2.6

The hydrodynamic volume fractions of interest range from 5% to 30%; at higher volume fractions, steric interactions between the colloids start to dominate and frustrated systems can occur[417]. All quantities are described in dimensionless units with mass in units of m_s (the mass of the solvent particles), energy in units of ϵ, length in units of σ, force in units of $\frac{\epsilon}{\sigma}$, and time in units of $\tau = \sqrt{m_s\sigma^2/\epsilon}$. Parameters are chosen to model micrometer-sized active particles within water, and using a temperature of 310 K with the viscosity of water at that temperature of $694.2\,\frac{\mu Ns}{m^2}$, physical values can be assigned to the micromotor clustering simulations [132]. Each SRD fluid point particle thus represents 4 water molecules, and $\sigma = 1\mu m$ is the radius of the CGMD active particle beads.

The focus of this work is to investigate the effects of density and driving force of active colloidal particles on their clustering behavior within a confined fluid system. In this paper we use a hybrid coarse-grained molecular dynamics model in order to simulate the clustering and aggregation behavior of colloidal particles of micrometer size. The fluid is explicit, due to the important effects of hydrodynamics on the clustering process. Stochastic rotation dynamics, also called multiparticle collision dynamics, is used in order to well replicate both long- and short-range hydrodynamic behavior at low Reynolds number. The active particle beads are modeled using coarse-grained molecular dynamics simulation with an inter-colloidal potential based on DLVO theory.

3. CLUSTERING BEHAVIOR OF ACTIVE PARTICLES

3.1. Model and Setup

Based on the coarse-graining and solvent schemes discussed in the previous chapter, I developed a simulational model in order to perform my own experiments for the clustering of active particles in a confined fluid environment. Presented in the following chapters is an investigation of the dynamic clustering behavior of active particles under confinement, including the effects of both particle density as well as active driving force. This chapter will discuss how the simulation was set up, the potentials used in this study, and the analysis methods that were carried out, the results of which will be discussed in the following chapters. A hybrid coarse-grained molecular dynamics scheme is used with stochastic rotation dynamics to allow for accurate hydrodynamic interactions, and the diffusion-limited aggregation behavior is studied. The variables of interest are θ and F. The variable θ is the 2D projection area coverage ratio of the colloidal particles to the 2D size of the simulation box; i.e. $\theta = 25\%$ means that the total area of all particle projections equals 25% of the area of the box. The variable F indicates the driving force on the colloidal particles along their axial direction, with $F = 0$ indicating passive (nondriven) particles. Results indicate that both coverage and driving force have strong effects on the aggregation behavior of the colloidal particles, with the coverage effects dictating the clustering speed at low driving forces, whereas large driving forces dominate behavior. Power scaling laws were found to well fit the rate of cluster formation over time, with

anywhere from two to four different dynamic regions depending on the coverage. The findings presented here allow for a series of scaling laws based on power relationships for the clustering time as a function of both density of active particles, as well as the applied driving force. There are up to four distinct dynamic regions in terms of clustering as a function of time, dependent on the density of the particles within the system. As driving force increases, the aggregation behavior also is accelerated, whereas an increase in density of active particles changes the dynamic procession of the system.

The system of interest is passive or active particles of the micrometer scale, which can be termed as a colloid [194-196]. In these colloidal systems the suspended particles may interact through hydrodynamic, interparticle, and Brownian (or thermal) forces[422]. The model setup used for all following simulations and results will directly model hydrodynamic and Brownian forces through stochastic rotation dynamics, and the interparticle interactions will be modeled with the Derjaguin-Landau-Verwey-Overbeek (DLVO) interaction. A multiparticle collision-based method called stochastic rotation dynamics will be used to model the solvent.

3.2. CGMD Active Particles / DLVO

This work studies specifically the common scheme of diffusion-limited colloidal aggregation; that is, when two colloidal particles are close enough, they will certainly form a cluster together [207, 419]. This progression is inherently a non-equilibrium kinetic process. Figure 3.1(a) displays a schematic representation of the attractive colloidal active particles under a quasi-2D confinement (Hele-Shaw confinement, as mentioned in Chapter 1) scheme, as expounded upon below. In the simulation, colloidal spheres of mass M are

propagated through the velocity Verlet algorithm with a timestep of $0.01\,\tau$. The colloids are embedded in the fluid, and interact with the fluid particles through a repulsive-only Weeks-Chandler-Andersen potential (van der Waals force). While the fluid-fluid interactions are coarse-grained using SRD, the colloid-colloid and colloid-fluid interactions are integrated using a normal molecular dynamics procedure.

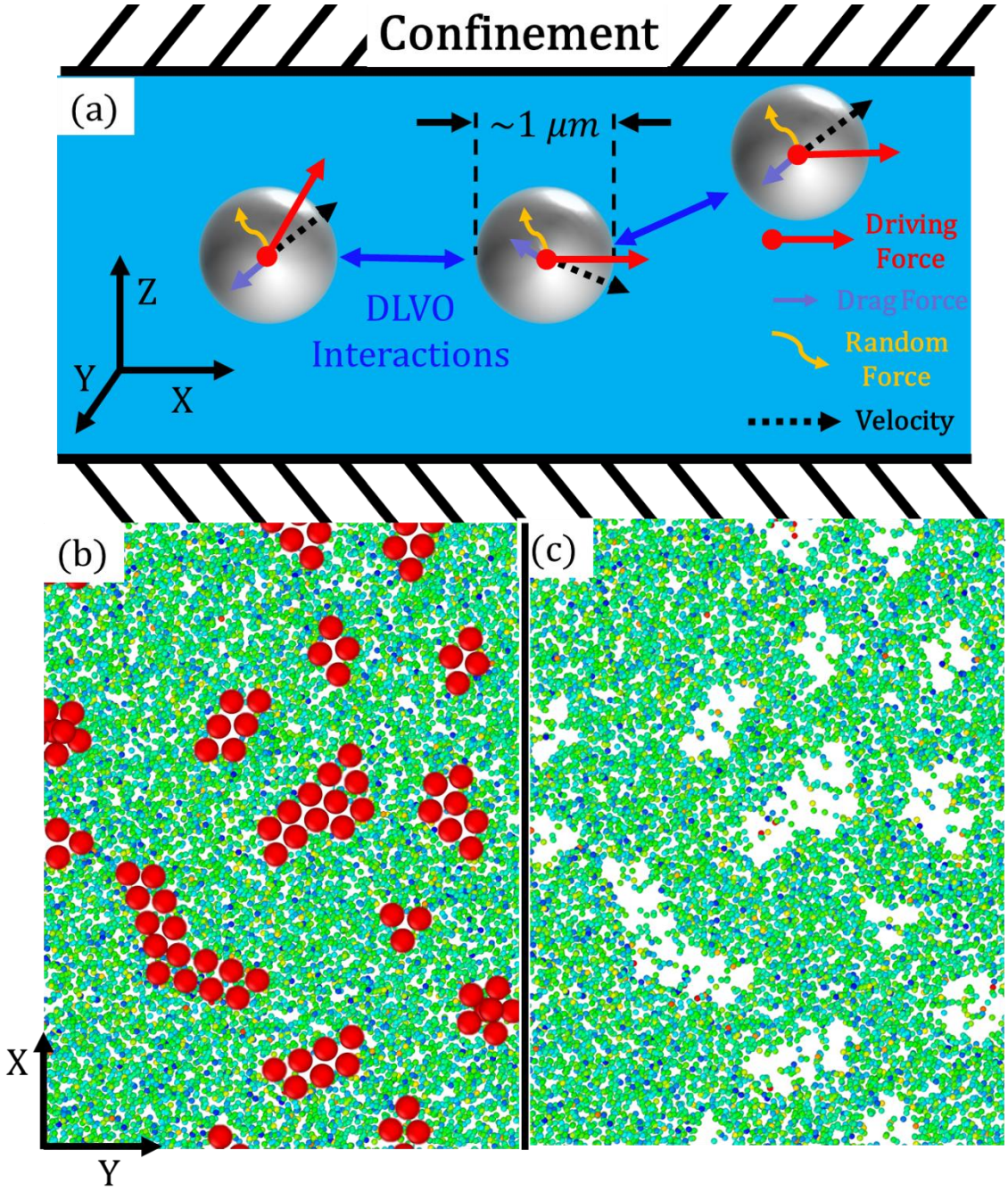

Figure 3.1: Model setup.

(a) Schematic of the spherical active particles, with on-axis driving force, under confinement. The particles can attract each other (cluster) at close distances due to the DLVO interactions. The explicit SRD fluid grants hydrodynamic effects such as drag forces

in the opposite direction of motion, and random thermal forces. Model setup: (a) The CGMD beads in SRD solvent, and (b) the solvent with transparent beads to show solvent density. Solvent beads are colored as a function of their relative velocity, to demonstrate the distribution.

The CGMD colloid-colloid interaction potential is the DLVO potential developed for colloidal interactions[420]. The total potential energy between two colloidal particles is the summation of the van der Waals (attractive) force, Coulombic (screened electrostatic) force, and Hertz (hard repulsive contact) force. The interbead colloidal forces are given by Equation 2.3, Equation 2.4, Equation 2.5, and Equation 2.6. The Derjaguin-Landau-Verwey-Overbeek interaction is suitable for use when coupling CGMD with SRD, and has been proven to give accurate hydrodynamic interactions for colloidal systems of Peclet number smaller than 20 [421]. To model steric repulsion between colloidal particles, and prevent overlap or penetration of the beads, a Hertz contact force is included, as given by Equation 2.6. The SRD fluid point particles interact with the CGMD beads via the Weeks-Chandler-Anderson potential as described in Equation 3.1.

$$\boldsymbol{U_{WCA}} = \begin{cases} \boldsymbol{4\epsilon\left(\left(\frac{\sigma}{r}\right)^{12} - \left(\frac{\sigma}{r}\right)^{6}\right) + \epsilon,} & \boldsymbol{r \leq 2^{\frac{1}{6}}\sigma} \\ \boldsymbol{0,} & \boldsymbol{r > 2^{1\backslash 6}\,\sigma} \end{cases}$$

Equation 3.1

The hydrodynamic volume fractions of interest range from 5% to 30%; at higher volume fractions, steric interactions between the colloids start to dominate and frustrated systems can occur[417]. All quantities are described in dimensionless units with mass in

units of m_s (the mass of the solvent particles), energy in units of ϵ, length in units of σ, force in units of $\frac{\epsilon}{\sigma}$, and time in units of $\tau = \sqrt{m_s\sigma^2/\epsilon}$.

Figure 3.1(b-c) shows a representative snapshot of the CGMD-SRD hybrid model used for the simulations in this work. The SRD point particles allow for good representation of long- and short-range hydrodynamic behaviors, while the CGMD beads model the colloidal micron-sized active particles (micromotors). The CGMD beads are finite-sized spheres with radius 1σ and density $1\frac{m_s}{\sigma^3}$. The simulation box is 256σ x 256σ in the x-y plane, and 10σ in the z dimension with a harmonic restraining force perpendicular to the z-direction on the CGMD colloidal particles only. The simulation box is periodic in all dimensions. The confining force in keeps the CGMD beads within a plane of approximate thickness 3σ at the center, in a quasi-2D setup. This size disfavors bead stacking in the z-dimension, while still allowing beads to cross over and past each other. Figure 3.2 displays the initial quasi-2D setup of the particles on a square lattice with areal density $\theta = 30\%$. The number of beads for each geometrical setup; that is for $\theta = 5\%$, 10%, 15%, 20%, 25%, and 30%; correspond to $N = 1089$, 2116, 3136, 4225, 5184, and 6241, respectively. A quasi-2D setup is chosen to both reflect the high confinement found in vascular systems as well as to allow for ease of simulation and analysis, with the results being easily extrapolated to 3D behavior. After the beads are created, each bead has its orientation randomly set, so that any propelling force will also act in a random direction at the beginning of the simulation. Figure 3.3 demonstrates the clustering of beads as a function of time, as well as their nearest neighbors. For the driving force applied to the active particles, the force is applied constantly along the axis of the active particle, and thus

due to the reorientation of spherical particles in a fluid, there is no net directional movement due to the driving force.

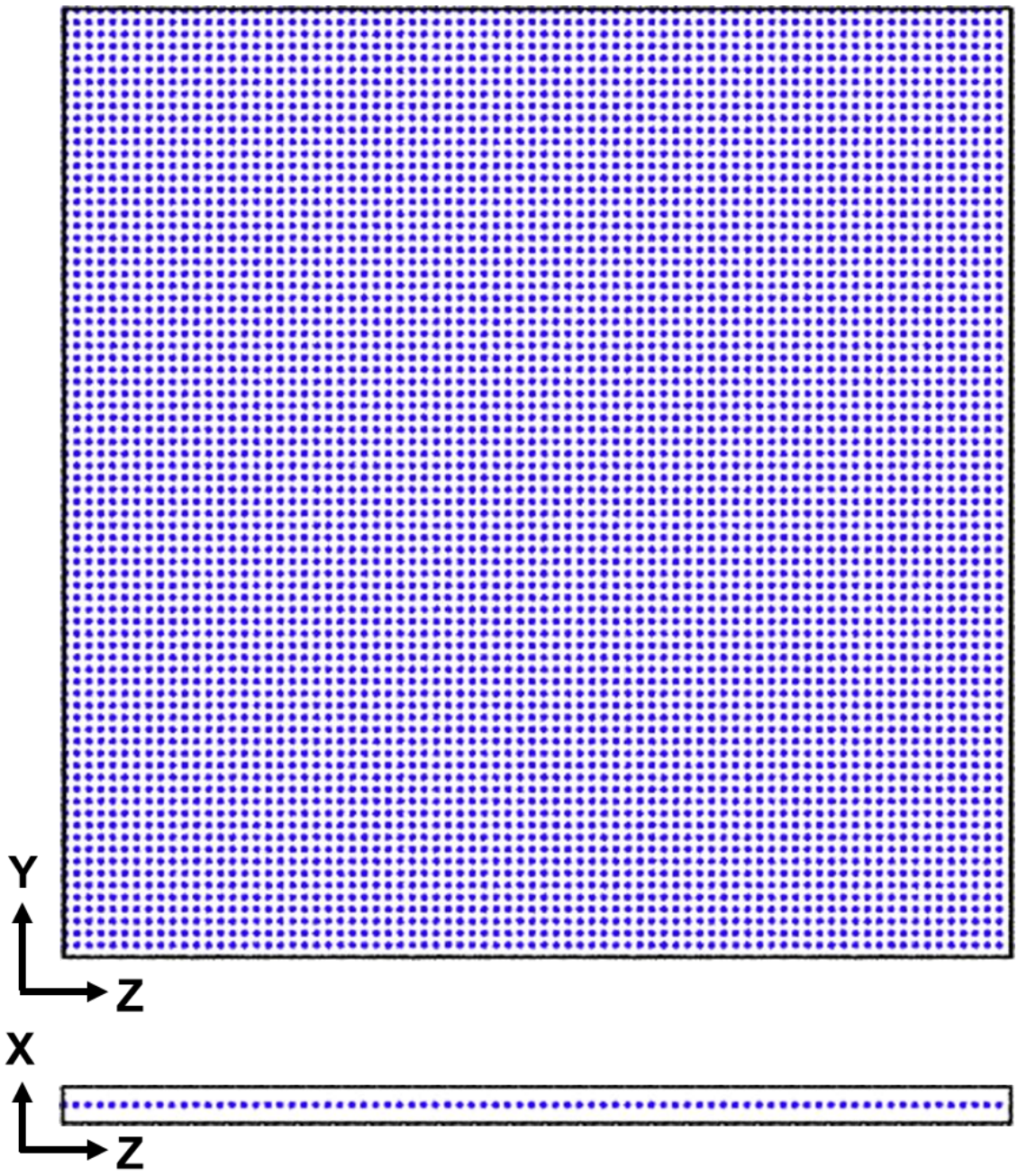

Figure 3.2: Axes and initial experimental setup for θ = 30%.

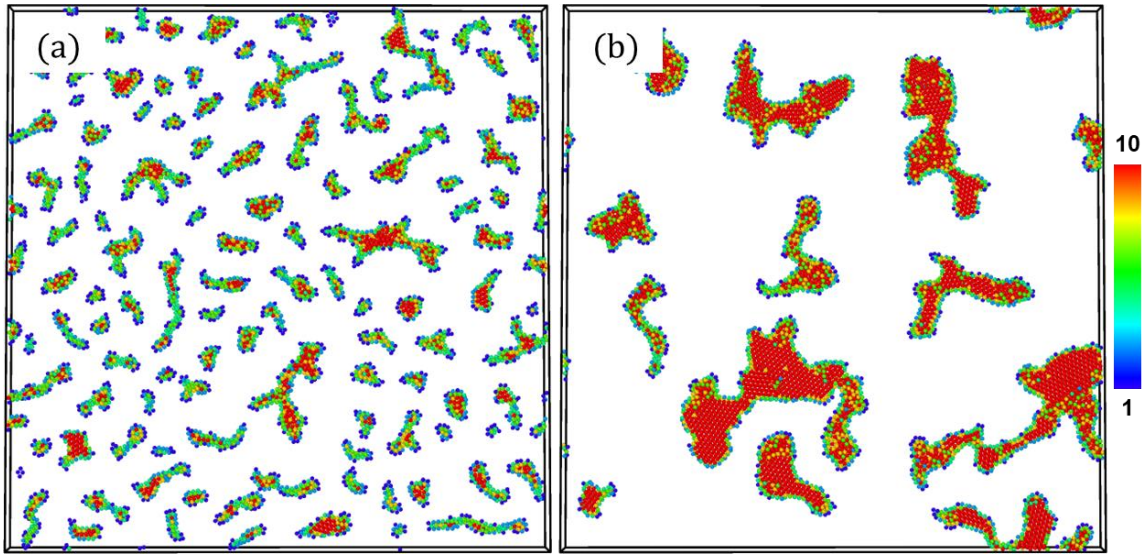

Figure 3.3: Coordination during clustering.

Case is for θ = 30% F = 5. (a) τ = 275, (b) τ = 2,500. The color bar indicates coordination of the beads.

3.3. Testing and Validation

For active particles, low-Reynold's number systems can be assumed. In the case of active particles for medical usage, blood within the body generally follows Stokes' law, as given by Equation 1.4. Peak Reynolds numbers within the human body (Re) are below 2000, and flow within the veins is generally laminar flow at $Re < 500$ [423]. Figure 3.4 demonstrates Stokes flow for a spherical bead traveling through the SRD particles. Figure 3.5 shows the mean squared displacement curves of particles with different applied forces as well as their trajectories. No applied driving force is equivalent to the Brownian motion of passive colloidal particles. The software LAMMPS was used for all simulations [424].

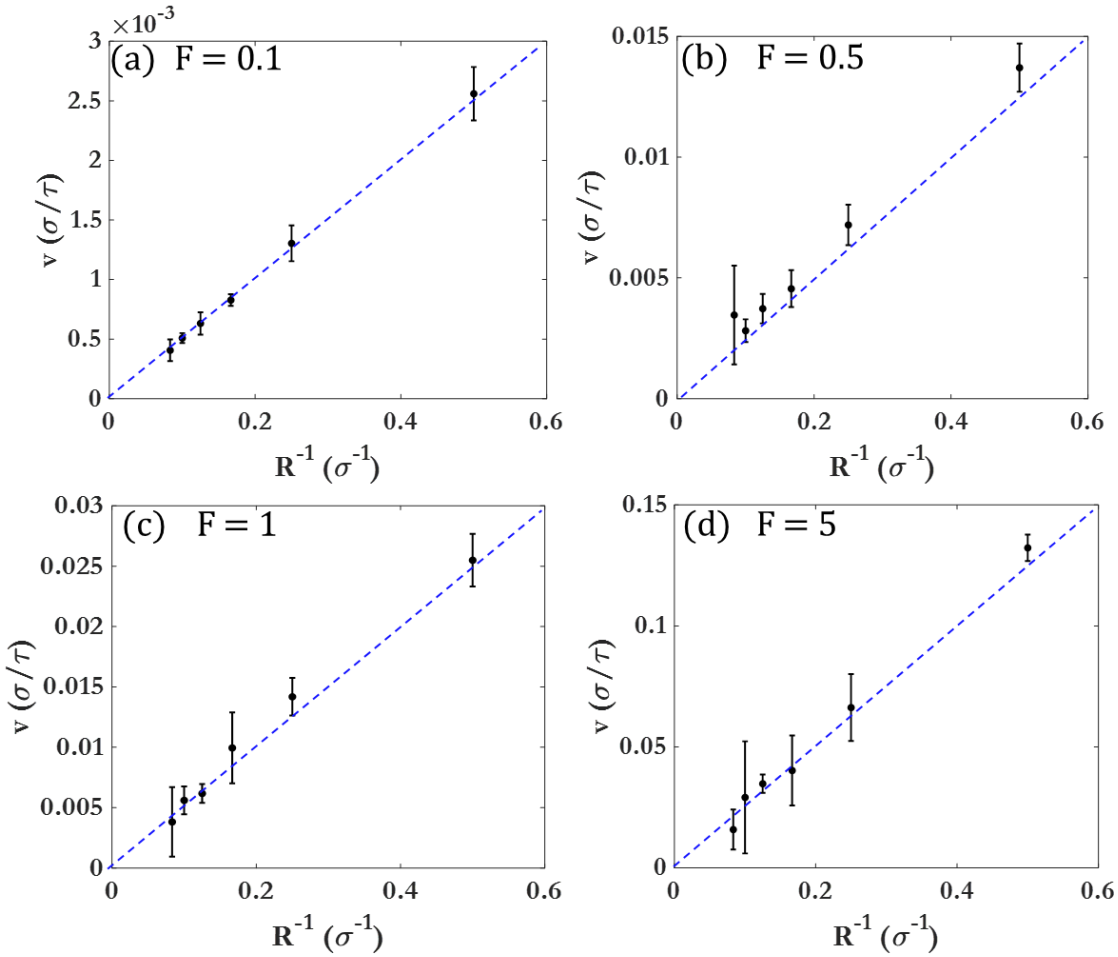

Figure 3.4: Low Reynolds regime for laminar flow test cases.

Cases are for spheres of different radii under driving force (a) F = 0.1, (b) F = 0.5, (c) F = 1, (d) F = 5. for F = 0.1The dotted line is from theory. N = 5 cases for each data point.

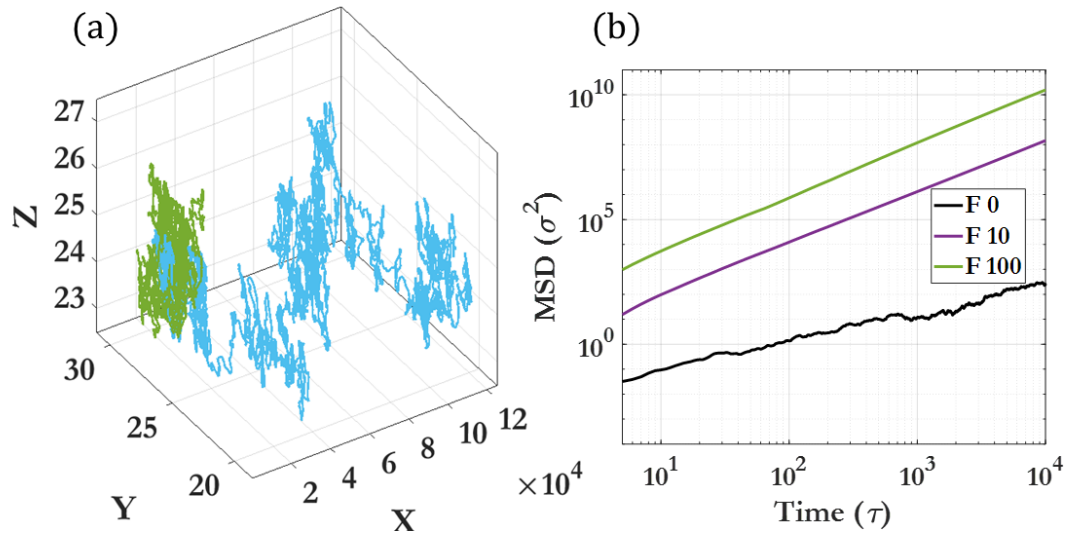

Figure 3.5: Validation of fluid.

Path of a single bead (a) and MSD (b) comparisons demonstrating enhanced diffusion of active particles when compared with passive particles.

Figure 3.6 shows all of the 5 independent runs for $\theta = 5\%$ at different driving forces. It can be seen that there is very little difference between cases, and this similarity holds true for all θ and F. At $F = 10$, occasionally a bead will temporarily detach from a cluster due to the similar magnitude of driving force and interbead attractive potential. Due to Figure 3.6, we can see that the average cluster number and therefore cluster size can be taken as a good approximation for all runs across each variation of driving force F for a given coverage density θ. Additionally, Figure 3.7 shows that only θ matters in terms of cluster number over time, and absolute bead number is not significant. For systems with $16x$ more and $16x$ fewer beads, there was no big difference in clustering behavior over time, although there were minor size effects towards the end of the run when the number

of beads was small ($N_0 < 500$). This can be attributed to the discreet behavior of very few ($N < 10$) clusters when compared with the more continuous behavior of many ($N \geq 100$) clusters.

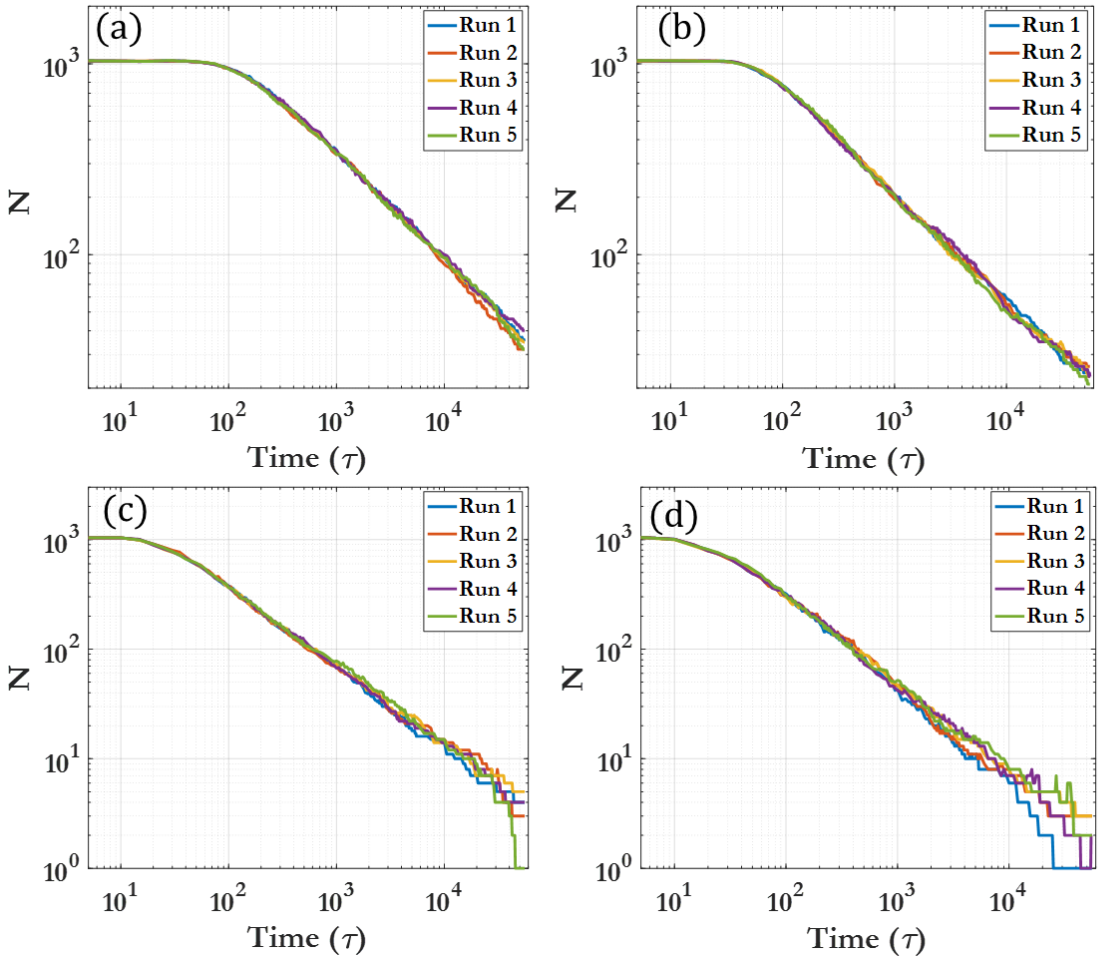

Figure 3.6: Comparison of different cases.

Five Different runs for θ = 5%, (a) F = 0, (b) F = 1, (c) F = 5, and (d) F = 10.

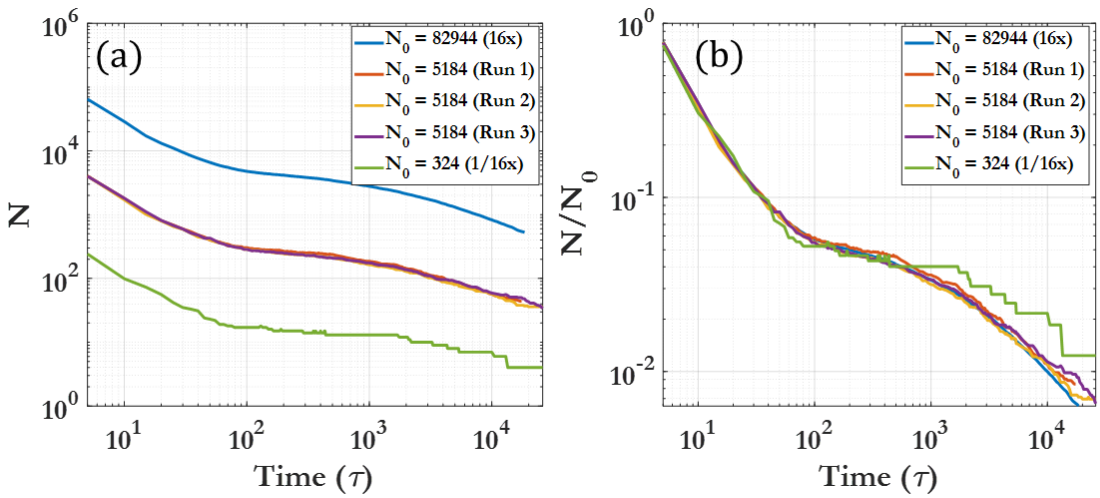

Figure 3.7: Size effects of the system.

Different sized simulation boxes and effects on clustering behavior. θ = 25% F = 0.

3.4. Analysis Methods

Cluster number tracking: A cluster here is defined as an arrangement of particles where at least two particles are within the skin distance of each other. The skin distance is $r_{ij} < 2.3\ \mu m$ where r_{ij} is the distance between two particles. Two particles are a part of the same cluster if a path can be drawn from one to the other solely by connecting particles within skin distance.

A program was written using MATLAB to count the clusters and their sizes for each snapshot of the system (301 snapshots for each of the five runs for each given force and coverage density (see Appendix). The clusters and sizes were used to generate a histogram of cluster size distributions which could be well-fit by the gamma distribution, given below:

$$P(S) = \frac{b^{-a} S^{a-1} e^{-\frac{S}{b}}}{\Gamma(a)}$$

Equation 3.2

Equation 3.2 gives the probability distribution defined by the gamma function, termed as the gamma distribution. Here, $P(S)$ is the probability of a cluster being size S. The gamma distribution has a shape parameter ($a > 0$), a scale parameter ($b > 0$), a cluster size ($S > 0$), and $\Gamma(a)$ is the gamma function. As a increases the distribution approaches a normal distribution. The gamma distribution is useful in applications with a physical lower bound but no non-statistical upper bound.

The periodic system can be analyzed through fast Fourier transformation (FFT) of snapshots of the system taken in the x-y plane, as the quasi-2D nature of this system allows for ease of spatial analysis. For each snapshot of the system used for analysis, an image was generated. The image was composed of 1024x1024 pixels for the 256x256 μm system (16 pixels/μm^2 resolution), and generated as completely black-and-white. From this initial image, a 2D-fast Fourier transform (FFT) was performed. In the clustering image, white pixels (background) are treated as zeros, while black pixels (colloidal particles) are treated as one. The circular average of the power of the 2D FFT transform was calculated, and the k-space power spectra was determined. The code used is given in the Appendix. This k-space was used to determine the representative length of the system, which denotes the average cluster size and spacing between clusters. The inverse length scale of the system is termed as k_r, while the circularly averaged FFT power spectra is denoted as

$PSD(k_r)$. To find the representative length k_0, a Gaussian curve was fit to the first peak for every snapshot, and k_0 and $PSD(k_0)$ were found and plotted.

4. TIME-DEPENDENT BEHAVIOR

4.1. Clustering Behavior

The fundamental quantity of interest for this system is the number and distribution of clusters, which changes over time due to the diffusion-limited aggregation of the individual particles and clusters which, in this confined setup with a set number of particles, drives towards fewer and fewer clusters. The individual particles aggregate into clusters, which further aggregate with the increment of time. Figure 4.1 gives a visual representation of how both time and driving force affect the clustering behavior for a given coverage (in this case, $\theta = 15\%$). An increase in the active driving force causes more rapid clustering behavior, especially near the beginning of the simulation. This causes clusters to form and aggregate more rapidly when compared with the passive colloidal particles (those with no driving force; $F = 0$). The dynamics of clustering are intrinsically changed by the addition of a driving force, with more complicated effects overall than a mere acceleration of the clustering seen. As evidenced in Figure 4.2, the coverage and driving force both contribute heavily to the time evolution of clustering behavior; the snapshot time for each given force and coverage is $t = 1000\tau$. At higher coverages, clustering proceeds more rapidly, especially at smaller times, due to the decreased average interbead distances which arise due to the geometrical realities of increased particle coverage.

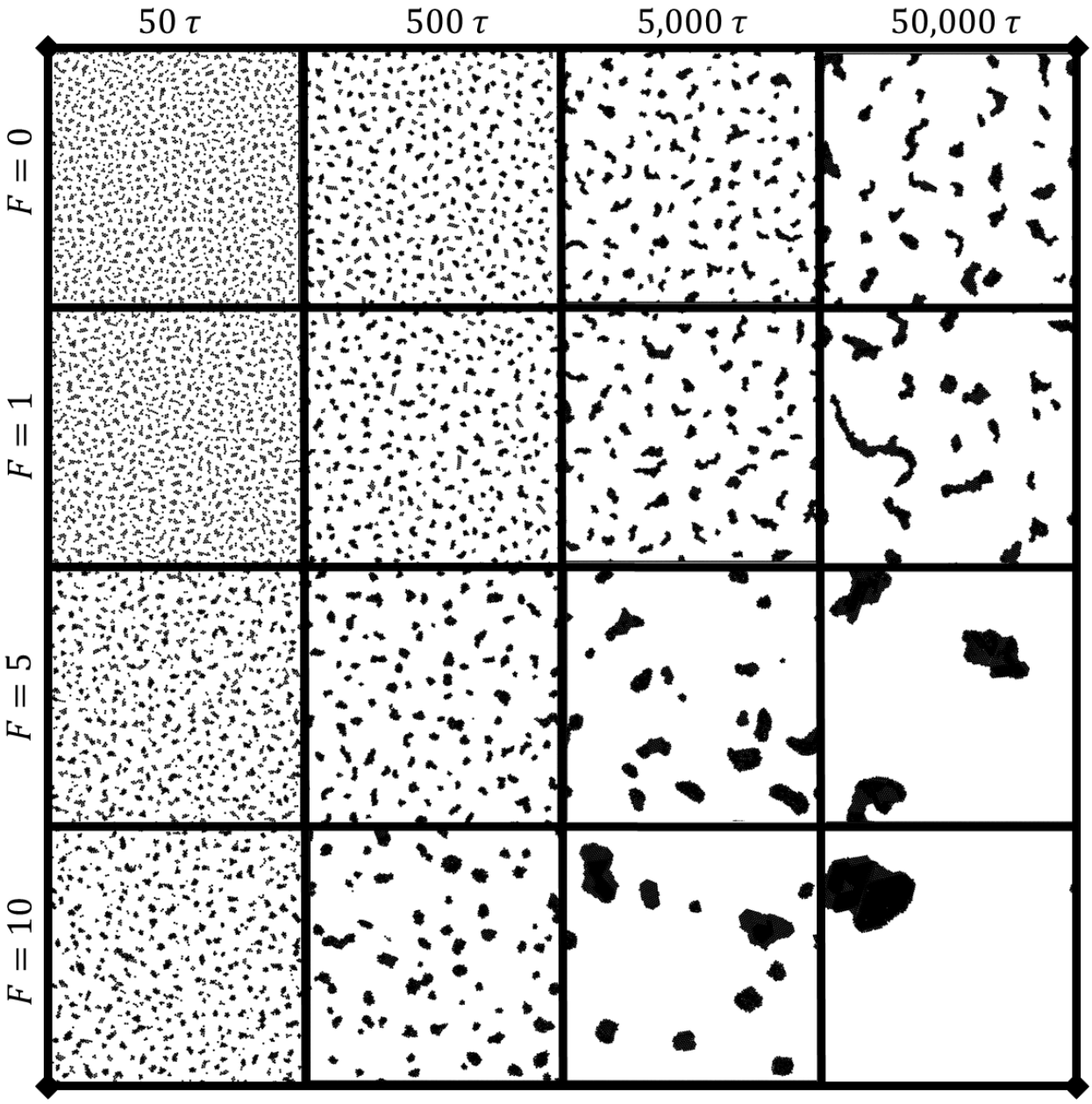

Figure 4.1: Clustering behavior over time.

Time is $50\ \tau$ *to* $50{,}000\ \tau$ *for* $\theta = 15\%$*, for different applied force* F.

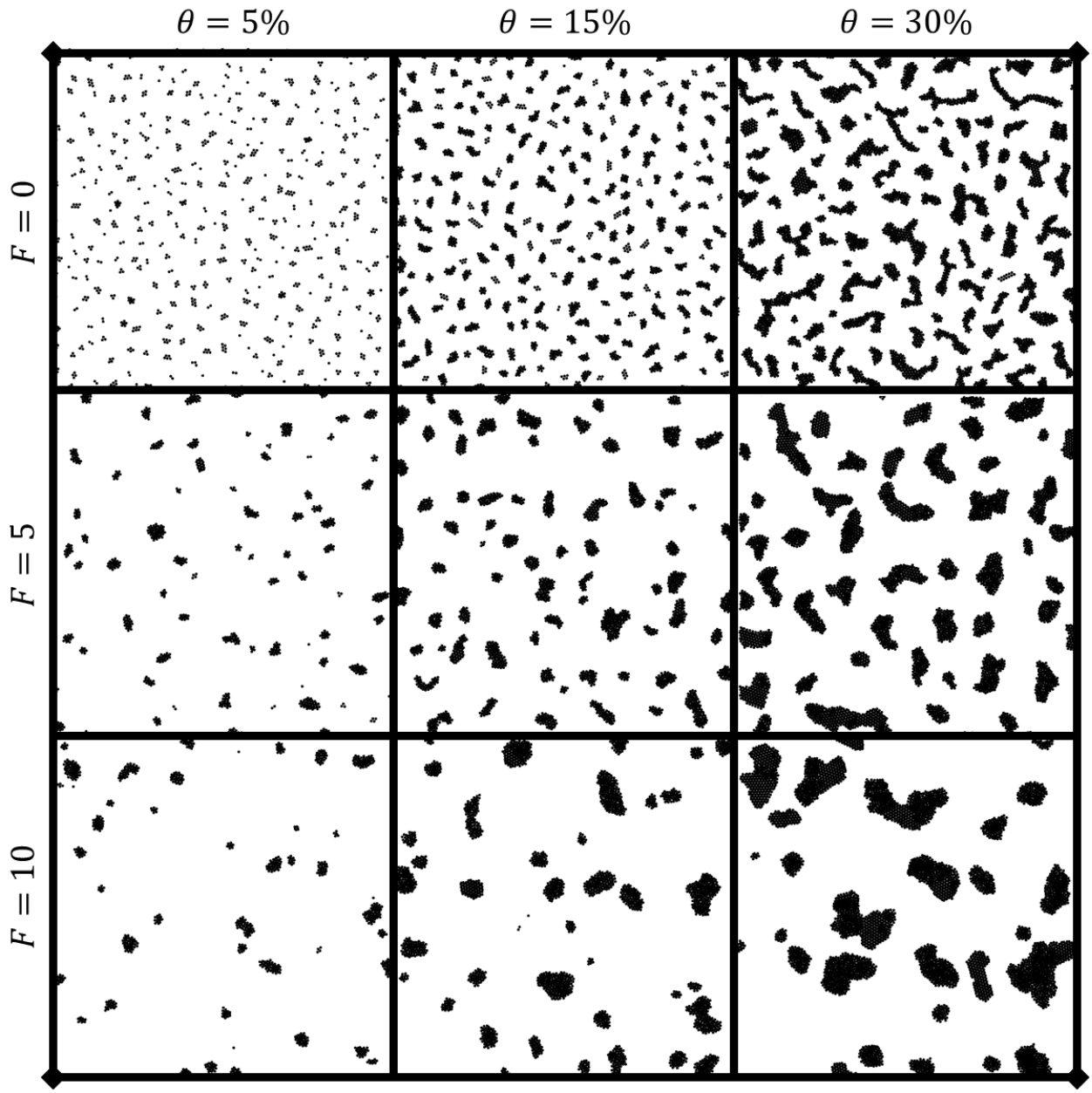

Figure 4.2: Clustering behaviors at different densities and driving forces.

Time is $t = 1000\ \tau$.

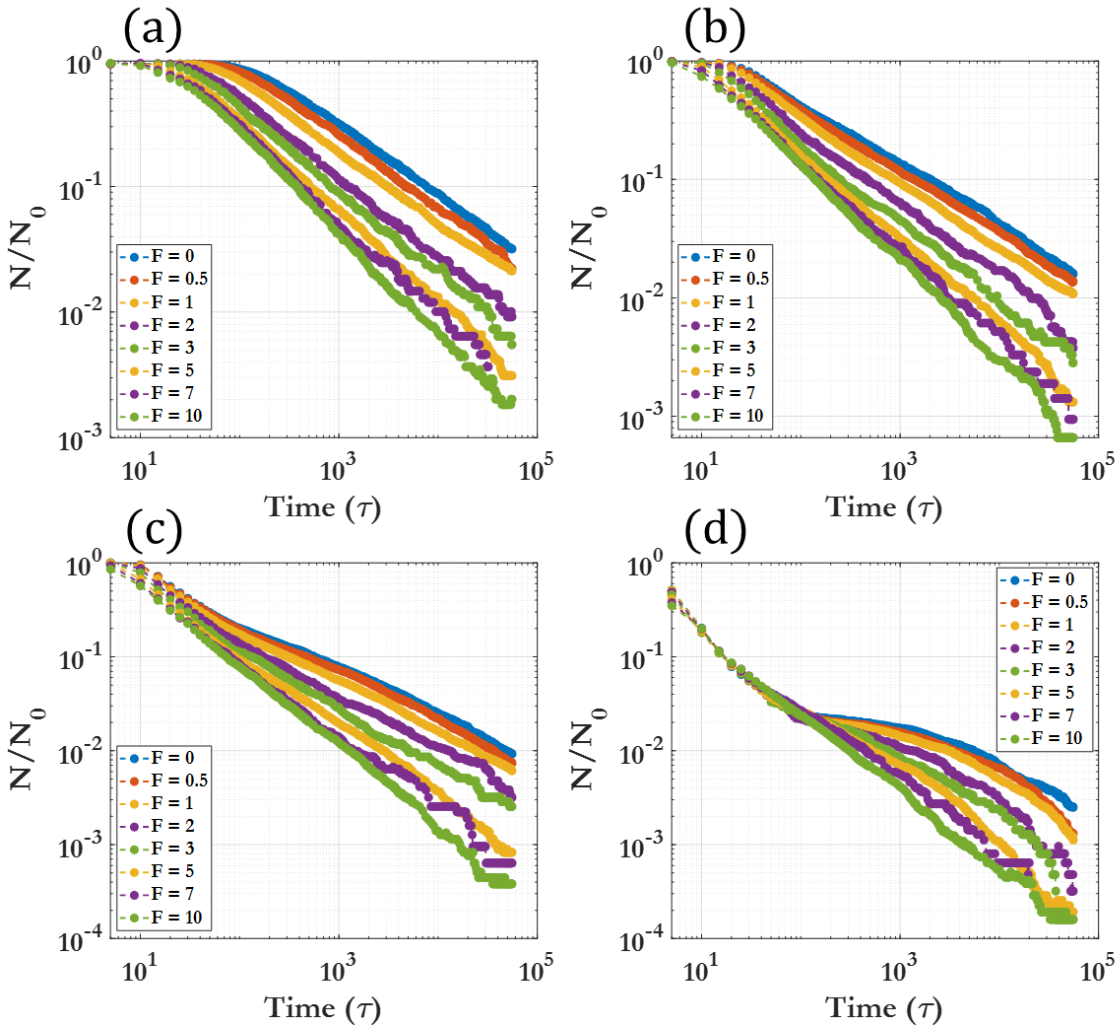

Figure 4.3: Cluster number versus time.

Clustering behavior over time for (a) $\theta = 5\%$*, (b)* $\theta = 10\%$*, (c)* $\theta = 15\%$*, and (d)* $\theta = 30\%$.

As the CGMD particles collide, they will stick together and form cluster aggregates. Figure 4.3 gives an overview of how the number of clusters proceeds over time, demonstrating how the number of clusters decreases monotonically over time, due to the DLCA assumption outlined in Chapter 1. As the driving force increases, the rate of cluster formation increases in a monotonic fashion. The clustering behavior can be well described

by Equation 4.1, which describes the number of clusters as a function of the time and number of particles in the system:

$$\boldsymbol{N \propto N_0 * t^m}$$

Equation 4.1

Where N is the total number of clusters at a given time t (a monomer is considered as a cluster of one particle), N_0 is the number of particles in the system (determined by the coverage), and m is a scaling exponent for the cluster number with respect to time, which will be discussed at greater length in Chapter 5.

As particle aggregation into clusters proceeds, the cluster size is an important metric used in conjunction with total cluster number to determine uniformity of clustering behavior. The size of each cluster is calculated for this section as the total number of particles within the cluster. Figure 4.4 gives a depiction of the cluster size distribution $P(S)$ and the mean cluster size $\bar{S}$, where S represents the number of particles within an individual cluster. The fitting lines for determining the time evolution of $\bar{S}$ and the peak of the probability distribution are given, as well as demonstrating how the exponents can be used to scale the cluster size distributions to a single curve. From this it can be seen that, for a given section of the curve, the clustering behavior can be well represented by the simple power law given in Equation 4.1. This form of scaling law for diffusion-limited cluster aggregation and growth has been shown to fit quite well in previous literature [425, 426]. This power law allows for not only the instantaneous but also dynamic behavior of such a clustering process to be well documented and characterized for future reference. This scaling is based upon the stochastic nature of clustering, which smooths out for large

sample sizes. Figure 4.5 demonstrates power law behavior and how division by the scaling exponent allows the graphs to collapse to a single curve for $\theta = 20\%$, $F = 0.5$, $465\tau < t < 6{,}000\tau$. The lower number of clusters at this time causes more obvious scattering from the fit when compared to that seen at lower time intervals.

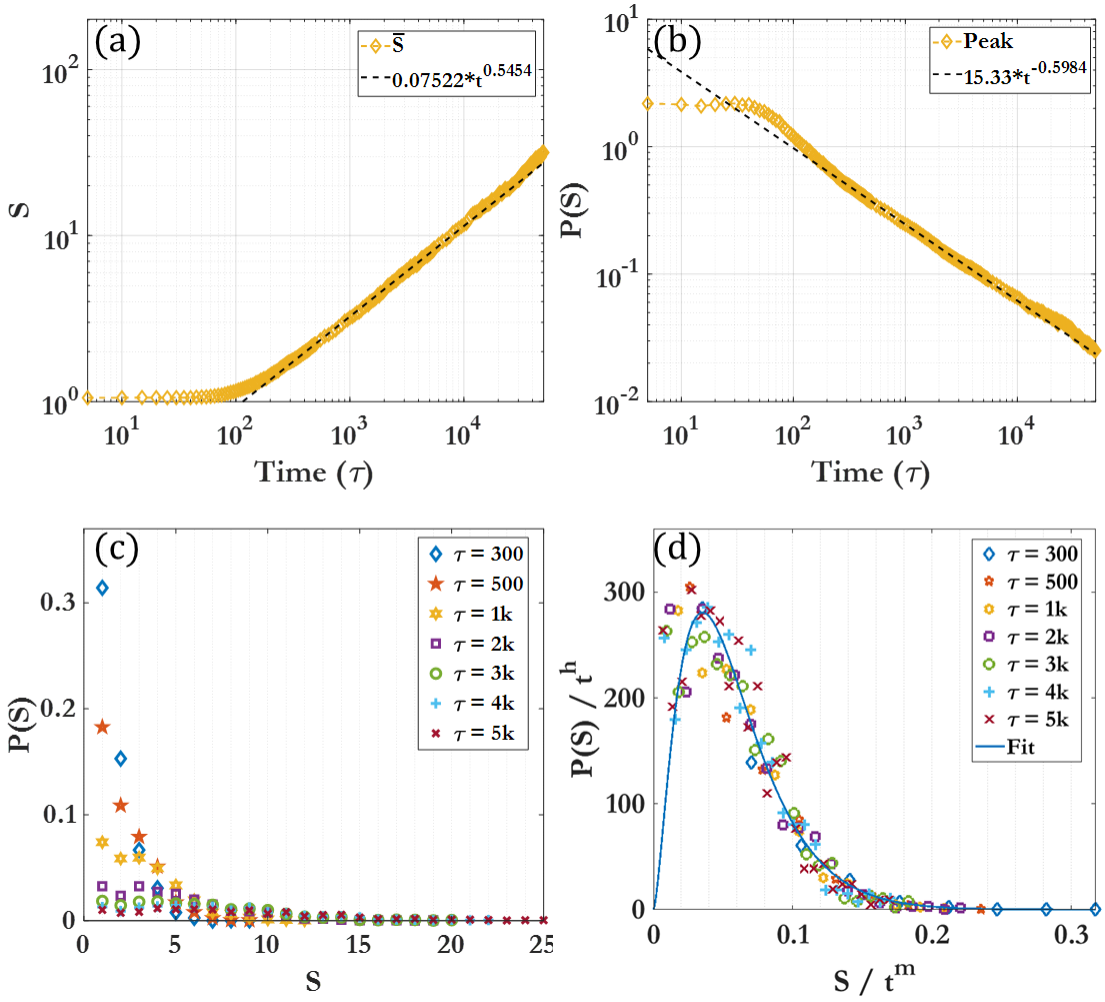

Figure 4.4: Cluster size distributions over time.

Case is for $\theta = 5\%$, $F = 0$. (a) The mean of the cluster number distribution, with fitting line for Region II; (b) the peak height of the cluster number distribution, with fitting line

for Region II. (c) The cluster size distributions for $t = 300\ \tau$ to $t = 5{,}000\ \tau$. (d) The same cluster size distribution after being scaled by the scaling function for the pertinent region.

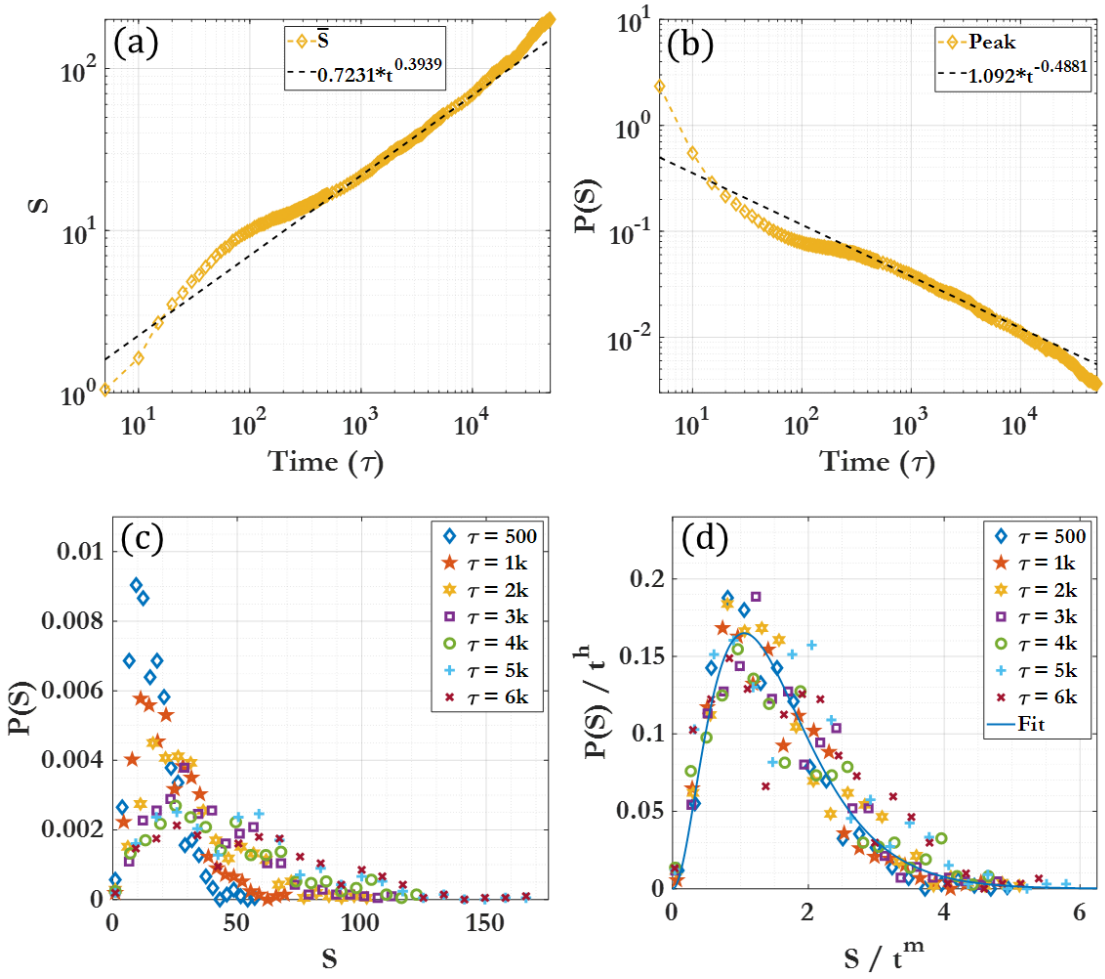

Figure 4.5: Cluster size probability distribution.

Labeled Region 4 for θ = 20%, F = 0.5. (a) Mean size fitting, (b) size peak probability fitting, (c) cluster sizes for Region 4, (d) scaled cluster sizes for Region 4.

The probability distribution of the cluster size can be fit well by the gamma distribution, as previously discussed in Chapter 3. Figure 4.6 demonstrates a fitting of the

gamma distribution to the cluster size over time for various θ and F. The fitting can be plotted as parameters a and b, and from this the skew and the mean can be easily seen. The mean of the distribution $\bar{S} = ab$, and the skew is inversely proportional to the shape $\frac{2}{\sqrt{a}}$. From Figure 4.6 it can be seen that the flattening, or reduced clustering, of the middle region is quite apparent in the plots of the scale parameter, which is closely linked with cluster size.

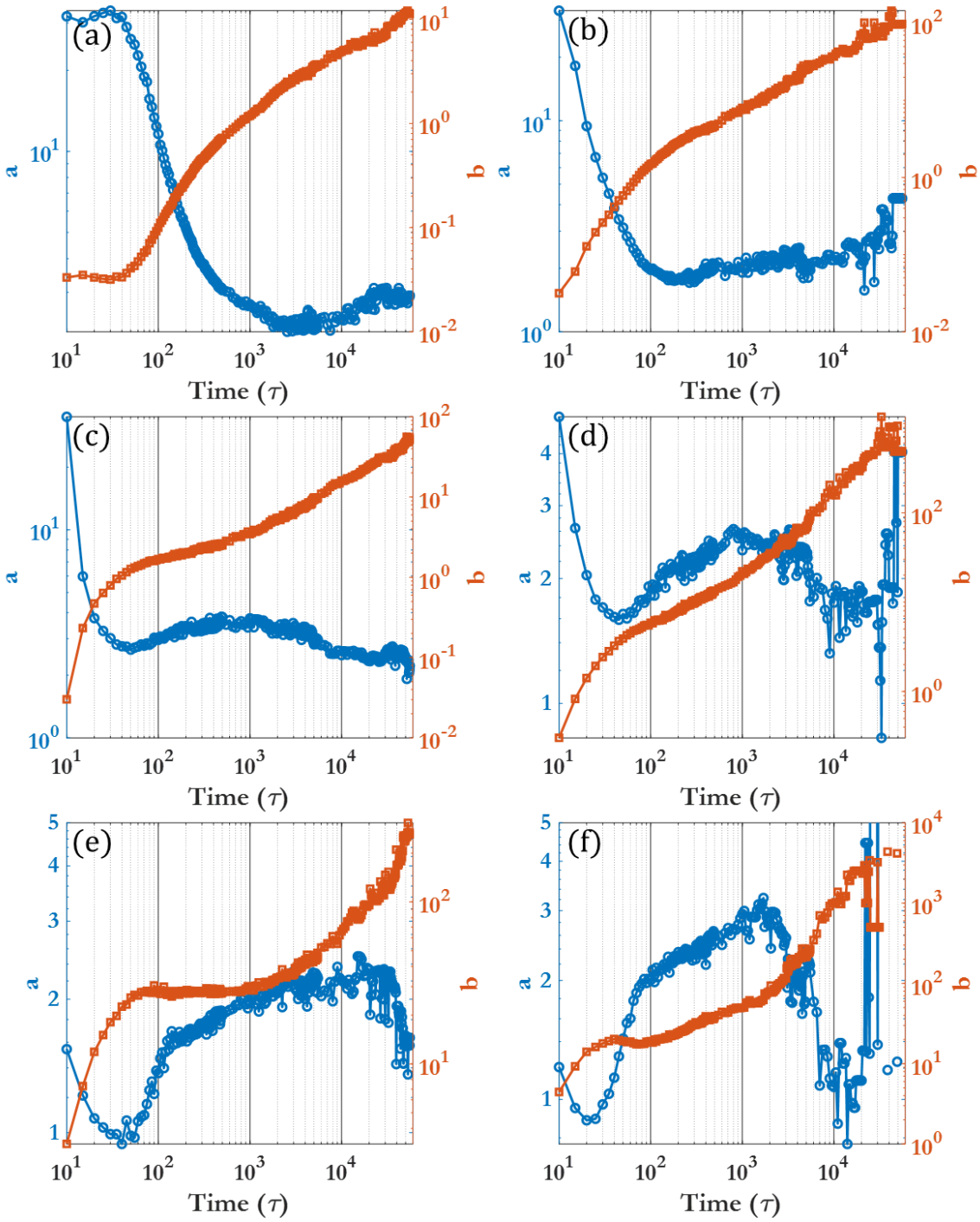

Figure 4.6: Gamma function plots.

Gamma function parameters a (shape) and b (scale) parameters over time for (a) $\theta = 5\%, F = 0$, (b) $\theta = 5\%, F = 5$; (c) $\theta = 15\%, F = 0$, (d) $\theta = 15\%, F = 5$; (e) $\theta = 30\%, F = 0$, (f) $\theta = 30\%, F = 5$. The solid vertical lines mark the transition between regions.

Another aspect of clustering behavior, along with cluster size and number, is the physical distribution of the clusters in space. The periodic system can be analyzed as discussed in Chapter 3 through fast Fourier transformation (FFT) of snapshots of the system taken in the x-y plane, as the quasi-2D nature of this system allows for ease of spatial analysis. Figure 4.7(a) shows a representative 2D-fast Fourier transform (FFT) of the clustering image in Figure 4.7(b). The circular average of the power of the FFT transform was calculated, and the k-space power spectra was plotted as seen in Figure 4.7 (c, d). To find the representative length k_0, a Gaussian curve was fit to the first peak for every snapshot, and k_0 and the power spectra $PSD(k_0)$ were found and plotted as shown in Figure 4.8. Figure 4.8 demonstrates that, for each given dynamic region (here, Region II for $\theta = 5\%$, $F = 0$) a fitting power law allows for scaling of the FFT spectra by the power law exponent, which allows for all snapshot spectra over the given region to collapse to a single curve after scaling. Figure 4.9 shows a representative FFT transformation of an image of clustering, as well as the circularly averaged power profile for $\theta = 15\%$, $F = 0$, $t = 5000\tau$.

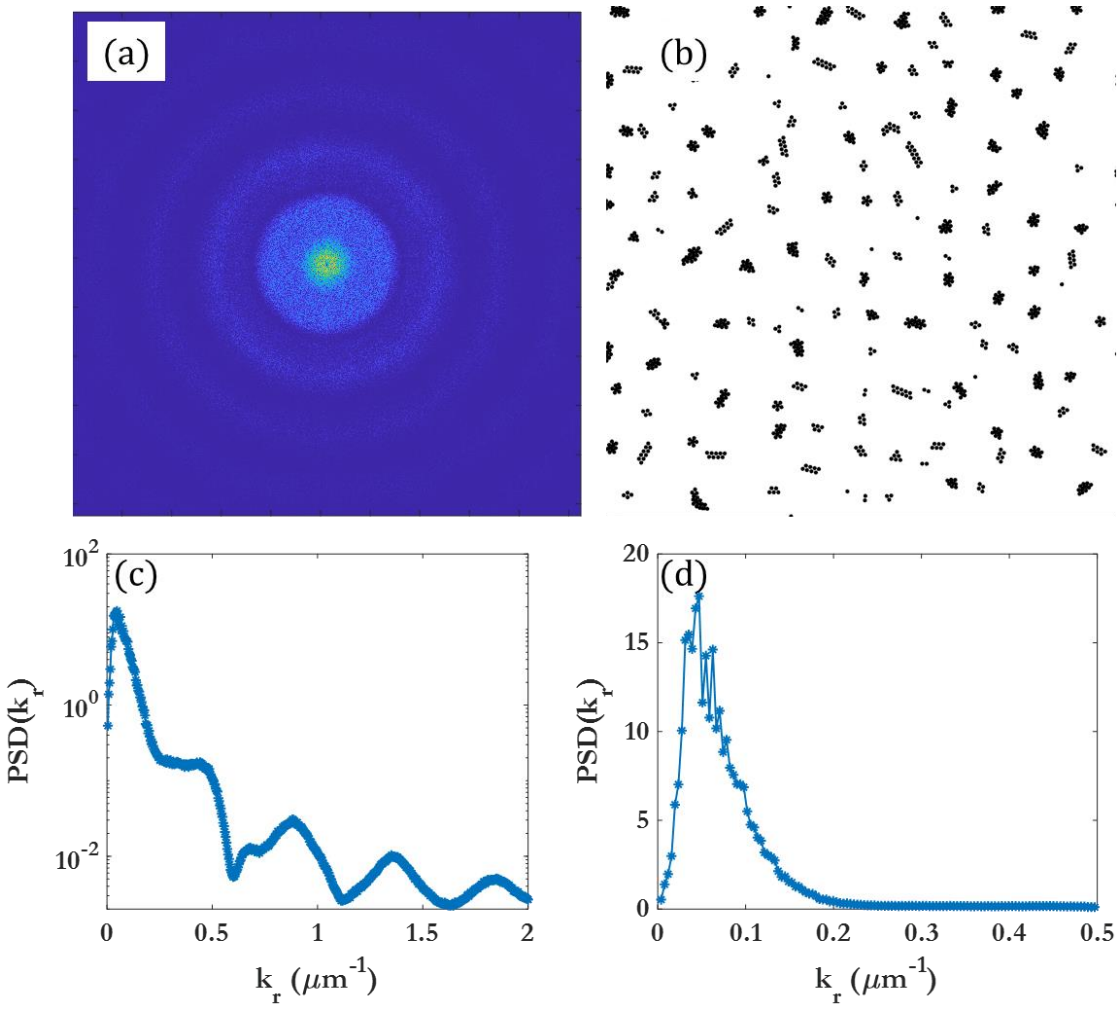

Figure 4.7: Cluster spatial distributions.

(a) FFT of image in (b) for $\theta = 5\%$, $F = 0$, $t = 5000\,\tau$; (c) and (d) show the circularly averaged intensity profile plotted at different scales.

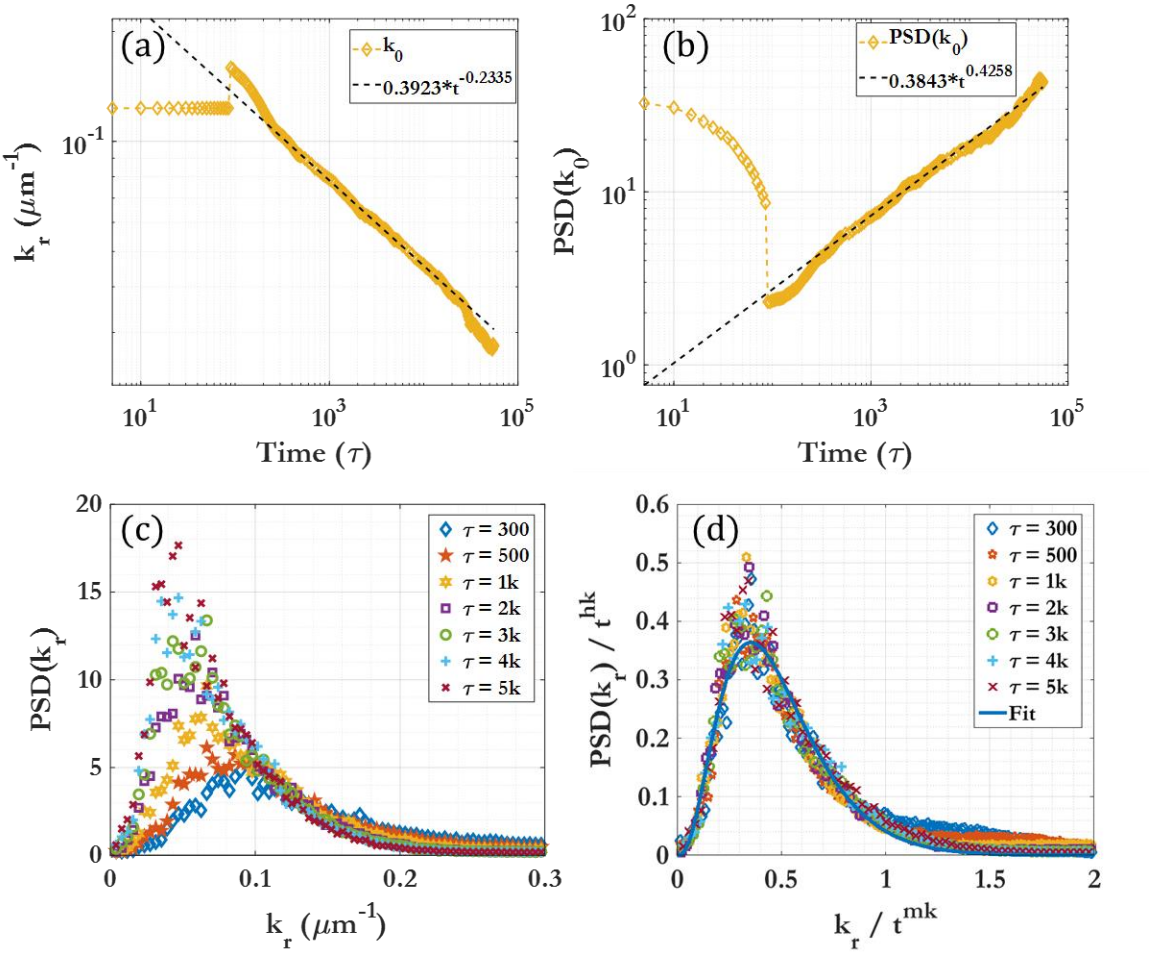

Figure 4.8: 2D circularly averaged FFT spectra over time.

Case is for $\theta = 5\%$, $F = 0$. (a) The FFT power spectra peak center for k_0, with fitting line for Region 2; (b) the power spectra peak intensity of k_0, with fitting line for Region 2. (c) The FFT power spectra for $t = 300\,\tau$ to $t = 5{,}000\,\tau$. (d) The same spectra after being scaled by the scaling function for the pertinent region.

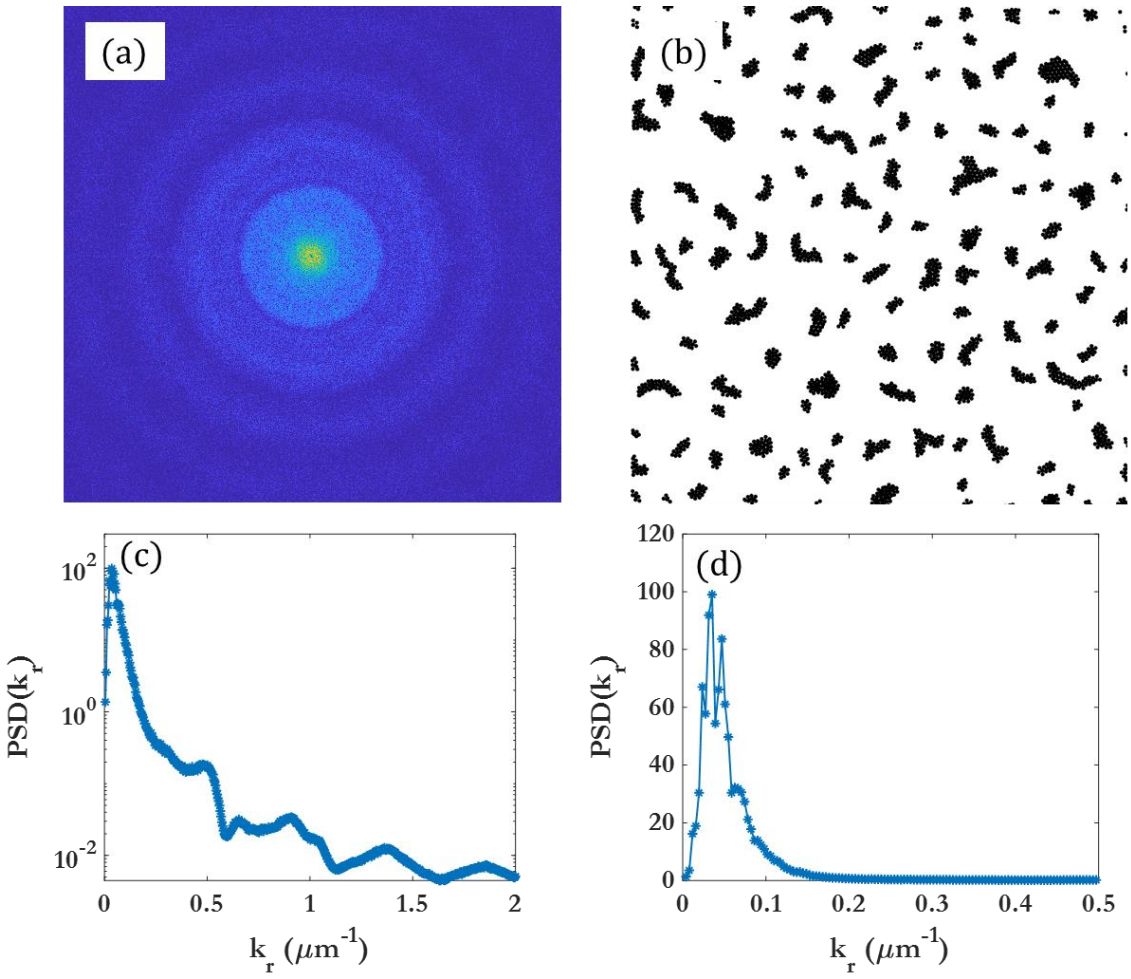

Figure 4.9: Cluster spatial distribution.

(a) FFT of image in (b) for θ = 15%, F =0, t = 5000 τ (c) and (d) show the circularly averaged intensity profile.

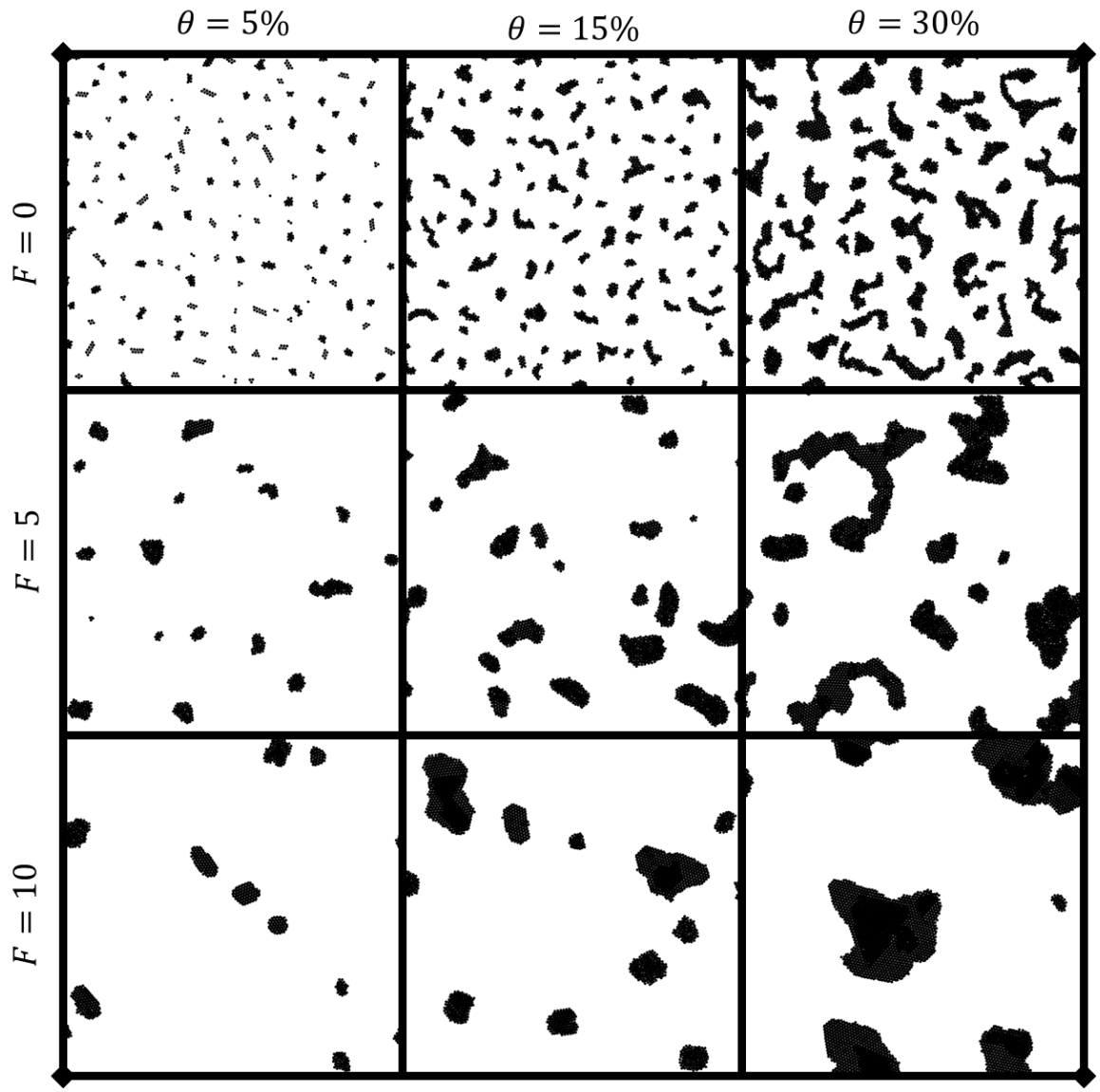

Figure 4.10: Snapshots taken at τ = 5,000.

Figure 4.10 shows representative snapshots of low, medium, and high coverage and force, at a chosen timestep of 5000τ, to demonstrate how the snapshots used for FFT analysis change as a function of these parameters. After this much time, the clustering has proceeded towards fewer, smaller clusters across each of the cases. However, it can be seen

still that the spatial distribution of clusters is relatively uniform, and this is the case for each of the 5 independent runs for every variation of F and θ. Due to this spatial uniformity, the FFT analysis used can be reasonably relied upon to determine the average intercluster spacing distance, as portrayed by Figure 4.7 and Figure 4.8. This intercluster spacing distance is represented by its inverse, k_0. It can be seen that higher coverage and driving force both accelerate the rate of clustering. At higher θ, there are more particles in solution, and thus the rate of collision and clustering is increased. For higher F, the effective diffusion constant for the colloidal particles is higher, and thus clustering proceeds following a scaling law with a higher exponent. Both FFT spatial distribution and clustering number can be well represented by their power law scaling exponents.

4.2. Dynamic Regions

This section presents definitions and descriptions of the different dynamic regions observed during clustering, from both the evolution of the number of clusters, cluster size distribution, as well as the spatial analyses which are discussed in detail in the preceding sections. Figure 4.11 shows the power law curves fitting the different dynamic regions, and their intersection is termed as the critical time for the distinction of regions. As seen in Figure 4.11, there are only two distinct dynamic regions for $\theta = 5\%$ and 10%, but for $\theta = 15 - 30\%$, four distinct dynamic regions occur, each of which follow the power law given by Equation 4.1.

Table 4.1 briefly describes the different dynamic regions, with a detailed description as follows: The first dynamic region, Region I, is pre-clustering, where the

average cluster size is approximately one (monomer region). It can be considered for Region I that the scaling exponent is 0 for all cases, as there is no functional change to the system. As the coverage density grows higher, the time for this region grows shorter due to the decrease in inter-bead spacing in the initial configuration. The length of Region I also decreases in time as the driving force F increases, due to the increased average velocity of the active particles. During Region I, effectively no clustering can be seen, this pre-clustering region can be considered as the preliminary stage where the average cluster size is effectively zero. This region can be seen in Figure 4.11(a) at $t < 100\tau$, or in the initial stages of Figure 4.12(c). Region I becomes vanishingly small as the coverage or the driving force increases, due to the more rapid initiation of clustering at higher particle densities and velocities (Figure 4.12).

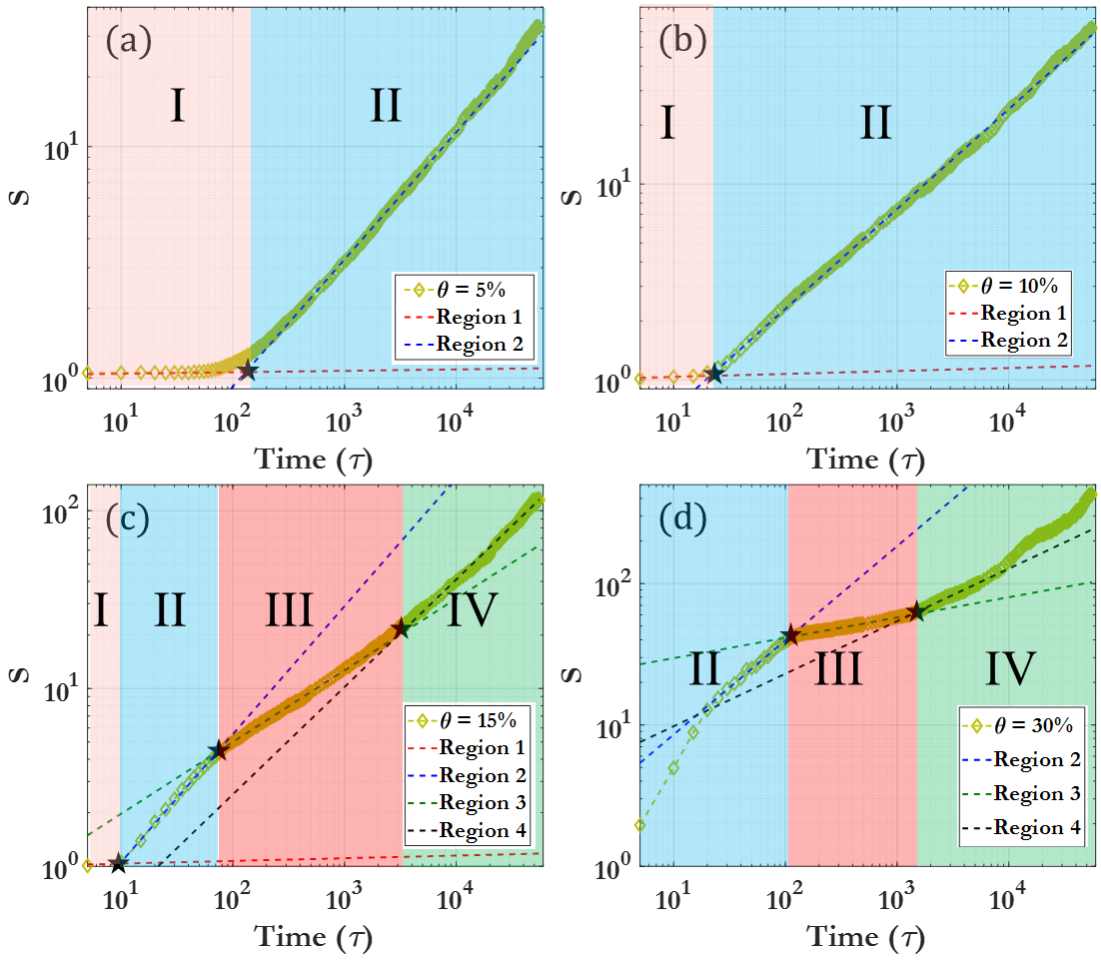

Figure 4.11: Dynamic Regions.

Demonstration of fitting curves for the average cluster size $\bar{S}$ and the associated different dynamic regions for (a) $\theta = 5\%$, (b) $\theta = 10\%$, (c) $\theta = 15\%$, and (d) $\theta = 30\%$.

Table 4.1: Different dynamic regions

Region 1	Effectively no clustering seen	$\theta = 5 - 30\%$
Region 2	Initial rapid clustering	$\theta = 5 - 30\%$
Region 3	Marked slowing of clustering	$\theta = 15 - 30\%$
Region 4	Long-time clustering behavior	$\theta = 15 - 30\%$

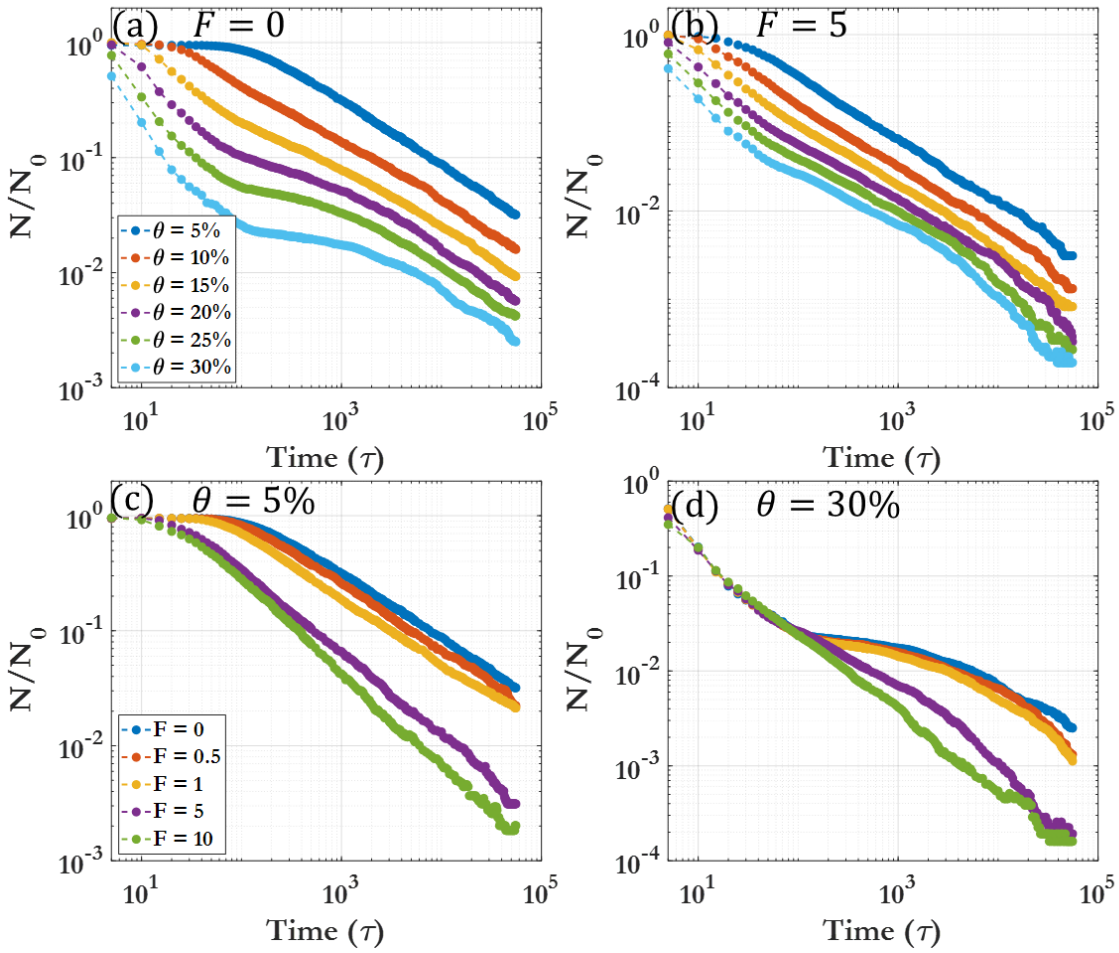

Figure 4.12: Normalized cluster number.

(a) $F = 0$, (b) $F = 5$, (c) $\theta = 5\%$, (d) $\theta = 30\%$. Each case is an average of five runs.

Region II can be considered as the initial clustering behavior, and this region dominates for $\theta = 5 - 10\%$. As seen in Figure 4.12(d), the driving force F has minimal effect on the clustering behavior of this region at higher coverage densities. Region III demonstrates a marked slowing of clustering, especially prominent at higher θ and lower F. This region is characterized by larger clusters, and a near-disappearance of the monomer phase, as seen in the 500 τ snapshots given in Figure 4.2. At very large driving forces, this

region becomes far less prominent. The final region is Region IV, the long-time clustering behavior. The clustering here is comparable to that seen in Region II, as discussed below, and this region is characterized by large clusters flocculating towards the limit of one single cluster within the system. Figure 4.13displays a 3D representation of the different dynamic regions, and the critical time separating them, as a function of both driving force F and coverage θ. It can be seen that the transition between Region I and Region II is smooth and monotonic across all F and θ; however, there is much greater variation in the transition between Region III and Region IV. Table 4.2 gives a detailed breakdown of the critical times for the transitions between dynamic regions. Figure 4.14 demonstrates that, for each given dynamic region (represented by Region IV, $\theta = 15\%$ and $F = 0$) a fitting power law allows for scaling of the FFT spectra by the power law exponent, which allows for all snapshot FFT spectra over the given region to collapse to a single curve.

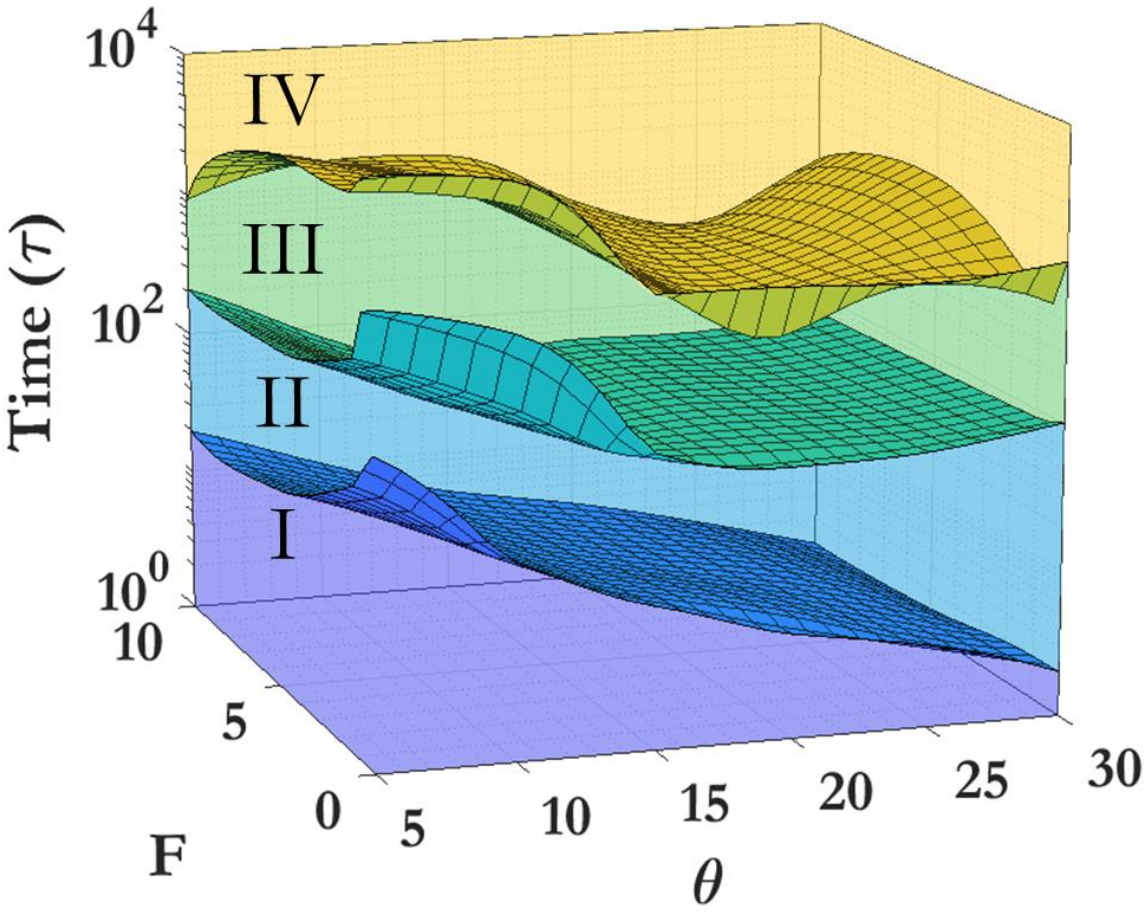

Figure 4.13: Parameter space of Regions I, II, III, and IV.

Here are the Regions as parameter spaces plotted as filled colored volumes, and the transition times between them (plotted as gridded surfaces), as a function of both coverage (θ) and driving force (F). The surfaces have been smoothed between discrete points using a modified cubic spline interpolation.

Table 4.2: Critical time for region transitions (t_1, t_2, t_3).

	$F = 0$	$F = 0.5$	$F = 1$	$F = 5$	$F = 10$
$\theta = 05\%$	129.4	93.82	65.05	23.88	19.52
$\theta = 10\%$	22.05	20.71	18.42	11.83	9.78
$\theta = 15\%$	9.49 99.93 1,114	9.17 84.58 1,186	8.72 75.60 1,207	6.44 55.16 1,180	5.21 44.21 1,519
$\theta = 20\%$	5.19 69.41 1,094	5.09 65.74 464.3	5.56 70.78 497.2	4.22 67.26 501.7	3.61 60.06 636.7
$\theta = 25\%$	3.66 75.41 1,014	3.15 72.80 901.6	3.11 72.29 803.6	2.88 64.64 687.7	2.25 59.54 383.2
$\theta = 30\%$	2.01 102.2 1,234	1.99 91.96 589.4	1.98 88.46 623.5	1.49 80.81 1,813	1.31 73.54 1,013

Units are in τ.

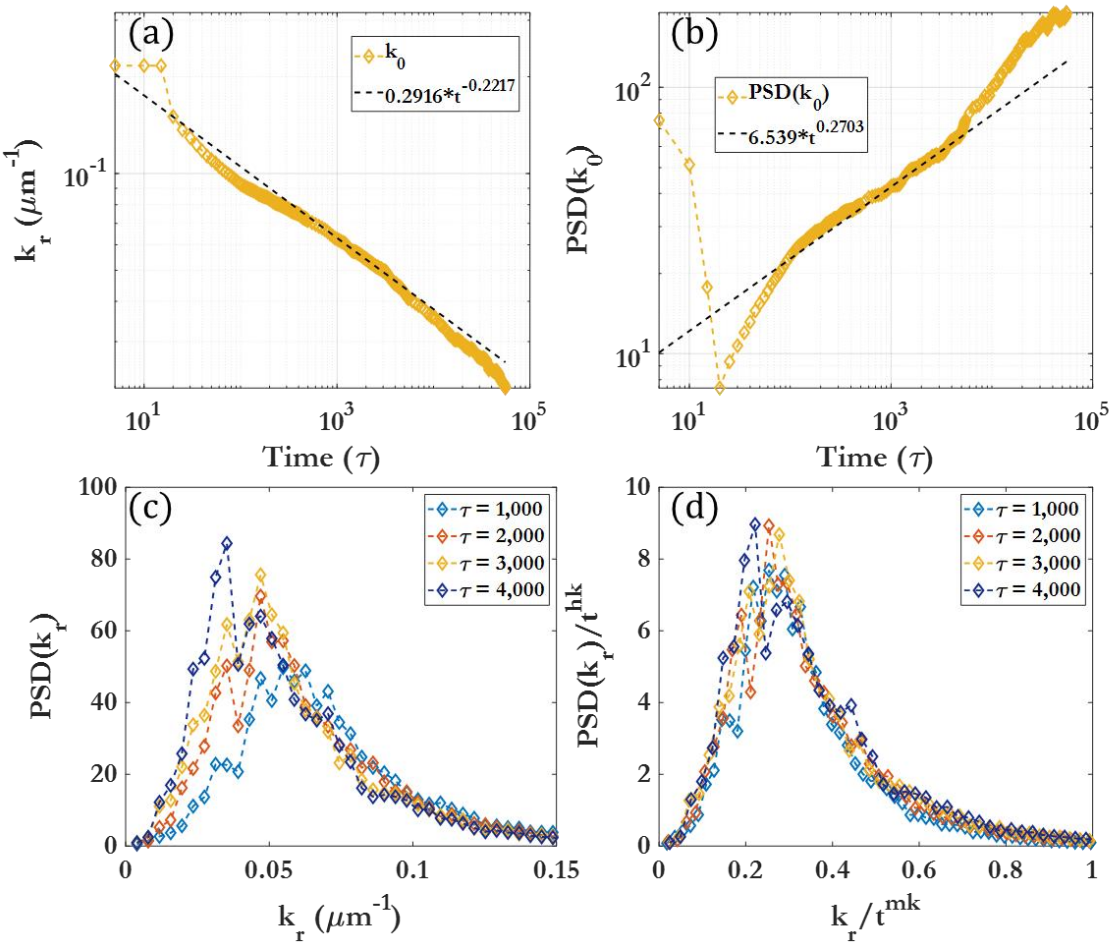

Figure 4.14: 2D circularly averaged FFT spectra over time.

Case is for θ = 15%, F =0. (a) The peak center for k_0, with fitting line for Region 4; (b) the peak intensity of k_0, with fitting line for Region 4. (c) The FFT spectra for t = 1,000 τ to t = 4,000 τ. (d) The same spectra after being scaled by the scaling function for the pertinent region.

To give a comparison with the clustering behavior demonstrated for $\theta = 15\%$ as given in Figure 4.1, representative snapshots of clustering over time were taken and given for the remainder of the coverage parameters, and displayed in the following figures.

Figure 4.15 shows an overview of the clustering process over time for $\theta = 5\%$, for various driving forces. Figure 4.16 shows an overview of the clustering process over time for $\theta = 10\%$, for various driving forces. Figure 4.17 shows an overview of the clustering process over time for $\theta = 20\%$, for various driving forces. Figure 4.18 shows an overview of the clustering process over time for $\theta = 25\%$, for various driving forces. Figure 4.19 shows an overview of the clustering process over time for $\theta = 30\%$, for various driving forces. Together these figures show representative clustering behavior evolution over time for each coverage θ and driving force F, in order to give a full overview of the procession of the clustering process. Chapter 5 will go in-depth into the scaling laws and the effects of coverage and driving force on how the clustering behavior proceeds over time.

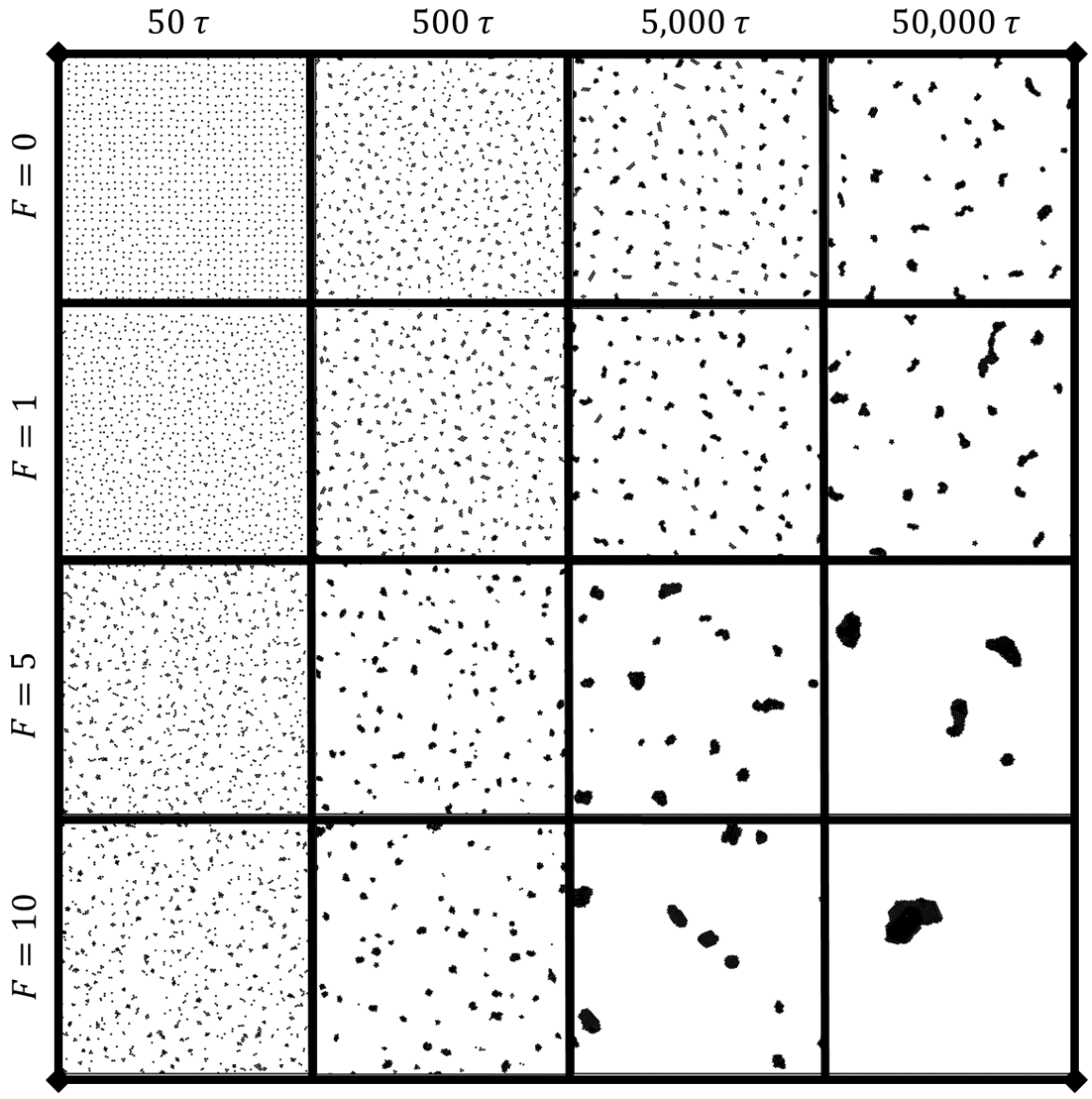

Figure 4.15: Clustering behavior over time for θ = 5%.

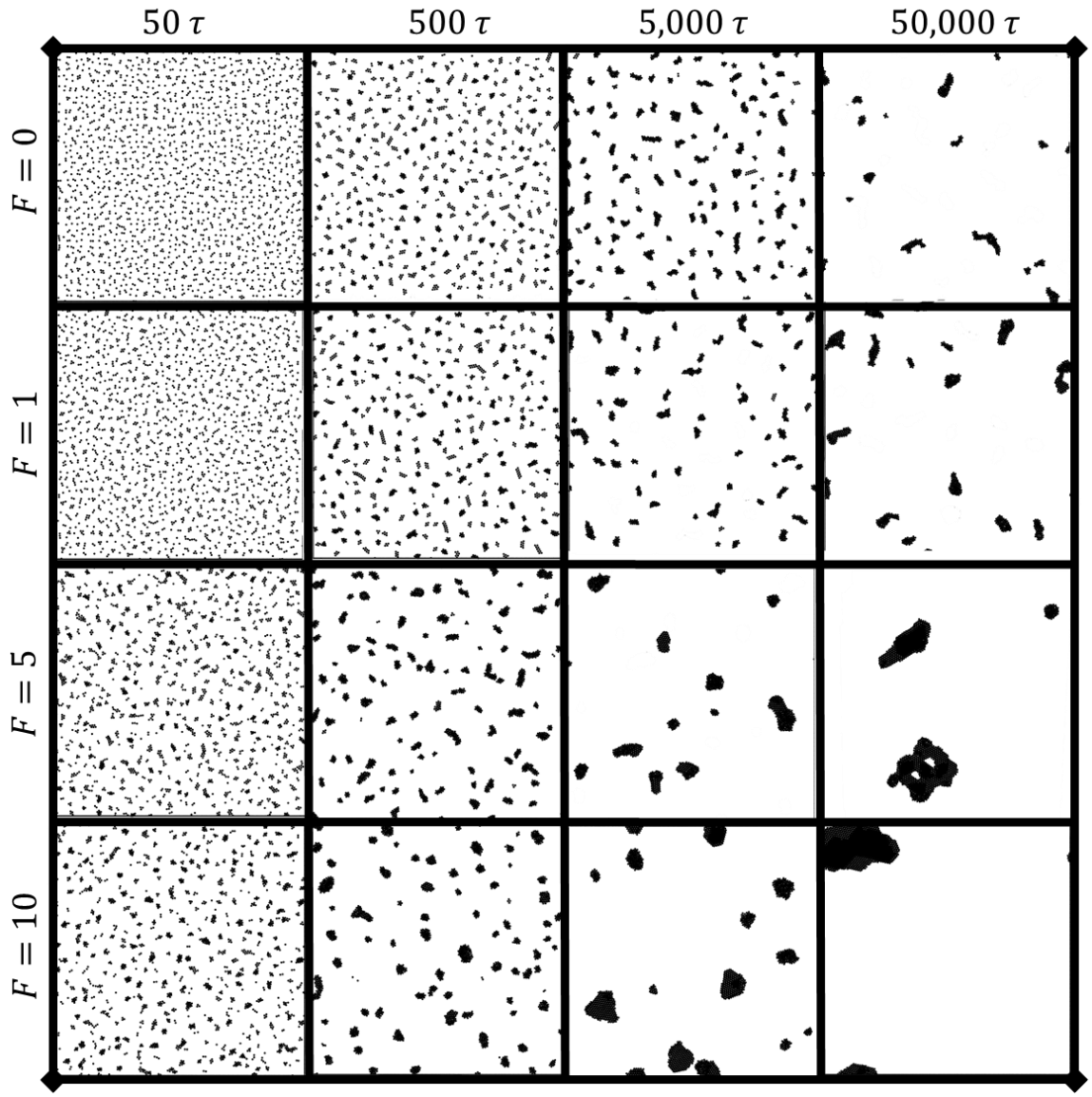

Figure 4.16: Clustering behavior over time for θ = 10%.

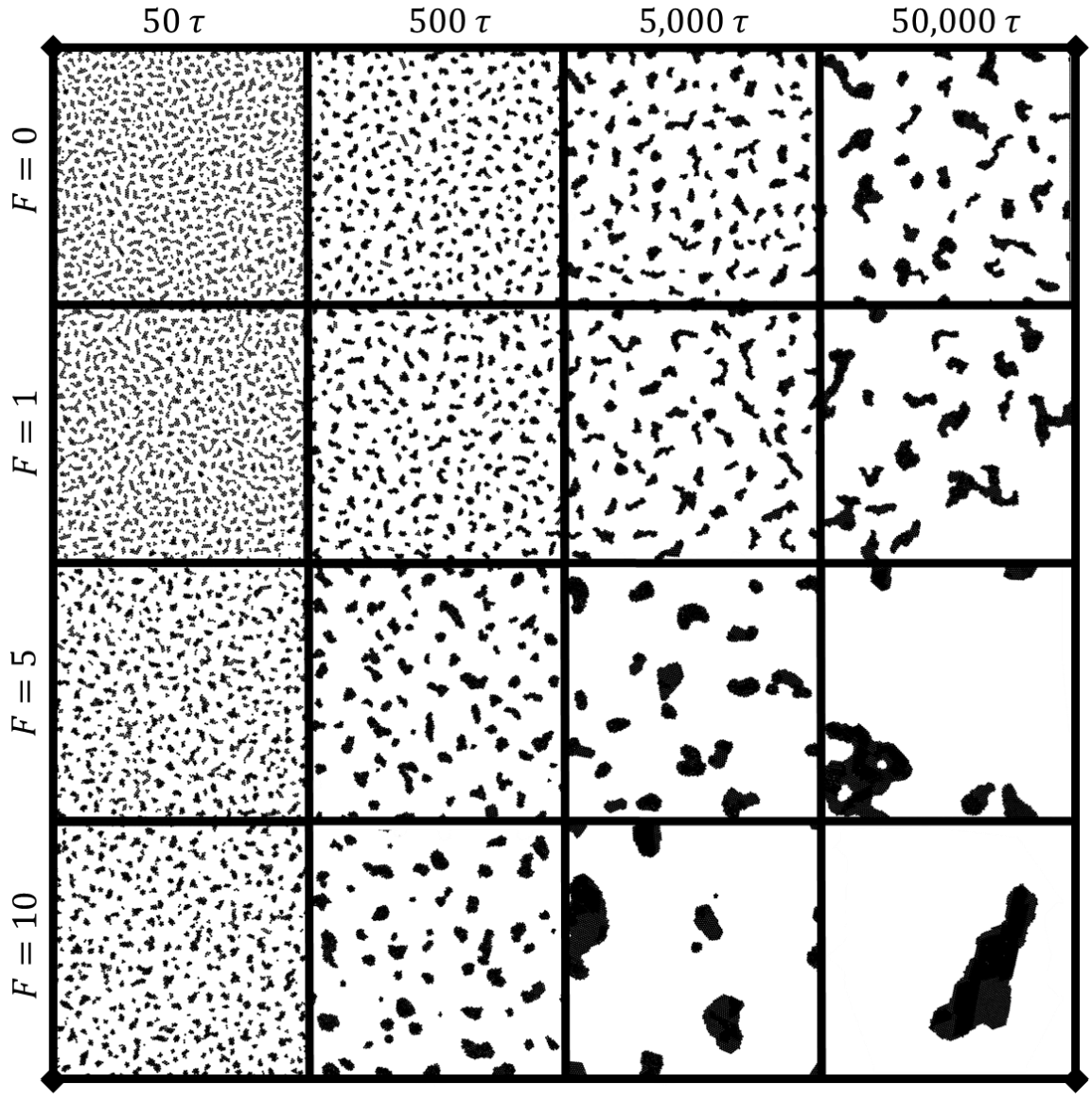

Figure 4.17: Clustering behavior over time for θ = 20%.

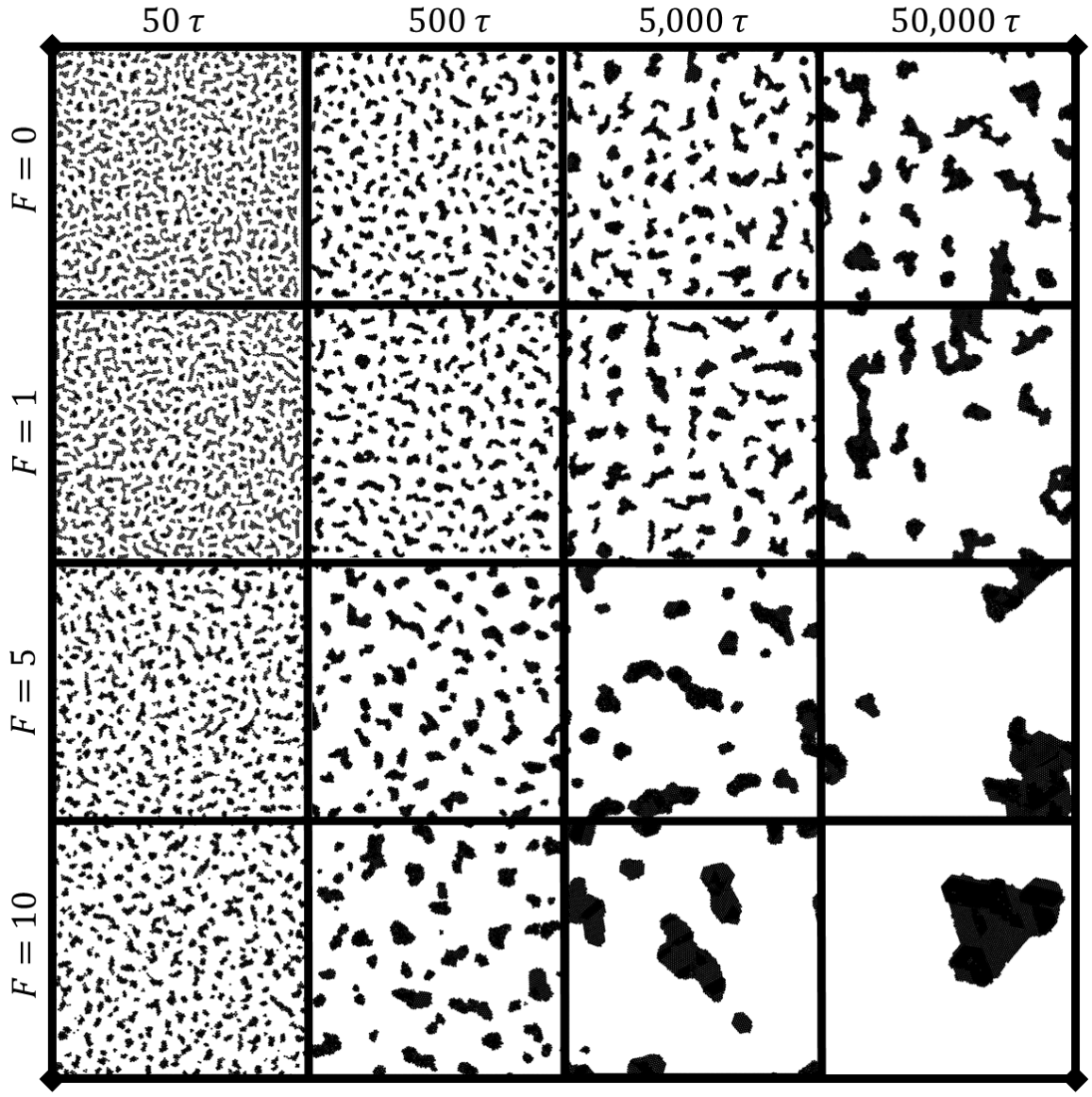

Figure 4.18: Clustering behavior over time for θ = 25%.

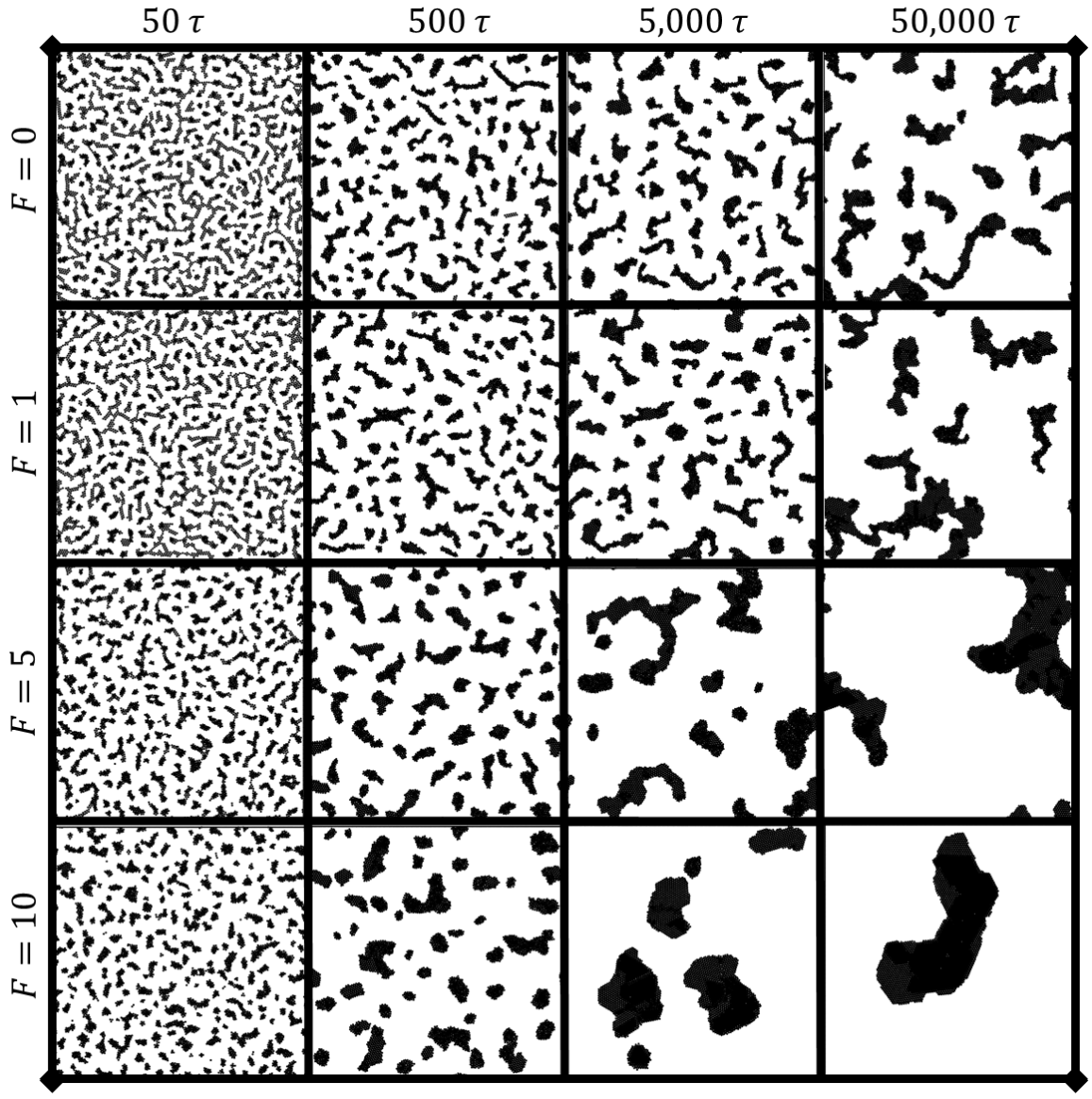

Figure 4.19: Clustering behavior over time for θ = 30%.

4.3. Limitations

The pre-clustering of Region I, defined as the individually separated particles prior to clustering, was not suitable for FFT calculation as demonstrated by Figure 4.20, wherein the initial square-lattice geometrical configuration of particles at setup causes a crystalline

FFT power spectra distribution, and the crystalline peaks disappear as the system evolves to amorphous clustering. In addition to the fact that there is little to no clustering happening during this period, and as such there are no scaling laws for cluster distribution or spacing presented or discussed for the pre-clustering behavior in this work. That is to say, for Dynamic Region I, there are no scaling laws due to the lack of cluster evolution in the system. Due to this, where scaling law exponents are reported for this work, there are no exponents given for Region I, where clustering is assumed to be nonexistent.

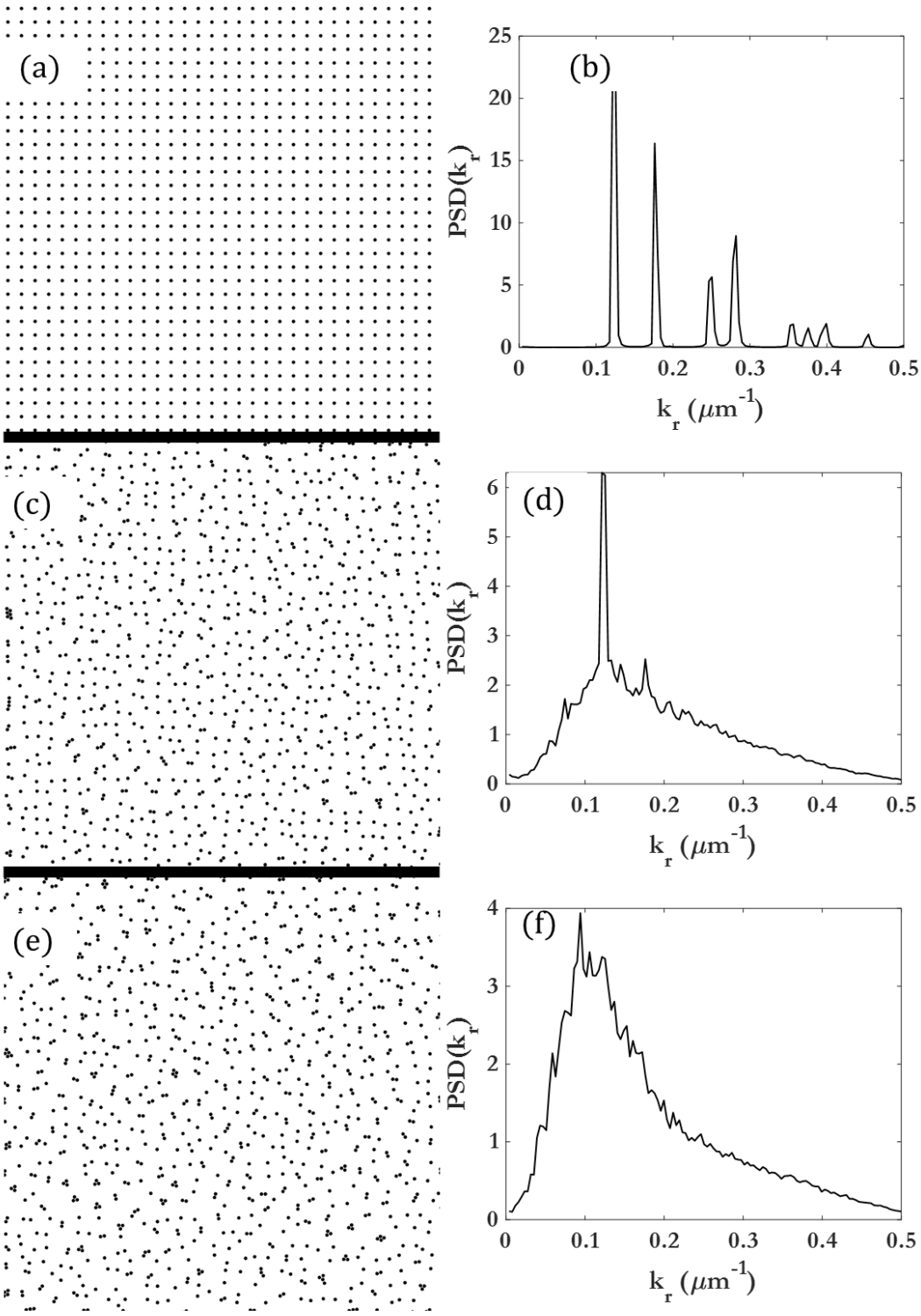

Figure 4.20: FFT peaks during pre-clustering.

(a, c, e) Cluster distribution and (b, d, e) FFT power spectra showing presence and disappearance of crystalline peaks due to the initial setup geometry for θ = 5%, F = 0 for (a, b) τ = 0, (c, d) τ = 100, (e, f) τ = 200.

The applied driving forces above $F = 10$ were strong enough that the assumption of diffusion-limited colloidal aggregation no longer holds. As can be seen in Figure 4.21, as the applied driving force increments for $10 < F < 20$, the driving force is large enough to overcome the attractive potential between CGMD beads, leading to a breakdown of clustering behavior. Once the driving force is able to overcome the attractive interaction between colloidal particles, the diffusion-limited colloidal aggregation theory no longer holds, as active particles have a certain probability to either fail to form a cluster upon collision, or else detach from a cluster which they were previously part of. This result implies that there is a balance between the interaction potential and the driving force of an active particle, such that clustering behavior is a metric that is influenced not only by coverage and surface interaction potential, as in passive clustering, but also is heavily influenced by the driving force of the active matter.

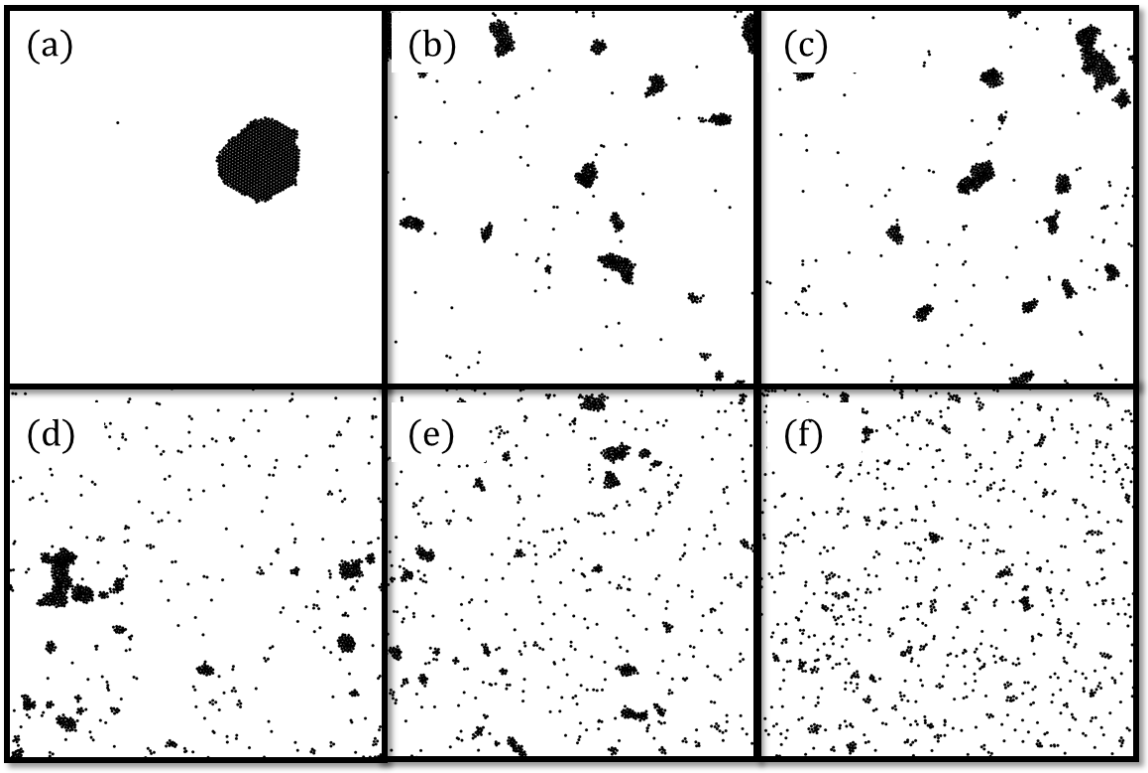

Figure 4.21: Reversible clustering at high driving forces.

For the snapshots shown, the applied driving forces in the simulation are (a) $F = 12$*, (b)* $F = 13$*, (c)* $F = 14$*, (d)* $F = 15$*, (e)* $F = 16$*, (f)* $F = 17$*. For all cases* $\theta = 5\%$ *and* $t = 50{,}000\tau$.

Of course, due to the complex nature of these simulations, there is a limit to the size and time scale which is reachable with current resources. Due to this, the studies performed and described in this work only reach a limited parameter space. However, the results presented in this dissertation may be used to inform and guide future works in order to test and validate them. The particles here were uncharged, and the solvent viscosity was that of water. The fluid parameters and the interaction potential between beads are very impornat parameters for clustering dynamics, and as such there is still much research to be carried

out in order to better flesh out current understanding of this field. This work does not consider chemical species or reactions, and as such is not suitable for the modeling of chemically propelled micromotors.

5. SCALING LAWS AND RELATIONSHIPS

5.1. Coverage-based Scaling

One of the most important parameters for the clustering of colloidal particles is how densely packed they are, represented in this work by the coverage, θ. The clearly different behaviors seen in the previous section for low and high coverages has much to do with the increased particle proximity at the beginning of the simulation, as well as the overall larger and more numerous clusters seen as time proceeds. Here we take the qualitative behavior discussed in the previous section and use the fitting exponents to describe the behavior, which can be quantified and scaled. For each given dynamic Region except Region I (as defined in Chapter 4), the power law fitting exponent for Equation 4.1 is given in Table 5.1. Different clustering evolution behaviors occur for various F and θ. The clustering coverage θ, has a pronounced effect on the shape of the cluster number curve, with simple clustering behavior observed for low coverage ($\theta = 5, 10\%$), and more complex time evolution of the cluster number for higher coverage ($\theta > 10\%$). The simple clustering behavior means that there are only two clear Dynamic Regions, Region I (pre-clustering), and Region II (initial clustering). Due to the active particles being spaced out in the initial setup at the low coverages of $\theta = 5\%$ and $\theta = 10\%$), Region I is extended, and clustering does not initiate immediately, even at higher applied driving forces.

Table 5.1: Dynamic region scaling exponent m for Regions II-IV, respectively.

	$F = 0$	$F = 0.5$	$F = 1$	$F = 5$	$F = 10$
$\theta = 05\%$	0.5454	0.5837	0.5781	0.7252	0.8177
$\theta = 10\%$	0.4867	0.5078	0.5587	0.6969	0.8226
$\theta = 15\%$	0.6388	0.6484	0.7126	0.8629	0.9273
	0.4065	0.4115	0.4859	0.6931	0.7962
	0.4824	0.5433	0.5779	0.7468	0.8922
$\theta = 20\%$	0.6840	0.7057	0.7327	0.8302	0.8711
	0.3039	0.3100	0.3595	0.6246	0.8389
	0.4793	0.4939	0.5018	0.7161	0.8896
$\theta = 25\%$	0.6682	0.6946	0.7227	0.7740	0.8778
	0.2197	0.2379	0.2886	0.6132	0.7971
	0.5359	0.4422	0.5107	0.6647	0.9489
$\theta = 30\%$	0.6660	0.7582	0.7302	0.7729	0.8195
	0.1432	0.1323	0.1848	0.6006	0.7693
	0.3621	0.3955	0.4053	0.7583	0.9453

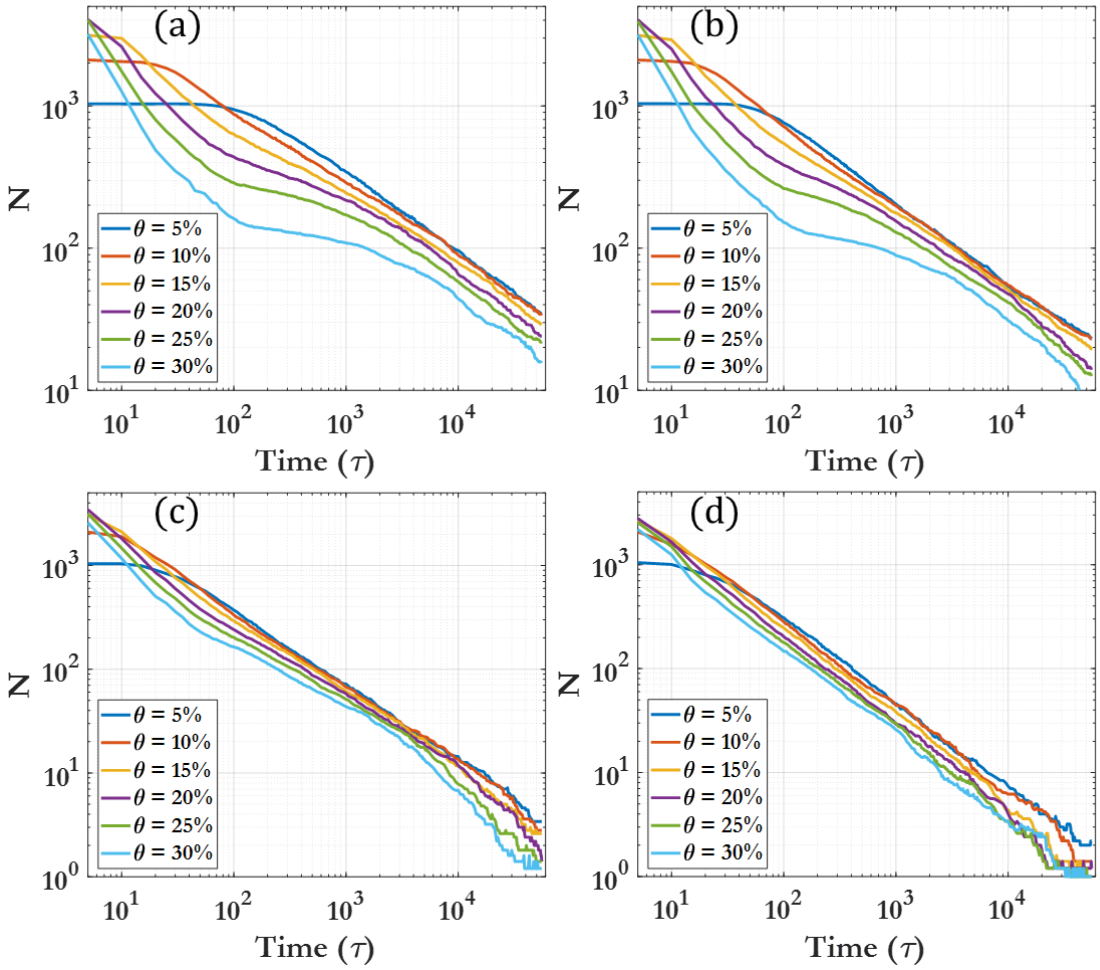

Figure 5.1: Cluster number.

Given are plots for (a) F = 0, (b) F = 1, (c) F = 5, (d) F = 10.

Figure 5.1 shows the absolute cluster number over time for various θ and F (rather than the normalized number shown in Figure 4.12). This visualization helps to highlight the rapid clustering behavior seen at higher θ, the extended Region I dynamic region for lower θ, and also the similarities in long-time behavior ($t > 3000\tau$).

5.2. Force-based Scaling

The addition of a driving force is what differentiates passive particles from active particles. Due to this, it can be inferred that the magnitude of the driving force, given by F, is a key parameter to consider when determining cluster aggregation behavior. Looking at Figure 5.2, which plots the different scaling exponents for the cluster size distribution and 2D cluster spatial distribution power laws across all coverages and driving forces for Region II, it can be seen that within a given region, there is some clear variation in the clustering behavior as a function of F. The differences become more pronounced, however, for Region III and Region IV. As can be seen, driving force F tends to flatten and accelerate the clustering behavior, in line with previous reports of driving force causing an increased effective diffusion coefficient for active particles. Figure 5.3 demonstrates the differences between cluster size scaling exponents, while Figure 5.4 demonstrates the differences between cluster spatial distribution scaling exponents (m_k, h_k), for Regions II, III, and IV for $\theta = 15 - 30\%$. These figures make it easy to see that the scaling exponent for Region II is not heavily affected by the coverage percentage; this early clustering behavior can thus be attributed to diffusion-driven (or enhanced diffusion for $F > 0$) clustering behavior, with less dependence on the density of colloidal particles or micromotors. As θ becomes larger, the scaling exponent for Region III decreases, indicating a marked slowing of the clustering behavior. However, as F increases, the scaling exponent for Region III increases rapidly, to the extent that for $F = 10$, there is no noticeable difference in scaling exponents for different θ; it can be seen in Figure 5.3 that for $F = 10$, Region III, the scaling exponent

m is always near 0.8. The different behaviors seen at low and high driving force represent the difference between passive colloidal clustering and the clustering of active colloidal micromotors; active motion not only increases the effective diffusion coefficient of Brownian particles, but causes a difference in the scaling of clustering times as well.

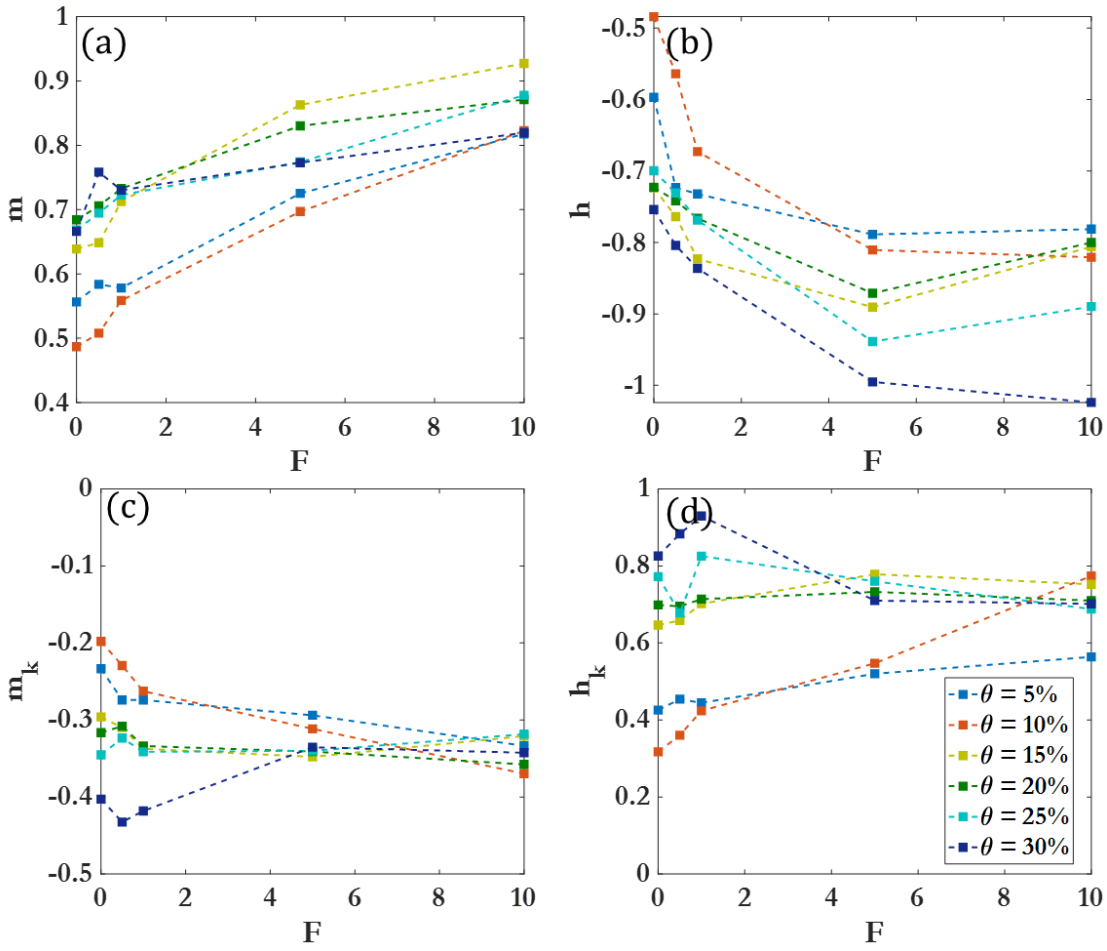

Figure 5.2: Scaling exponents.

Scaling exponents (a) m, (b) h, (c) m_k, and (d) h_k for Region 2 across all θ and F tested.

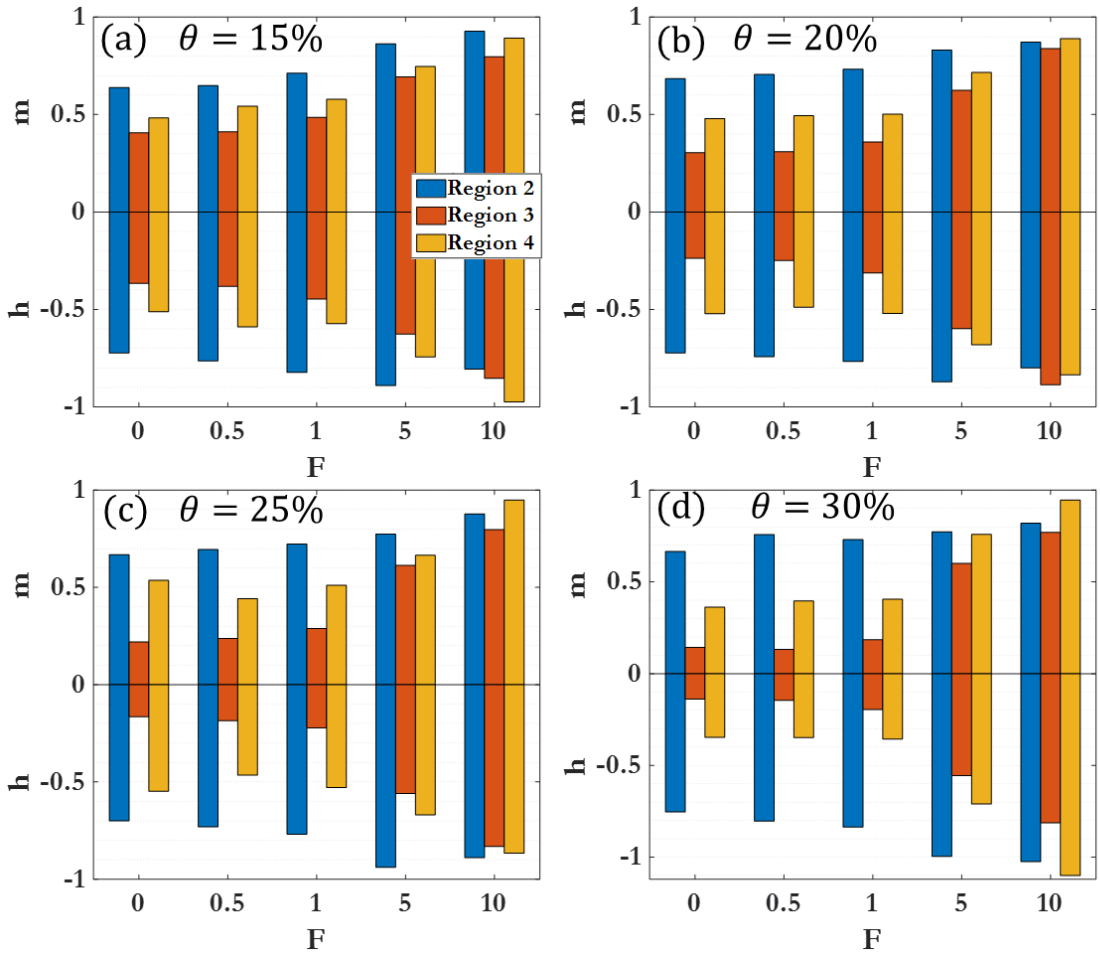

Figure 5.3: Scaling exponents m and h for different dynamic regions.

Scaling exponent results for (a) $\theta = 15\%$ at different F; (b) $\theta = 20\%$ at different F; (c) $\theta = 25\%$ at different F; (d) $\theta = 30\%$ at different F.

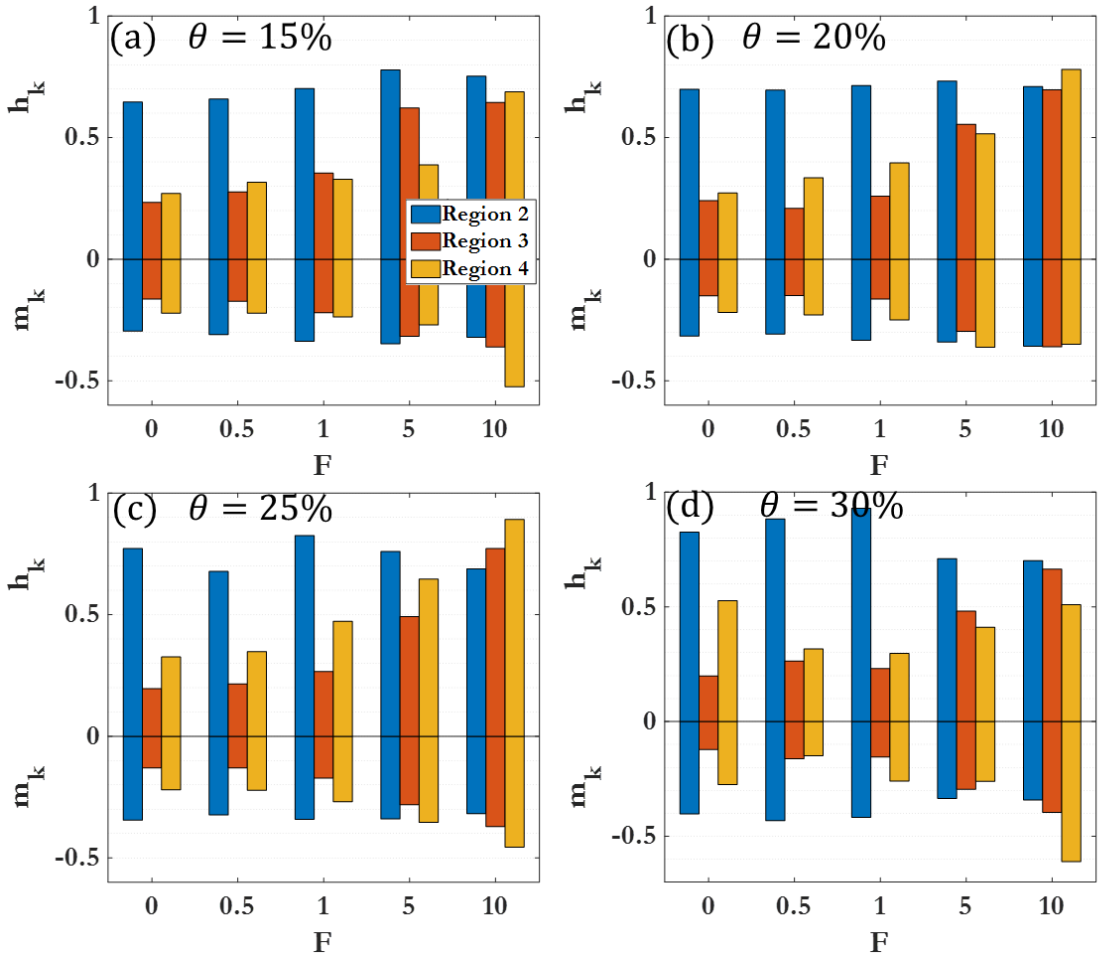

Figure 5.4: Scaling exponents m_k and h_k for different dynamic regions.

Spatial scaling exponent results for (a) $\theta = 15\%$ at different F; (b) $\theta = 20\%$ at different F; (c) $\theta = 25\%$ at different F; (d) $\theta = 30\%$ at different F.

5.3. Potential-based Scaling

For clustering colloidal particles, the level of attraction between discrete particles is a very important parameter which is strongly influenced by multiple factors, including surface potential, charge, and the chemistry of the solution. However, via simulation, it is

much easier to control the interaction between particles. In order to examine the effect of different interbead potentials between CGMD beads, the strength of the van der Waals force (Equation 2.4) was modulated and the clustering results plotted to observe how changing the interaction strength affected the clustering behavior over time.

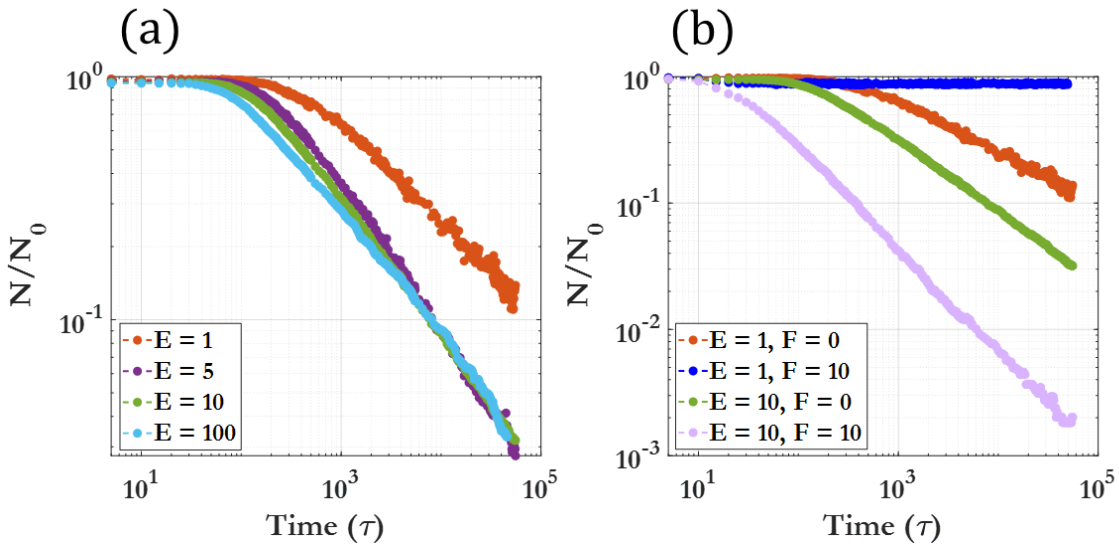

Figure 5.5: Interbead potential vs clustering over time.

For different CGMD potential strengths, (a) demonstrates the effect of potential on clustering with (a) no added force, and (b) with driving force for comparison. For all cases, $\theta = 5\%$. $E = 10$ *is the potential strength used in all other cases presented.*

Figure 5.5 demonstrates that, for a given coverage, once the interbead potential is great enough for clustering to proceed in the diffusion-limited aggregation regime, there is very little change in clustering behavior. That is, if two beads will definitely form a cluster upon contact, the strength of their adhesion is negligible in terms of how clustering is

affected. However, if there is a driving force applied, a weak interbead potential will not prevent beads from separating and de-clustering. These results can be compared with the results from Figure 4.21, which show that for a given potential strength, there is a force threshold where the beads do not remain in a cluster. Due to time and equipment constraints, it was not possible to run a thorough investigation into how potential strength effects clustering behavior. As discussed in Chapter 6, this can be considered to be an open-ended question to be answered by future investigation.

The scaling laws demonstrated here show that, for all driving forces, coverages, and potential strengths presented, diffusion-limited colloidal aggregation can well explain the clustering behaviors observed. For these DLCA-based active particle confined fluid systems, the scaling law presented in Equation 4.1 fits the data completely for the dynamic regions defined in Chapter 4. This scaling law and the scaling law time exponents presented in Table 5.1, and in Figure 5.2, Figure 5.3, and Figure 5.4 allow for an increment into understanding the behavior of colloid-sized active particles and their time-dependent rate of aggregation.

6. CONCLUSIONS

Active systems operate out of equilibrium, which makes it challenging to understand and predict the operation of these systems. However, it is precisely this representative characteristic which allows systems containing active particles to demonstrate unique and diverse behavior. By studying models of active systems, where the parameters are all under control, and comparing them with experimental observations and theory, explanations of the emergent phenomena arising from collective motion of active particles may be developed, in order to allow scientists to make better use of these wondrous tools. For the propelled active particles studied in Chapters 4-6, the particle-fluid interactions and the particle-particle interactions are well-described in accordance with modern theory. Of course, due to the complex nature of these simulations, there is a limit to the size and time scale which is reachable with current resources. Due to this, the studies performed and described in this work only reach a limited parameter space. However, the results presented in this dissertation may be used to inform and guide future works in order to test and validate them. The particles here were uncharged, and the solvent viscosity was that of water. The fluid parameters and the interaction potential between beads are very impornat parameters for clustering dynamics, and as such there is still much research to be carried out in order to better flesh out current understanding of this field. This work does not consider chemical species or reactions, and as such is not suitable for the modeling of chemically propelled micromotors.

To summarize this work, Chapter 1 was on overview and introduction to the state of the art for active particles, including definitions and applications. Chapter 2 gave a more in-depth presentation of recent experimental, theoretical, and simulational works in the field, with special attention given to the DLVO interaction potential and methods of modeling fluids for active matter simulation. Chapter 3 described the simulational model used in the studies presented in this work, along with testing and validation, and the methods of data analysis used. Chapter 4 presented the results of the simulations, and defined dynamic regions of clustering which are observable for the forces and coverages tested. Scaling laws of clustering behavior were given in Chapter 5.

The study of active particles is irrevocably tied to the future of all scientific fields, especially those pertaining to medicine or health. This can be considered as the logical next step in the medical fields, as our bodies perform their most important functions at the microscale. Active particles on this scale, such as micromotors, are demonstrably able to synthetically and controllably perform tasks in a similar fashion to natural bacteria or cells. As the field of active matter grows and expands, we will see active particles becoming a larger and larger part of not only scientific work, but also potentially our daily lives. Systems containing active particles pose challenges for understanding their behavior due to the fact that they are complex, operate out of equilibrium, and can display a wide range of phenomena which cannot be directly predicted from first principles. Thus, simulational models across different levels of fidelity can be used to observe, predict, and ultimately understand the origins of these phenomena. Due to the high variability in active particle type and system geometry, the field is definitely still expanding and being refined.

This work has presented the state of the art in the field of active matter simulation, performed novel simulations of colloidal active particles under confinement, and from that defined scaling laws for the clustering of passive and active colloidal particles under confinement at Reynolds numbers and Peclet numbers that are biologically relevant to micromotors within laminar blood flow. The overall goal of this research is developing a better understanding of the aggregation and possible removal of micromotors in the medical and waste removal fields. Future work on this topic could use the framework presented here in order to investigate differently shaped active particles, systems containing active particles of different sizes, and active particles within a non-water fluid environment, such as the modeling of active particles within the blood of an animal or human capillary.

APPENDIX

The following are the software scripts written to organize and process the data in this Dissertation. All scripts listed here were written by myself, and used with MATLAB R2019a which was generously provided by the College of Engineering at the University of Georgia.

The following code was used to generate FFT power spectra and their associated Gaussian curves for 301x5 snapshots (5 runs, of 301 snapshots each), as seen in Figure 4.7, Figure 4.8, Figure 4.9, Figure 4.14, and Figure 4.20:

```
% 2d_fft_image_five_runs
gaussEqn =  'a1*exp(-((x-b1)/c1)^2)'; % Gaussian equation
for i = 0:300  % 0 - 300
I{1} = abs(1-double(imbinarize(rgb2gray(imread(sprintf('oxNMCC-
SRD_d2_c30_f100_r41_%04d.png',i)))))); %#ok<*CTPCT>
I{2} = abs(1-double(imbinarize(rgb2gray(imread(sprintf('oxNMCC-
SRD_d2_c30_f100_r42_%04d.png',i))))));
I{3} = abs(1-double(imbinarize(rgb2gray(imread(sprintf('oxNMCC-
SRD_d2_c30_f100_r44_%04d.png',i))))));
I{4} = abs(1-double(imbinarize(rgb2gray(imread(sprintf('oxNMCC-
SRD_d2_c30_f100_r46_%04d.png',i))))));
```

```
I{5} = abs(1-double(imbinarize(rgb2gray(imread(sprintf('oxNMCC-
SRD_d2_c30_f100_r50_%04d.png',i))))));
for j = 1:5
f{j} = fft2(I{j}-mean(I{j}(:)));P{j}=(abs(fftshift(f{j}))).^2/(1024.^2);
[Zrp{j}, Rp{j}] =
radialavg(P{j},512);Rp{j}=Rp{j}.*2;[M{j},I{j}]=max(Zrp{j});k0{j}=Rp{j}(I{j});
D2C30F100_Parray{i+1,j}=[Zrp{j}]; % Power spectra for all images
fnan{j}=find(isnan(Zrp{j}));
f{j}=fit(Rp{j}',Zrp{j}',gaussEqn,'Startpoint',[M{j} k0{j} 0.01],'Exclude',
fnan{j});coeffs{j}=coeffvalues(f{j});
end
for h = 1:3
coeff{h}=mean(coeffs{j}(h));
D2C30F100_k0(i+1,h)=coeff{h}; % Gaussian curves for all images
end
end
```

The following code was used to find the scaling exponents m_k and h_k for the power law fit to the power spectra data, as seen in Figure 4.8:

```
b = D2C30F100_k0; % Data
k2 = b(:,2); % k0
I2 = b(:,1); % Intensity
```

```
tn = [tc1 tc2]; % Chosen start and end values
j = [];
for i = 1:2
j(i) = find(t300 == tn(i));%#ok<*SAGROW>  % find appropriate indices
end

PowerEqn =  'a1*x^b1';
fitk=fit(t300(j(1):j(2)),k2(j(1):j(2)),PowerEqn,'Startpoint',[0.5 0.5]);
coeffk=coeffvalues(fitk)
fitI=fit(t300(j(1):j(2)),I2(j(1):j(2)),PowerEqn,'Startpoint',[0.5 0.5]);
coeffI=coeffvalues(fitI)
```

The following code was used to plot the chosen cluster size data and scale it by the scaling exponents m and k, as seen in Figure 4.4 and Figure 4.5:

```
set(0,'DefaultFigureWindowStyle','docked') % Docked Figures
ha = D2C20F05_harray; % Chosen array
tn = [500 1000 2000 3000 4000 5000 6000]; % Chosen values for tau
m = 0.3939; % Scaling factor for mean
h = -0.4881; % Scaling factor for peak
nb = 20; % Number of bins for histogram
j = [];
for i = 1:length(tn)
```

```
j(i) = find(t300 == tn(i));%#ok<*SAGROW>   % find appropriate indices
end
figure; hold on;
for i = j(1:end) % Plot histogram data
   if (max(ha{i}-1)./nb) < 1
      q = 1;
      bn = max(ha{i});
   else
      q = (max(ha{i}-1)./nb);
      bn = nb+1;
   end
p = plot((1:q:(max(ha{i}))),... % X values
    histcounts(ha{i},bn)./sum(ha{i}),'DisplayName',num2str(t300(i))); % Y values
p.LineStyle = 'none'; p.MarkerSize = 10; p.Marker = '+'; p.LineWidth = 3;
end
xlabel('S','FontSize', 20,'FontWeight','bold');ylabel('P(S)','FontSize',
20,'FontWeight','bold');
set(gca,'fontsize',30,'FontName','Garamond','fontweight','bold');
figure; hold on;
x3 = [];y3 = [];
for i = j(1:end) % Plot scaled histogram data
   if (max(ha{i}-1)./nb) < 1
```

```
    q = 1;
    bn = max(ha{i});
  else
    q = (max(ha{i}-1)./nb);
    bn = nb+1;
  end
p = plot((1:q:(max(ha{i}))./(t300(i).^m),... % Scaled X values
  histcounts(ha{i},bn)./sum(ha{i})./(t300(i).^h),'DisplayName',num2str(t300(i)));
% Scaled Y values
p.LineStyle = 'none'; p.MarkerSize = 10; p.Marker = '+'; p.LineWidth = 3;
x3 = horzcat(x3,(1:q:(max(ha{i}))./(t300(i).^m));
y3 = horzcat(y3,histcounts(ha{i},bn)./sum(ha{i})./(t300(i).^h));
end
xlabel('S / t^m','FontSize', 20,'FontWeight','bold');ylabel('P(S) / t^h','FontSize',
20,'FontWeight','bold');
set(gca,'fontsize',30,'FontName','Garamond','fontweight','bold');
x1 = [];y1 = []; hb = [];% Define blank x1, y1
for i = j(1):1:j(end)
  if (max(ha{i}-1)./nb) < 1
    q = 1;
    bn = max(ha{i});
  else
```

```
      q = (max(ha{i}-1)./nb);
      bn = nb+1;
   end
x1 = horzcat(x1,(1:q:(max(ha{i}))))./(t300(i).^m));
y1 = horzcat(y1,histcounts(ha{i},bn)./sum(ha{i})./(t300(i).^h));
hb = horzcat(hb,(ha{i}./t300(i)^m));
end
 q = (max(hb)./nb);
 bn = nb;
x2 = (q:q:(max(hb))); y2 = histcounts(hb,bn)./sum(hb); %#ok<BDSCI> % Scaled
histogram data
pd = fitdist(hb','gamma');
pd.a
pd.b
figure
histfit(hb,nb,'gamma');
xlabel('Scaled Cluster Size','FontSize',
20,'FontWeight','bold');ylabel('Count','FontSize', 20,'FontWeight','bold');
set(gca,'fontsize',20,'FontName','Garamond','fontweight','bold');
```

REFERENCES

[1] H. Fujita, Microactuators and micromachines, P Ieee, 86 (1998) 1721-1732.

[2] X. Chen, C. Zhou, W. Wang, Colloidal Motors 101: A Beginner's Guide to Colloidal Motor Research, Chem-Asian J, 14 (2019) 2388-2405.

[3] G. Wang, X.L. Xu, Y. Yang, S.X. Li, Y.Z. Dai, H. Zhu, W. Guan, Y.H. Yu, C. Lv, H. Xia, In microchannel driven micromotor by microfluid liquid as potential multi-functional devices towards lab on a chip, Optik, 206 (2020).

[4] S. Michelin, E. Lauga, Universal optimal geometry of minimal phoretic pumps, Sci Rep-Uk, 9 (2019).

[5] Y.Z. He, L.F. Wang, Q. Li, L.J. Yang, W.B. Rong, L.N. Sun, Characterization of rotary magnetic micromotor supported on single droplet, J Micromech Microeng, 29 (2019).

[6] D.L. Koch, G. Subramanian, Collective Hydrodynamics of Swimming Microorganisms: Living Fluids, Annual Review of Fluid Mechanics, Vol 43, 43 (2011) 637-659.

[7] C. Maes, S.R. Thomas, Archimedes' law and its corrections for an active particle in a granular sea, J Phys a-Math Theor, 44 (2011).

[8] A. Baskaran, M.C. Marchetti, Self-regulation in self-propelled nematic fluids, Eur Phys J E, 35 (2012).

[9] G. Foffano, J.S. Lintuvuori, A.N. Morozov, K. Stratford, M.E. Cates, D. Marenduzzo, Bulk rheology and microrheology of active fluids, Eur Phys J E, 35 (2012).

[10] G. Foffano, J.S. Lintuvuori, K. Stratford, M.E. Cates, D. Marenduzzo, Colloids in Active Fluids: Anomalous Microrheology and Negative Drag, Phys Rev Lett, 109 (2012).

[11] N. Khurana, N.T. Ouellette, Interactions between active particles and dynamical structures in chaotic flow, Phys Fluids, 24 (2012).

[12] A. Pototsky, H. Stark, Active Brownian particles in two-dimensional traps, Epl-Europhys Lett, 98 (2012).

[13] F. Alarcon, I. Pagonabarraga, Spontaneous aggregation and global polar ordering in squirmer suspensions, J Mol Liq, 185 (2013) 56-61.

[14] M. Hennes, K. Wolff, H. Stark, Self-Induced Polar Order of Active Brownian Particles in a Harmonic Trap, Phys Rev Lett, 112 (2014).

[15] D. Levis, L. Berthier, Clustering and heterogeneous dynamics in a kinetic Monte Carlo model of self-propelled hard disks, Phys Rev E, 89 (2014).

[16] M. Sandoval, N.K. Marath, G. Subramanian, E. Lauga, Stochastic dynamics of active swimmers in linear flows, J Fluid Mech, 742 (2014) 50-70.

[17] V. Bratanov, F. Jenko, E. Frey, New class of turbulence in active fluids, P Natl Acad Sci USA, 112 (2015) 15048-15053.

[18] C. Datt, G. Natale, S.G. Hatzikiriakos, G.J. Elfring, An active particle in a complex fluid, J Fluid Mech, 823 (2017) 675-688.

[19] L. Deprez, P. de Buyl, Passive and active colloidal chemotaxis in a microfluidic channel: mesoscopic and stochastic models, Soft Matter, 13 (2017) 3532-3543.

[20] G.J. Elfring, Force moments of an active particle in a complex fluid, J Fluid Mech, 829 (2017).

[21] J.T. Siebert, J. Letz, T. Speck, P. Virnau, Phase behavior of active Brownian disks, spheres, and dimers, Soft Matter, 13 (2017) 1020-1026.

[22] C. Datt, B. Nasouri, G.J. Elfring, Two-sphere swimmers in viscoelastic fluids, Phys Rev Fluids, 3 (2018).

[23] B. Nasouri, G.J. Elfring, Higher-order force moments of active particles, Phys Rev Fluids, 3 (2018).

[24] D. Saintillan, Rheology of Active Fluids, Annu Rev Fluid Mech, 50 (2018) 563-592.

[25] M. Borgnino, K. Gustavsson, F. De Lillo, G. Boffetta, M. Cencini, B. Mehlig, Alignment of Nonspherical Active Particles in Chaotic Flows, Phys Rev Lett, 123 (2019).

[26] A.I. Campbell, S.J. Ebbens, P. Illien, R. Golestanian, Experimental observation of flow fields around active Janus spheres, Nat Commun, 10 (2019).

[27] P. Krinninger, M. Schmidt, Power functional theory for active Brownian particles: General formulation and power sum rules, J Chem Phys, 150 (2019).

[28] A. Martin-Gomez, T. Eisenstecken, G. Gompper, R.G. Winkler, Active Brownian filaments with hydrodynamic interactions: conformations and dynamics, Soft Matter, 15 (2019) 3957-3969.

[29] N. Narinder, J.R. Gomez-Solano, C. Bechinger, Active particles in geometrically confined viscoelastic fluids, New J Phys, 21 (2019).

[30] S. Ramaswamy, Active fluids, Nat Rev Phys, 1 (2019) 640-642.

[31] M.S. Rizvi, A. Nait-Ouhra, A. Farutin, P. Peyla, S. Rafai, C. Misbah, Rheological signature of microswimmer phase-locking under flow, Phys Rev Fluids, 4 (2019).

[32] L.L. Zhang, Z.Y. Xiao, X. Chen, J.Y. Chen, W. Wang, Confined 1D Propulsion of Metallodielectric Janus Micromotors on Microelectrodes under Alternating Current Electric Fields, Acs Nano, 13 (2019) 8842-8853.

[33] H. Fadlallah, M. Jarrahi, E. Herbert, R. Ferrari, A. Mejean, H. Peerhossaini, Active Fluids: Effects of Hydrodynamic Stress on Growth of Self-Propelled Fluid Particles, J Appl Fluid Mech, 13 (2020) 561-570.

[34] R.C. Maloney, C.K. Hall, Clustering and Phase Separation in Mixtures of Dipolar and Active Particles in an External Field, Langmuir, 36 (2020) 6378-6387.

[35] B. Khezri, J.G.S. Moo, P. Song, A.C. Fisher, M. Pumera, Detecting the complex motion of self-propelled micromotors in microchannels by electrochemistry, Rsc Adv, 6 (2016) 99977-99982.

[36] R. Omori, K. Shima, A. Suzuki, Rotation of optically trapped particles in air, Jpn J Appl Phys 2, 38 (1999) L743-L745.

[37] M.R. Shaebani, A. Wysocki, R.G. Winkler, G. Gompper, H. Rieger, Computational models for active matter, Nat Rev Phys, 2 (2020) 181-199.

[38] R. Alert, X. Trepat, Physical Models of Collective Cell Migration, Annu Rev Conden Ma P, 11 (2020) 77-101.

[39] Z.Y. Xiao, M.S. Wei, W. Wang, A Review of Micromotors in Confinements: Pores, Channels, Grooves, Steps, Interfaces, Chains, and Swimming in the Bulk, Acs Appl Mater Inter, 11 (2019) 6667-6684.

[40] R.N. Zia, Active and Passive Microrheology: Theory and Simulation, Annu Rev Fluid Mech, 50 (2018) 371-405.

[41] B.E.F. de Avila, P. Angsantikul, J.X. Li, W. Gao, L.F. Zhang, J. Wang, Micromotors Go In Vivo: From Test Tubes to Live Animals, Adv Funct Mater, 28 (2018).

[42] J. Zhang, E. Luijten, B.A. Grzybowski, S. Granick, Active colloids with collective mobility status and research opportunities, Chem Soc Rev, 46 (2017) 5551-5569.

[43] L.S. Liu, T. Bai, Q.J. Chi, Z. Wang, S. Xu, Q.W. Liu, Q. Wang, How to Make a Fast, Efficient Bubble-Driven Micromotor: A Mechanical View, Micromachines-Basel, 8 (2017).

[44] A.E. Patteson, A. Gopinath, P.E. Arratia, Active colloids in complex fluids, Curr Opin Colloid In, 21 (2016) 86-96.

[45] M. Alarcon-Correa, D. Walker, T. Qiu, P. Fischer, Nanomotors, Eur Phys J-Spec Top, 225 (2016) 2241-2254.

[46] V.V. Singh, J. Wang, Nano/micromotors for security/defense applications. A review, Nanoscale, 7 (2015) 19377-19389.

[47] H.H. Wensink, H. Lowen, M. Marechal, A. Hartel, R. Wittkowski, U. Zimmermann, A. Kaiser, A.M. Menzel, Differently shaped hard body colloids in confinement: From passive to active particles, Eur Phys J-Spec Top, 222 (2013) 3023-3037.

[48] C. Misbah, C. Wagner, Living fluids, Cr Phys, 14 (2013) 447-450.

[49] I.S. Aranson, Collective behavior in out-of-equilibrium colloidal suspensions, Cr Phys, 14 (2013) 518-527.

[50] H.C. Feng, H.L. Chang, X. Zhong, T.N. Wong, Recent advancement in induced-charge electrokinetic phenomena and their micro- and nano-fluidic applications, Adv Colloid Interfac, 280 (2020).

[51] R.M. Lee, W. Losert, Dynamics phenotyping across length and time scales in collective cell migration, Semin Cell Dev Biol, 93 (2019) 69-76.

[52] A. Jakli, B. Senyuk, G.X. Liao, O.D. Lavrentovich, Colloidal micromotor in smectic A liquid crystal driven by DC electric field, Soft Matter, 4 (2008) 2471-2474.

[53] W. Gao, A. Pei, J. Wang, Water-Driven Micromotors, Acs Nano, 6 (2012) 8432-8438.

[54] G. Jayaraman, S. Ramachandran, S. Ghose, A. Laskar, M.S. Bhamla, P.B.S. Kumar, R. Adhikari, Autonomous Motility of Active Filaments due to Spontaneous Flow-Symmetry Breaking, Phys Rev Lett, 109 (2012).

[55] L.Q. Li, J.Y. Wang, T.L. Li, W.P. Song, G.Y. Zhang, Hydrodynamics and propulsion mechanism of self-propelled catalytic micromotors: model and experiment, Soft Matter, 10 (2014) 7511-7518.

[56] A.K. Singh, K.K. Dey, A. Chattopadhyay, T.K. Mandal, D. Bandyopadhyay, Multimodal chemo-magnetic control of self-propelling microbots, Nanoscale, 6 (2014) 1398-1405.

[57] M. Liu, L.M. Liu, W.L. Gao, M.D. Su, Y. Ge, L.L. Shi, H. Zhang, B. Dong, C.Y. Li, Nanoparticle mediated micromotor motion, Nanoscale, 7 (2015) 4949-4955.

[58] L.M. Liu, M. Liu, Y.J. Su, Y.G. Dong, W. Zhou, L.N. Zhang, H. Zhang, B. Dong, L.F. Chi, Tadpole-like artificial micromotor, Nanoscale, 7 (2015) 2276-2280.

[59] V.V. Singh, F. Soto, K. Kaufmann, J. Wang, Micromotor-Based Energy Generation, Angew Chem Int Edit, 54 (2015) 6896-6899.

[60] R.F. Dong, Q.L. Zhang, W. Gao, A. Pei, B.Y. Ren, Highly Efficient Light-Driven TiO2-Au Janus Micromotors, Acs Nano, 10 (2016) 839-844.

[61] M.J. Huang, J. Schofield, R. Kapral, A microscopic model for chemically-powered Janus motors, Soft Matter, 12 (2016) 5581-5589.

[62] A.X. Lu, Y.J. Liu, H. Oh, A. Gargava, E. Kendall, Z.H. Nie, D.L. DeVoe, S.R. Raghavan, Catalytic Propulsion and Magnetic Steering of Soft, Patchy Microcapsules: Ability to Pick-Up and Drop-Off Microscale Cargo, Acs Appl Mater Inter, 8 (2016) 15676-15683.

[63] J.M. Yeomans, The hydrodynamics of active systems, P Int Sch Phys, 193 (2016) 383-416.

[64] X. Zhou, Z.T. Li, L.H. Tan, Y. Zhang, Y.P. Jiao, Near-Infrared Light-Steered Graphene Aerogel Micromotor with High Speed and Precise Navigation for Active Transport and Microassembly, Acs Appl Mater Inter, 12 (2020) 23134-23144.

[65] U. Ohiri, C.W. Shields, K. Han, T. Tyler, O.D. Velev, N. Jokerst, Reconfigurable engineered motile semiconductor microparticles, Nat Commun, 9 (2018).

[66] R. Maria-Hormigos, B. Jurado-Sanchez, A. Escarpa, Surfactant-Free beta-Galactosidase Micromotors for "On-The-Move" Lactose Hydrolysis, Adv Funct Mater, 28 (2018).

[67] T. Maric, M.Z.M. Nasir, R.D. Webster, M. Pumera, Tailoring Metal/TiO2 Interface to Influence Motion of Light-Activated Janus Micromotors, Adv Funct Mater, 30 (2020).

[68] J.X. Li, V.V. Singh, S. Sattayasamitsathit, J. Orozco, K. Kaufmann, R.F. Dong, W. Gao, B. Jurado-Sanchez, Y. Fedorak, J. Wang, Water-Driven Micromotors for Rapid Photocatalytic Degradation of Biological and Chemical Warfare Agents, Acs Nano, 8 (2014) 11118-11125.

[69] Z.G. Wu, J.X. Li, B.E.F. de Avila, T.L. Li, W.W. Gao, Q. He, L.F. Zhang, J. Wang, Water-Powered Cell-Mimicking Janus Micromotor, Adv Funct Mater, 25 (2015) 7497-7501.

[70] K.S. Yuan, V. de la Asuncion-Nadal, B. Jurado-Sanchez, A. Escarpa, 2D Nanomaterials Wrapped Janus Micromotors with Built-in Multiengines for Bubble, Magnetic, and Light Driven Propulsion, Chem Mater, 32 (2020) 1983-1992.

[71] Y. Liu, J. Li, J.Y. Li, X.H. Yan, F.D. Wang, W.N. Yang, D.H.L. Ng, J. Yang, Active magnetic Fe3+-doped BiOBr micromotors as efficient solar photo-fenton catalyst, J Clean Prod, 252 (2020).

[72] D. Das, E. Lauga, Active Particles Powered by Quincke Rotation in a Bulk Fluid, Phys Rev Lett, 122 (2019).

[73] O. Dincel, T. Ueta, J. Kameoka, Acoustic driven microbubble motor device, Sensor Actuat a-Phys, 295 (2019) 343-347.

[74] A. Poddar, A. Bandopadhyay, S. Chakraborty, Activated micromotor propulsion by enzyme catalysis in a biofluid medium, Appl Phys Lett, 114 (2019).

[75] S. Ramachandran, P.B.S. Kumar, I. Pagonabarraga, A Lattice-Boltzmann model for suspensions of self-propelling colloidal particles, Eur Phys J E, 20 (2006) 151-158.

[76] L. Schwarz, M. Medina-Sanchez, O.G. Schmidt, Sperm-hybrid micromotors: on-board assistance for nature's bustling swimmers, Reproduction, 159 (2020) R83-R96.

[77] S. Heidenreich, S.H.L. Klapp, M. Bar, Numerical simulations of a minimal model for the fluid dynamics of dense bacterial suspensions, 2nd International Conference on Mathematical Modeling in Physical Sciences 2013 (Ic-Msquare 2013), 490 (2014).

[78] G. Caviglia, A. Morro, Continuum model of cell motility and chemotaxis, Eur J Mech B-Fluid, 49 (2015) 235-242.

[79] A. Decoene, S. Martin, B. Maury, Microscopic Modelling of Active Bacterial Suspensions, Math Model Nat Pheno, 6 (2011) 98-129.

[80] C. Valeriani, M. Li, J. Novosel, J. Arlt, D. Marenduzzo, Colloids in a bacterial bath: simulations and experiments, Soft Matter, 7 (2011) 5228-5238.

[81] E. Benjacob, I. Cohen, O. Shochet, A. Tenenbaum, T. Vicsek, A. Czirok, Cooperative Formation of Chiral Patterns during Growth of Bacterial Colonies, Phys Rev Lett, 75 (1995) 2899-2902.

[82] E. Mehes, E. Mones, V. Nemeth, T. Vicsek, Collective Motion of Cells Mediates Segregation and Pattern Formation in Co-Cultures, Plos One, 7 (2012).

[83] Y. Hatwalne, S. Ramaswamy, M. Rao, R.A. Simha, Rheology of active-particle suspensions, Phys Rev Lett, 92 (2004).

[84] J. Dunkel, I.M. Zaid, Noisy swimming at low Reynolds numbers, Phys Rev E, 80 (2009).

[85] J. Dunkel, V.B. Putz, I.M. Zaid, J.M. Yeomans, Swimmer-tracer scattering at low Reynolds number, Soft Matter, 6 (2010) 4268-4276.

[86] M. Leoni, T.B. Liverpool, Swimmers in Thin Films: From Swarming to Hydrodynamic Instabilities, Phys Rev Lett, 105 (2010).

[87] M.J. Huang, H.Y. Chen, A.S. Mikhailov, Nano-swimmers in biological membranes and propulsion hydrodynamics in two dimensions, Eur Phys J E, 35 (2012).

[88] Y.F. Chen, S. Xiao, H.Y. Chen, Y.J. Sheng, H.K. Tsao, Enhancing rectification of a nano-swimmer system by multi-layered asymmetric barriers, Nanoscale, 7 (2015) 16451-16459.

[89] M. Alarcon-Correa, J.P. Gunther, J. Troll, V.M. Kadiri, J. Bill, P. Fischer, D. Rothenstein, Self-Assembled Phage-Based Colloids for High Localized Enzymatic Activity, Acs Nano, 13 (2019) 5810-5815.

[90] M. Spellings, M. Engel, D. Klotsa, S. Sabrina, A.M. Drews, N.H.P. Nguyen, K.J.M. Bishop, S.C. Glotzer, Shape control and compartmentalization in active colloidal cells, P Natl Acad Sci USA, 112 (2015) E4642-E4650.

[91] S. Gonzalez, R. Soto, Active colloidal chains with cilia- and flagella-like motion, New J Phys, 20 (2018).

[92] F.G. Woodhouse, J. Dunkel, Active matter logic for autonomous microfluidics, Nat Commun, 8 (2017).

[93] X.L. Cui, J. Li, D.H.L. Ng, J. Liu, Y. Liu, W.N. Yang, 3D hierarchical ACFs-based micromotors as efficient photo-Fentonlike catalysts, Carbon, 158 (2020) 738-748.

[94] B. Jurado-Sanchez, M. Pacheco, J. Rojo, A. Escarpa, Magnetocatalytic Graphene Quantum Dots Janus Micromotors for Bacterial Endotoxin Detection, Angew Chem Int Edit, 56 (2017) 6957-6961.

[95] B.E.F. de Avila, M.A. Lopez-Ramirez, D.F. Baez, A. Jodra, V.V. Singh, K. Kaufmann, J. Wang, Aptamer-Modified Graphene-Based Catalytic Micromotors: Off-On Fluorescent Detection of Ricin, Acs Sensors, 1 (2016) 217-221.

[96] L.J. Cai, H. Wang, Y.R. Yu, F.K. Bian, Y. Wang, K.Q. Shi, F.F. Ye, Y.J. Zhao, Stomatocyte structural color-barcode micromotors for multiplex assays, Natl Sci Rev, 7 (2020) 644-651.

[97] Y. Li, F.Z. Mou, C.R. Chen, M. You, Y.X. Yin, L.L. Xu, J.G. Guan, Light-controlled bubble propulsion of amorphous TiO2/Au Janus micromotors, Rsc Adv, 6 (2016) 10697-10703.

[98] D. Rojas, B. Jurado-Sanchez, A. Escarpa, "Shoot and Sense" Janus Micromotors-Based Strategy for the Simultaneous Degradation and Detection of Persistent Organic Pollutants in Food and Biological Samples, Anal Chem, 88 (2016) 4153-4160.

[99] Z.J. Zhang, A.D. Zhao, F.M. Wang, J.S. Ren, X.G. Qu, Design of a plasmonic micromotor for enhanced photo-remediation of polluted anaerobic stagnant waters, Chem Commun, 52 (2016) 5550-5553.

[100] J.A.M. Delezuk, D.E. Ramirez-Herrera, B.E.F. de Avila, J. Wang, Chitosan-based water-propelled micromotors with strong antibacterial activity, Nanoscale, 9 (2017) 2195-2200.

[101] S.K. Srivastava, M. Guix, O.G. Schmidt, Wastewater Mediated Activation of Micromotors for Efficient Water Cleaning, Nano Lett, 16 (2016) 817-821.

[102] K. Wybieralska, A. Wajda, Removal of organic dyes from aqueous solutions with surfactant-modified magnetic nanoparticles, Pol J Chem Technol, 16 (2014) 27-30.

[103] Y.Z. Zhang, J. Yeom, Pollutant-Degrading Multifunctional Micromotors, 2017 Ieee 12th International Conference on Nano/Micro Engineered and Molecular Systems (Nems), DOI (2017) 16-20.

[104] C.S. Lee, J.Y. Gong, D.S. Oh, J.R. Jeon, Y.S. Chang, Zerovalent-Iron/Platinum Janus Micromotors with Spatially Separated Functionalities for Efficient Water Decontamination, Acs Appl Nano Mater, 1 (2018) 768-776.

[105] M. Uygun, V.V. Singh, K. Kaufmann, D.A. Uygun, S.D.S. de Oliveira, J. Wang, Micromotor-Based Biomimetic Carbon Dioxide Sequestration: Towards Mobile Microscrubbers, Angew Chem Int Edit, 54 (2015) 12900-12904.

[106] V.V. Singh, A. Martin, K. Kaufmann, S.D.S. de Oliveira, J. Wang, Zirconia/Graphene Oxide Hybrid Micromotors for Selective Capture of Nerve Agents, Chem Mater, 27 (2015) 8162-8169.

[107] V.V. Singh, B. Jurado-Sanchez, S. Sattayasamitsathit, J. Orozco, J.X. Li, M. Galarnyk, Y. Fedorak, J. Wang, Multifunctional Silver-Exchanged Zeolite Micromotors for Catalytic Detoxification of Chemical and Biological Threats, Adv Funct Mater, 25 (2015) 2147-2155.

[108] V.V. Singh, K. Kaufmann, J. Orozco, J.X. Li, M. Galarnyk, G. Arya, J. Wang, Micromotor-based on-off fluorescence detection of sarin and soman simulants, Chem Commun, 51 (2015) 11190-11193.

[109] Y. Yuan, C.Y. Gao, D.L. Wang, C. Zhou, B.H. Zhu, Q. He, Janus-micromotor-based on-off luminescence sensor for active TNT detection, Beilstein J Nanotech, 10 (2019) 1324-1331.

[110] S.K. Srivastava, F. Ajalloueian, A. Boisen, Thread-Like Radical-Polymerization via Autonomously Propelled (TRAP) Bots, Adv Mater, 31 (2019).

[111] X.C. Chang, C.R. Chen, J.X. Li, X.L. Lu, Y.Y. Liang, D.K. Zhou, H.C. Wang, G.Y. Zhang, T.L. Li, J. Wang, L.Q. Li, Motile Micropump Based on Synthetic Micromotors for Dynamic Micropatterning, Acs Appl Mater Inter, 11 (2019) 28507-28514.

[112] O. Rotariu, L.E. Udrea, N.J.C. Strachan, S.D. Heys, A.C. Schofield, F.J. Gilbert, V. Badescu, Studies of magnetic carrier particles capture for blood vessel embolization, J Optoelectron Adv M, 8 (2006) 1758-1760.

[113] L.E. Udrea, O. Rotariu, M.I. Popa, Magnetic Support Nanoparticles for the Targeting of Drugs: Physical Characterization and Manipulation in Magnetic Field, Sci Study Res-Chem C, 7 (2006) 151-156.

[114] C. Alexiou, R. Tietze, E. Schreiber, S. Lyer, Nanomedicine, Bundesgesundheitsbla, 53 (2010) 839-845.

[115] R. Chhabra, G. Tosi, A.M. Grabrucker, Emerging Use of Nanotechnology in the Treatment of Neurological Disorders, Curr Pharm Design, 21 (2015) 3111-3130.

[116] M. Talelli, A. Aires, M. Marciello, Protein-modified Magnetic Nanoparticles for Biomedical Applications, Curr Org Chem, 20 (2016) 1252-1261.

[117] A. Choi, K.D. Seo, D.W. Kim, B.C. Kim, D.S. Kim, Recent advances in engineering microparticles and their nascent utilization in biomedical delivery and diagnostic applications, Lab Chip, 17 (2017) 591-613.

[118] E. Karshalev, B.E.F. de Avila, M. Beltran-Gastelum, P. Angsantikul, S.S. Tang, R. Mundaca-Uribe, F.Y. Zhang, J. Zhao, L.F. Zhang, J. Wang, Micromotor Pills as a Dynamic Oral Delivery Platform, Acs Nano, 12 (2018) 8397-8405.

[119] X.M. Bing, X.L. Zhang, J. Li, D.H.L. Ng, W.N. Yang, J. Yang, 3D hierarchical tubular micromotors with highly selective recognition and capture for antibiotics, J Mater Chem A, 8 (2020) 2809-2819.

[120] Y.R. Yu, J.H. Guo, Y.T. Wang, C.M. Shao, Y. Wang, Y.J. Zhao, Bioinspired Helical Micromotors as Dynamic Cell Microcarriers, Acs Appl Mater Inter, 12 (2020) 16097-16103.

[121] S.S. Tang, F.Y. Zhang, H. Gong, F.N. Wei, J. Zhuang, E. Karshalev, B.E.F. de Avila, C.Y. Huang, Z.D. Zhou, Z.X. Li, L. Yin, H.F. Dong, R.H. Fang, X.J. Zhang, L.F. Zhang, J. Wang, Enzyme-powered Janus platelet cell robots for active and targeted drug delivery, Sci Robot, 5 (2020).

[122] W.S. Jiang, L. Ma, X.B. Xu, Recent progress on the design and fabrication of micromotors and their biomedical applications, Bio-Des Manuf, 1 (2018) 225-236.

[123] Q.H. Cui, T.H. Le, Y.J. Lin, Y.B. Miao, I.T. Sung, W.B. Tsai, H.Y. Chan, Z.H. Lin, H.W. Sung, A self-powered battery-driven drug delivery device that can function as a micromotor and galvanically actuate localized payload release, Nano Energy, 66 (2019).

[124] M.L. Li, M. Brinkmann, I. Pagonabarraga, R. Seemann, J.B. Fleury, Spatiotemporal control of cargo delivery performed by programmable self-propelled Janus droplets, Commun Phys-Uk, 1 (2018).

[125] Y. Dong, C. Yi, S.S. Yang, J. Wang, P. Chen, X. Liu, W. Du, S. Wang, B.F. Liu, A substrate-free graphene oxide-based micromotor for rapid adsorption of antibiotics, Nanoscale, 11 (2019) 4562-4570.

[126] M. Yoon, P. Borrmann, D. Tomanek, Targeted medication delivery using magnetic nanostructures, J Phys-Condens Mat, 19 (2007).

[127] J. Li, F. Ji, D.H.L. Ng, J. Liu, X.M. Bing, P. Wang, Bioinspired Pt-free molecularly imprinted hydrogel-based magnetic Janus micromotors for temperature-responsive recognition and adsorption of erythromycin in water, Chem Eng J, 369 (2019) 611-620.

[128] A. Nourhani, E. Karshalev, F. Soto, J. Wang, Multigear Bubble Propulsion of Transient Micromotors, Research-China, 2020 (2020).

[129] L.L.A. Adams, D. Lee, Y.F. Mei, D.A. Weitz, A.A. Solovev, Nanoparticle-Shelled Catalytic Bubble Micromotor, Adv Mater Interfaces, 7 (2020).

[130] H. Zhu, S. Nawar, J.G. Werner, J.R. Liu, G.S. Huang, Y.F. Mei, D.A. Weitz, A.A. Solovev, Hydrogel micromotors with catalyst-containing liquid core and shell, J Phys-Condens Mat, 31 (2019).

[131] Y.Y. Su, M.J. Zhang, W. Wang, C.F. Deng, J. Peng, Z. Liu, Y. Faraj, X.J. Ju, R. Xie, L.Y. Chu, Bubble-Propelled Hierarchical Porous Micromotors from Evolved Double Emulsions, Ind Eng Chem Res, 58 (2019) 1590-1600.

[132] P.H. Colberg, Collective Motion of Chemically Powered Nanomotors, University of Toronto (Canada), Ann Arbor, 2018, pp. 131.

[133] N. Moradi, M. Shamsipur, A. Taherpour, N. Rahimdad, A. Pashabadi, Fabrication of Template-Less Self-Propelled Micromotors Based on A Metal-Sandwiched Polytryptophan Body: An Experimental and DFT Study, Chempluschem, 85 (2020) 1129-1136.

[134] X.Q. Zhang, C.T. Chen, J. Wu, H.X. Ju, Bubble-Propelled Jellyfish-like Micromotors for DNA Sensing, Acs Appl Mater Inter, 11 (2019) 13581-13588.

[135] C.Y. Gu, Z. Yang, Hundred body length velocity self-actuating platinum micromotor in H2O2, 2019 14th Annual Ieee International Conference on Nano/Micro Engineered and Molecular Systems (Ieee-Nems 2019), DOI (2019) 381-384.

[136] B. Jurado-Sanchez, J. Wang, Micromotors for environmental applications: a review, Environ Sci-Nano, 5 (2018) 1530-1544.

[137] B.M. Tansi, M.L. Peris, O.E. Shklyaev, A.C. Balazs, A. Sen, Organization of Particle Islands through Light-Powered Fluid Pumping, Angew Chem Int Edit, 58 (2019) 2295-2299.

[138] S.S. Tang, F.Y. Zhang, J. Zhao, W. Talaat, F. Soto, E. Karshalev, C.R. Chen, Z.H. Hu, X.L. Lu, J.X. Li, Z.H. Lin, H.F. Dong, X.J. Zhang, A. Nourhani, J. Wang, Structure-Dependent Optical Modulation of Propulsion and Collective Behavior of Acoustic/Light-Driven Hybrid Microbowls, Adv Funct Mater, 29 (2019).

[139] Y.Y. Sun, Y. Liu, B. Song, H. Zhang, R.M. Duan, D.F. Zhang, B. Dong, A Light-Driven Micromotor with Complex Motion Behaviors for Controlled Release, Adv Mater Interfaces, 6 (2019).

[140] Y. Zhang, S.Y. Lin, Z.H. Liu, Y.X. Zhang, J.Z. Zhang, J. Yang, L.B. Yuan, Laser-induced rotary micromotor with high energy conversion efficiency, Photonics Res, 8 (2020) 534-538.

[141] N. Yu, X. Lou, K. Chen, M.C. Yang, Phototaxis of active colloids by self-thermophoresis, Soft Matter, 15 (2019) 408-414.

[142] Y. Wu, A. Fu, G. Yossifon, Active particles as mobile microelectrodes for selective bacteria electroporation and transport, Sci Adv, 6 (2020).

[143] D. Yamamoto, K. Kosugi, K. Hiramatsu, W.Y. Zhang, A. Shioi, K. Kamata, T. Iyoda, K. Yoshikawa, Helical micromotor operating under stationary DC electrostatic field, J Chem Phys, 150 (2019).

[144] M.M. Sun, X.J. Fan, X.H. Meng, J.M. Song, W.N. Chen, L.N. Sun, H. Xie, Magnetic biohybrid micromotors with high maneuverability for efficient drug loading and targeted drug delivery, Nanoscale, 11 (2019) 18382-18392.

[145] Q.L. Wang, R.F. Dong, Q.X. Yang, J.J. Wang, S.Y. Xu, Y.P. Cai, Highly efficient visible-light-driven oxygen-vacancy-based Cu2+1O micromotors with biocompatible fuels, Nanoscale Horiz, 5 (2020) 325-330.

[146] X.Y. Zhang, B.R. Zhang, G.H. Wu, Y.M. Chen, B.R. Xu, A.N. Dong, Y.F. Mei, Epitaxial-assembled monolayer superlattices for efficient micromotor propulsion, J Phys D Appl Phys, 53 (2020).

[147] G. Salinas, A.L. Dauphin, C. Colin, E. Villani, S. Arbault, L. Bouffier, A. Kuhn, Chemo- and Magnetotaxis of Self-Propelled Light-Emitting Chemo-electronic Swimmers, Angew Chem Int Edit, 59 (2020) 7508-7513.

[148] F.Y. Wu, D.C. Yang, X.F. Huang, L.Z. Yi, M. Liu, L.Q. Pan, Ultrafast Bubble-Propelled and Magnetic-Field-Navigated Porous Catalytic Janus Micromotor, J Nanosci Nanotechno, 19 (2019) 4154-4159.

[149] F.R. Koessel, S. Jabbari-Farouji, Controlling stability and transport of magnetic microswimmers by an external field, Epl-Europhys Lett, 125 (2019).

[150] F. Soto, M.A. Lopez-Ramirez, I. Jeerapan, B.E.F. de Avila, R.K. Mishra, X.L. Lu, I. Chai, C.R. Chen, D. Kupor, A. Nourhani, J. Wang, Rotibot: Use of Rotifers as Self-Propelling Biohybrid Microcleaners, Adv Funct Mater, 29 (2019).

[151] C. Kruger, G. Klos, C. Bahr, C.C. Maass, Curling Liquid Crystal Microswimmers: A Cascade of Spontaneous Symmetry Breaking, Phys Rev Lett, 117 (2016).

[152] R. Pohnl, M.N. Popescu, W.E. Uspal, Axisymmetric spheroidal squirmers and self-diffusiophoretic particles, J Phys-Condens Mat, 32 (2020).

[153] M. Liu, Y.X. Wang, Y.B. Kuai, J.W. Cong, Y.L. Xu, H.G. Piao, L.Q. Pan, Y.M. Liu, Magnetically Powered Shape-Transformable Liquid Metal Micromotors, Small, 15 (2019).

[154] J. Burelbach, H. Stark, Linear and angular motion of self-diffusiophoretic Janus particles, Phys Rev E, 100 (2019).

[155] A. Czirok, T. Vicsek, Collective behavior of interacting self-propelled particles, Physica A, 281 (2000) 17-29.

[156] A. Deutsch, G. Theraulaz, T. Vicsek, Collective motion in biological systems, Interface Focus, 2 (2012) 689-692.

[157] E. Mehes, T. Vicsek, Collective motion of cells: from experiments to models, Integr Biol-Uk, 6 (2014) 831-854.

[158] B. Ferdinandy, K. Ozogany, T. Vicsek, Collective motion of groups of self-propelled particles following interacting leaders, Physica A, 479 (2017) 467-477.

[159] A. Czirok, M. Vicsek, T. Vicsek, Collective motion of organisms in three dimensions, Physica A, 264 (1999) 299-304.

[160] A. Czirok, A.L. Barabasi, T. Vicsek, Collective motion of self-propelled particles: Kinetic phase transition in one dimension, Phys Rev Lett, 82 (1999) 209-212.

[161] L.M. Chen, J. Toner, C.F. Lee, Critical phenomenon of the order-disorder transition in incompressible active fluids, New J Phys, 17 (2015).

[162] J. Elgeti, R.G. Winkler, G. Gompper, Physics of microswimmers-single particle motion and collective behavior: a review, Rep Prog Phys, 78 (2015).

[163] T.C. Lee, M. Alarcon-Correa, C. Miksch, K. Hahn, J.G. Gibbs, P. Fischer, Self-Propelling Nanomotors in the Presence of Strong Brownian Forces, Nano Lett, 14 (2014) 2407-2412.

[164] A.S. Khair, J.F. Brady, Single particle motion in colloidal dispersions: a simple model for active and nonlinear microrheology, J Fluid Mech, 557 (2006) 73-117.

[165] X. Yang, D. Marenduzzo, M.C. Marchetti, Spiral and never-settling patterns in active systems, Phys Rev E, 89 (2014).

[166] C.G. Wagner, M.F. Hagan, A. Baskaran, Steady-state distributions of ideal active Brownian particles under confinement and forcing, J Stat Mech-Theory E, DOI ARTN 043203

10.1088/1742-5468/aa60a8(2017).

[167] R.N. Zia, J.F. Brady, Stress development, relaxation, and memory in colloidal dispersions: Transient nonlinear microrheology, J Rheol, 57 (2013) 457-492.

[168] S.C. Takatori, J.F. Brady, Superfluid Behavior of Active Suspensions from Diffusive Stretching, Phys Rev Lett, 118 (2017).

[169] J.R. Gomez-Solano, C. Bechinger, Transient dynamics of a colloidal particle driven through a viscoelastic fluid, New J Phys, 17 (2015).

[170] S. Chakraborti, S. Mishra, P. Pradhan, Additivity, density fluctuations, and nonequilibrium thermodynamics for active Brownian particles, Phys Rev E, 93 (2016).

[171] R. Kapral, A.S. Mikhailov, Stirring a fluid at low Reynolds numbers: Hydrodynamic collective effects of active proteins in biological cells, Physica D, 318 (2016) 100-104.

[172] C.J. Miles, A.A. Evans, M.J. Shelley, S.E. Spagnolie, Active matter invasion of a viscous fluid: Unstable sheets and a no-flow theorem, Phys Rev Lett, 122 (2019).

[173] T. Vicsek, Universal patterns of collective motion from minimal models of flocking, Saso 2008: Second Ieee International Conference on Self-Adaptive and Self-Organizing Systems, Proceedings, DOI 10.1109/Saso.2008.23(2008) 3-11.

[174] A. Czirok, M. Matsushita, T. Vicsek, Theory of periodic swarming of bacteria: Application to Proteus mirabilis, Phys Rev E, 63 (2001).

[175] B. Szabo, G.J. Szollosi, B. Gonci, Z. Juranyi, D. Selmeczi, T. Vicsek, Phase transition in the collective migration of tissue cells: Experiment and model, Phys Rev E, 74 (2006).

[176] Z. Csahok, T. Vicsek, Lattice-Gas Model for Collective Biological Motion, Phys Rev E, 52 (1995) 5297-5303.

[177] T. Vicsek, A. Zafeiris, Collective motion, Phys Rep, 517 (2012) 71-140.

[178] I. Derenyi, P. Tegzes, T. Vicsek, Collective transport in locally asymmetric periodic structures, Chaos, 8 (1998) 657-664.

[179] T. Vicsek, Complexity in the collective behaviour of humans, Sci Cult Ser Phys, 26 (2005) 287-300.

[180] C. Viragh, G. Vasarhelyi, N. Tarcai, T. Szorenyi, G. Somorjai, T. Nepusz, T. Vicsek, Flocking algorithm for autonomous flying robots, Bioinspir Biomim, 9 (2014).

[181] G. Vasarhelyi, C. Viragh, G. Somorjai, T. Nepusz, A.E. Eiben, T. Vicsek, Optimized flocking of autonomous drones in confined environments, Sci Robot, 3 (2018).

[182] G. Vasarhelyi, C. Viragh, G. Somorjai, N. Tarcai, T. Szorenyi, T. Nepusz, T. Vicsek, Outdoor flocking and formation flight with autonomous aerial robots, 2014 Ieee/Rsj International Conference on Intelligent Robots and Systems (Iros 2014), DOI (2014) 3866-3873.

[183] I.J. Farkas, T. Vicsek, Patterns in the collective behavior of humans, Modeling Cooperative Behavior in the Social Sciences, 779 (2005) 1-15.

[184] D. Helbing, I.J. Farkas, P. Molnar, T. Vicsek, Simulation of pedestrian crowds in normal and evacuation situations, Pedestrian and Evacuation Dynamics, DOI (2002) 21-58.

[185] T. Vicsek, A. Czirok, E. Benjacob, I. Cohen, O. Shochet, Novel Type of Phase-Transition in a System of Self-Driven Particles, Phys Rev Lett, 75 (1995) 1226-1229.

[186] P. Degond, S. Merino-Aceituno, F. Vergnet, H. Yu, Coupled Self-Organized Hydrodynamics and Stokes Models for Suspensions of Active Particles, J Math Fluid Mech, 21 (2019).

[187] I. Derenyi, T. Vicsek, Cooperative Transport of Brownian Particles, Phys Rev Lett, 75 (1995) 374-377.

[188] E. BenJacob, O. Shochet, I. Cohen, A. Tenenbaum, A. Czirok, T. Vicsek, Cooperative strategies in formation of complex bacterial patterns, Fractals, 3 (1995) 849-868.

[189] H. Row, J.F. Brady, Reverse osmotic effect in active matter, Phys Rev E, 101 (2020).

[190] P. Gaspard, R. Kapral, Thermodynamics and statistical mechanics of chemically powered synthetic nanomotors, Adv Phys-X, 4 (2019).

[191] J. Giltinan, P. Katsamba, W.D. Wang, E. Lauga, M. Sitti, Selectively controlled magnetic microrobots with opposing helices, Appl Phys Lett, 116 (2020).

[192] R.C. Maloney, G.J. Liao, S.H.L. Klapp, C.K. Hall, Clustering and phase separation in mixtures of dipolar and active particles, Soft Matter, 16 (2020) 3779-3791.

[193] E. Fodor, T. Nemoto, S. Vaikuntanathan, Dissipation controls transport and phase transitions in active fluids: mobility, diffusion and biased ensembles, New J Phys, 22 (2020).

[194] A. Winkler, D. Winter, P. Chaudhuri, A. Statt, P. Virnau, J. Horbach, K. Binder, Computer simulations of structure, dynamics, and phase behavior of colloidal fluids in confined geometry and under shear, Eur Phys J-Spec Top, 222 (2013) 2787-2801.

[195] A.M. Puertas, T. Voigtmann, Microrheology of colloidal systems, J Phys-Condens Mat, 26 (2014).

[196] P. Tierno, Recent advances in anisotropic magnetic colloids: realization, assembly and applications, Phys Chem Chem Phys, 16 (2014) 23515-23528.

[197] I. Kryven, S. Lazzari, G. Storti, Population Balance Modeling of Aggregation and Coalescence in Colloidal Systems, Macromol Theor Simul, 23 (2014) 170-181.

[198] C.H. Rycroft, C.H. Wu, Y. Yu, K. Kamrin, Reference map technique for incompressible fluid-structure interaction, J Fluid Mech, 898 (2020).

[199] M. Theillard, D. Saintillan, Computational mean-field modeling of confined active fluids, J Comput Phys, 397 (2019).

[200] M. Tateno, H. Tanaka, Numerical prediction of colloidal phase separation by direct computation of Navier-Stokes equation, Npj Comput Mater, 5 (2019).

[201] M.P. Howard, A. Nikoubashman, J.C. Palmer, Modeling hydrodynamic interactions in soft materials with multiparticle collision dynamics, Curr Opin Chem Eng, 23 (2019) 34-43.

[202] R.P. Mohanty, R.N. Zia, Transient nonlinear microrheology in hydrodynamically interacting colloidal dispersions: flow cessation, J Fluid Mech, 884 (2020).

[203] M. De Marchis, B. Milici, Turbulence modulation by micro-particles in smooth and rough channels, Phys Fluids, 28 (2016).

[204] O.E. Shklyaev, H. Shum, A.C. Balazs, Using Chemical Pumps and Motors To Design Flows for Directed Particle Assembly, Accounts Chem Res, 51 (2018) 2672-2680.

[205] M.A. Desposito, C. Pallavicini, V. Levi, L. Bruno, Active transport in complex media: Relationship between persistence and superdiffusion, Physica A, 390 (2011) 1026-1032.

[206] A.S. Vishen, Heat dissipation rate in a nonequilibrium viscoelastic medium, J Stat Mech-Theory E, 2020 (2020).

[207] P. Meakin, Models for Colloidal Aggregation, Annual Review of Physical Chemistry, 39 (1988) 237-267.

[208] G. Mirabello, A. Ianiro, P.H.H. Bomans, T. Yoda, A. Arakaki, H. Friedrich, G. de With, N.A.J.M. Sommerdijk, Crystallization by particle attachment is a colloidal assembly process, Nat Mater, 19 (2020) 391-+.

[209] S. Das, J. Riest, R.G. Winkler, G. Gompper, J.K.G. Dhont, G. Nagele, Clustering and dynamics of particles in dispersions with competing interactions: theory and simulation, Soft Matter, 14 (2018) 92-103.

[210] R. Singh, M.E. Cates, Hydrodynamically Interrupted Droplet Growth in Scalar Active Matter, Phys Rev Lett, 123 (2019).

[211] A. Paul, S. Mukherjee, J. Dhar, S. Ghosal, S. Chakraborty, The effect of the finite size of ions and Debye layer overspill on the screened Coulomb interactions between charged flat plates, Electrophoresis, 41 (2020) 607-614.

[212] W. Wang, W.T. Duan, S. Ahmed, A. Sen, T.E. Mallouk, From One to Many: Dynamic Assembly and Collective Behavior of Self-Propelled Colloidal Motors, Accounts Chem Res, 48 (2015) 1938-1946.

[213] F. Orts, G. Ortega, E.M. Garzon, M. Fuchs, A.M. Puertas, Dynamics and friction of a large colloidal particle in a bath of hard spheres: Langevin dynamics simulations and hydrodynamic description, Phys Rev E, 101 (2020).

[214] M. Werner, P. Margaretti, A. Maciolek, Drag Force for Asymmetrically Grafted Colloids in Polymer Solutions, Front Phys-Lausanne, 7 (2019).

[215] F. Orts, G. Ortega, E.M. Garzon, A.M. Puertas, Finite size effects in active microrheology in colloids, Comput Phys Commun, 236 (2019) 8-14.

[216] D.E. Huang, R.N. Zia, Sticky, active microrheology: Part 1. Linear-response, J Colloid Interf Sci, 554 (2019) 580-591.

[217] M. Puljiz, A.M. Menzel, Memory-based mediated interactions between rigid particulate inclusions in viscoelastic environments, Phys Rev E, 99 (2019).

[218] E. Agoritsas, T. Maimbourg, F. Zamponi, Out-of-equilibrium dynamical equations of infinite-dimensional particle systems I. The isotropic case, J Phys a-Math Theor, 52 (2019).

[219] M. Dijkstra, E. Luijten, From predictive modelling to machine learning and reverse engineering of colloidal self-assembly, Nat Mater, 20 (2021) 762-773.

[220] S. Paul, R. Kumar, A. Banerjee, A quantitative analysis of memory effects in the viscously coupled dynamics of optically trapped Brownian particles, Soft Matter, 15 (2019) 8976-8981.

[221] G.J. Liao, C.K. Hall, S.H.L. Klapp, Dynamical self-assembly of dipolar active Brownian particles in two dimensions, Soft Matter, 16 (2020) 2208-2223.

[222] J. Toner, Giant number fluctuations in dry active polar fluids: A shocking analogy with lightning rods, J Chem Phys, 150 (2019).

[223] F. Novotny, M. Pumera, Nanomotor tracking experiments at the edge of reproducibility, Sci Rep-Uk, 9 (2019).

[224] Z.W. Lin, T. Gao, Direct-forcing fictitious domain method for simulating non-Brownian active particles, Phys Rev E, 100 (2019).

[225] S. Hermann, D. de las Heras, M. Schmidt, Non-negative Interfacial Tension in Phase-Separated Active Brownian Particles, Phys Rev Lett, 123 (2019).

[226] G. Gradenigo, S.N. Majumdar, A first-order dynamical transition in the displacement distribution of a driven run-and-tumble particle, J Stat Mech-Theory E, DOI ARTN 053206

10.1088/1742-5468/ab11be(2019).

[227] J.M. Epstein, K. Klymko, K.K. Mandadapu, Statistical mechanics of transport processes in active fluids. II. Equations of hydrodynamics for active Brownian particles, J Chem Phys, 150 (2019).

[228] S. Das, G. Gompper, R.G. Winkler, Local stress and pressure in an inhomogeneous system of spherical active Brownian particles, Sci Rep-Uk, 9 (2019).

[229] R.A. Williams, R.H. Zhou, Instability of active suspensions of liquid crystals, Radiat Eff Defect S, 174 (2019) 125-139.

[230] K. Han, G. Kokot, S. Das, R.G. Winkler, G. Gompper, A. Snezhko, Reconfigurable structure and tunable transport in synchronized active spinner materials, Sci Adv, 6 (2020).

[231] A.S. Vishen, J. Prost, M. Rao, Breakdown of effective temperature, power law interactions, and self-propulsion in a momentum-conserving active fluid, Phys Rev E, 100 (2019).

[232] O.E. Shklyaev, H. Shum, V.V. Yashin, A.C. Balazs, Convective Self-Sustained Motion in Mixtures of Chemically Active and Passive Particles, Langmuir, 33 (2017) 7873-7880.

[233] W.J. Fei, Y. Gu, K.J.M. Bishop, Active colloidal particles at fluid-fluid interfaces, Curr Opin Colloid In, 32 (2017) 57-68.

[234] I.S. Aranson, Active colloids, Phys-Usp+, 56 (2013) 79-92.

[235] G. Nagele, Colloidal hydrodynamics, Physics of Complex Colloids, 184 (2013) 507-601.

[236] G.S. Redner, M.F. Hagan, A. Baskaran, Structure and Dynamics of a Phase-Separating Active Colloidal Fluid, Phys Rev Lett, 110 (2013).

[237] D. Saintillan, M.J. Shelley, Active suspensions and their nonlinear models, Cr Phys, 14 (2013) 497-517.

[238] S. Ghose, R. Adhikari, Irreducible Representations of Oscillatory and Swirling Flows in Active Soft Matter, Phys Rev Lett, 112 (2014).

[239] G. D'Avino, P.L. Maffettone, Particle dynamics in viscoelastic liquids, J Non-Newton Fluid, 215 (2015) 80-104.

[240] M. Kuron, P. Kreissl, C. Holm, Toward Understanding of Self-Electrophoretic Propulsion under Realistic Conditions: From Bulk Reactions to Confinement Effects, Accounts Chem Res, 51 (2018) 2998-3005.

[241] U.M.B. Marconi, C. Maggi, Towards a statistical mechanical theory of active fluids, Soft Matter, 11 (2015) 8768-8781.

[242] A. Suma, L.F. Cugliandolo, G. Gonnella, Tracer motion in an active dumbbell fluid, J Stat Mech-Theory E, DOI Artn 054029

10.1088/1742-5468/2016/05/054029(2016).

[243] P. Malgaretti, M.N. Popescu, S. Dietrich, Active colloids at fluid interfaces, Soft Matter, 12 (2016) 4007-4023.

[244] O.D. Lavrentovich, Active colloids in liquid crystals, Curr Opin Colloid In, 21 (2016) 97-109.

[245] T. Jamali, A. Naji, Active fluids at circular boundaries: swim pressure and anomalous droplet ripening, Soft Matter, 14 (2018) 4820-4834.

[246] J. Dunkel, ACTIVE FLUIDS Rolling sound waves, Nat Mater, 17 (2018) 759-760.

[247] S.I. Martynov, L.Y. Tkach, Mechanism of Moving Particle Aggregates in a Viscous Fluid Subjected to a Varying Uniform External Field, Comp Math Math Phys+, 59 (2019) 475-483.

[248] Z.H. Liao, M. Han, M. Fruchart, V. Vitelli, S. Vaikuntanathan, A mechanism for anomalous transport in chiral active liquids, J Chem Phys, 151 (2019).

[249] K.K. Dey, Dynamic Coupling at Low Reynolds Number, Angew Chem Int Edit, 58 (2019) 2208-2228.

[250] P. Gaspard, R. Kapral, Active Matter, Microreversibility, and Thermodynamics, Research-China, 2020 (2020).

[251] E.J. Hemingway, A. Maitra, S. Banerjee, M.C. Marchetti, S. Ramaswamy, S.M. Fielding, M.E. Cates, Active Viscoelastic Matter: From Bacterial Drag Reduction to Turbulent Solids, Phys Rev Lett, 114 (2015).

[252] D. Klotsa, As above, so below, and also in between: mesoscale active matter in fluids, Soft Matter, 15 (2019) 8946-8950.

[253] S.A. Mallory, A. Saric, C. Valeriani, A. Cacciuto, Anomalous thermomechanical properties of a self-propelled colloidal fluid, Phys Rev E, 89 (2014).

[254] A. Morozov, D. Marenduzzo, Enhanced diffusion of tracer particles in dilute bacterial suspensions, Soft Matter, 10 (2014) 2748-2758.

[255] T. Speck, J. Bialke, A.M. Menzel, H. Lowen, Effective Cahn-Hilliard Equation for the Phase Separation of Active Brownian Particles, Phys Rev Lett, 112 (2014).

[256] A.P. Solon, Y. Fily, A. Baskaran, M.E. Cates, Y. Kafri, M. Kardar, J. Tailleur, Pressure is not a state function for generic active fluids, Nat Phys, 11 (2015) 673-678.

[257] F.G. Woodhouse, R.E. Goldstein, Spontaneous Circulation of Confined Active Suspensions, Phys Rev Lett, 109 (2012).

[258] G. Subramanian, D.L. Koch, S.R. Fitzgibbon, The stability of a homogeneous suspension of chemotactic bacteria, Phys Fluids, 23 (2011).

[259] C. Hohenegger, M.J. Shelley, Stability of active suspensions, Phys Rev E, 81 (2010).

[260] B. Hancock, A. Baskaran, Statistical mechanics and hydrodynamics of self-propelled hard spheres, J Stat Mech-Theory E, DOI 10.1088/1742-5468/aa5ed1(2017).

[261] G. Szamel, Theory for the dynamics of dense systems of athermal self-propelled particles, Phys Rev E, 93 (2016).

[262] V. Schaller, A.R. Bausch, Topological defects and density fluctuations in collectively moving systems, P Natl Acad Sci USA, 110 (2013) 4488-4493.

[263] A. Hartel, D. Richard, T. Speck, Three-body correlations and conditional forces in suspensions of active hard disks, Phys Rev E, 97 (2018).

[264] B. Vincenti, C. Douarche, E. Clement, Actuated rheology of magnetic micro-swimmers suspensions: Emergence of motor and brake states, Phys Rev Fluids, 3 (2018).

[265] F.Z. Mou, J.H. Zhang, Z. Wu, S.N. Du, Z.X. Zhang, L.L. Xu, J.G. Guan, Phototactic Flocking of Photochemical Micromotors, Iscience, 19 (2019) 415-+.

[266] M. Abkenar, K. Marx, T. Auth, G. Gompper, Collective behavior of penetrable self-propelled rods in two dimensions, Phys Rev E, 88 (2013).

[267] A. Zottl, H. Stark, Hydrodynamics Determines Collective Motion and Phase Behavior of Active Colloids in Quasi-Two-Dimensional Confinement, Phys Rev Lett, 112 (2014).

[268] A.M. Menzel, T. Ohta, H. Lowen, Active crystals and their stability, Phys Rev E, 89 (2014).

[269] L. Mohan, M. Cloitre, R.T. Bonnecaze, Active microrheology of soft particle glasses, J Rheol, 58 (2014) 1465-1482.

[270] Y. Sasaki, Y. Takikawa, V.S.R. Jampani, H. Hoshikawa, T. Seto, C. Bahr, S. Herminghaus, Y. Hidaka, H. Orihara, Colloidal caterpillars for cargo transportation, Soft Matter, 10 (2014) 8813-8820.

[271] S. Das, M.L. Bowers, C. Bakker, A. Cacciuto, Active sculpting of colloidal crystals, J Chem Phys, 150 (2019).

[272] T. Vicsek, A. Czirok, D. Helbing, Collective motion and optimal self-organisation in self-driven systems, Traffic and Granular Flow'99, DOI (2000) 147-160.

[273] K. Dietrich, G. Volpe, M.N. Sulaiman, D. Renggli, I. Buttinoni, L. Isa, Active Atoms and Interstitials in Two-Dimensional Colloidal Crystals, Phys Rev Lett, 120 (2018).

[274] Q.L. Zhang, R.F. Dong, X.Y. Chang, B.Y. Ren, Z. Tong, Spiropyran-Decorated SiO2-Pt Janus Micromotor: Preparation and Light-Induced Dynamic Self-Assembly and Disassembly, Acs Appl Mater Inter, 7 (2015) 24585-24591.

[275] Z.Y. Deng, F.Z. Mou, S.W. Tang, L.L. Xu, M. Luo, J.G. Guan, Swarming and collective migration of micromotors under near infrared light, Appl Mater Today, 13 (2018) 45-53.

[276] P. Grancic, F. Stepanek, Swarming behavior of gradient-responsive Brownian particles in a porous medium, Phys Rev E, 86 (2012).

[277] C.H. Peng, O.D. Lavrentovich, Liquid Crystals-Enabled AC Electrokinetics, Micromachines-Basel, 10 (2019).

[278] Z.M. Sherman, J.W. Swan, Transmutable Colloidal Crystals and Active Phase Separation via Dynamic, Directed Self-Assembly with Toggled External Fields, Acs Nano, 13 (2019) 764-771.

[279] G. Kokot, S. Das, R.G. Winkler, G. Gompper, I.S. Aranson, A. Snezhko, Active turbulence in a gas of self-assembled spinners, P Natl Acad Sci USA, 114 (2017) 12870-12875.

[280] Z.Y. Shen, A. Wurger, J.S. Lintuvuori, Hydrodynamic self-assembly of active colloids: chiral spinners and dynamic crystals, Soft Matter, 15 (2019) 1508-1521.

[281] G. Destgeer, A. Hashmi, J. Park, H. Ahmed, M. Afzal, H.J. Sung, Microparticle self-assembly induced by travelling surface acoustic waves, Rsc Adv, 9 (2019) 7916-7921.

[282] Y.K. Kim, J. Noh, K. Nayani, N.L. Abbott, Soft matter from liquid crystals, Soft Matter, 15 (2019) 6913-6929.

[283] A. Wysocki, R.G. Winkler, G. Gompper, Cooperative motion of active Brownian spheres in three-dimensional dense suspensions, Epl-Europhys Lett, 105 (2014).

[284] M. Maiti, M. Schmiedeberg, Energy landscape description of the clustering transition for active soft spheres, Epl-Europhys Lett, 126 (2019).

[285] M.E. Cates, J. Tailleur, Motility-Induced Phase Separation, Annual Review of Condensed Matter Physics, Vol 6, 6 (2015) 219-244.

[286] G.S. Redner, A. Baskaran, M.F. Hagan, Reentrant phase behavior in active colloids with attraction, Phys Rev E, 88 (2013).

[287] V. Prymidis, H. Sielcken, L. Filion, Self-assembly of active attractive spheres, Soft Matter, 11 (2015) 4158-4166.

[288] D. Bartolo, E. Lauga, Shaking-induced motility in suspensions of soft active particles, Phys Rev E, 81 (2010).

[289] J. Smrek, K. Kremer, Small Activity Differences Drive Phase Separation in Active-Passive Polymer Mixtures, Phys Rev Lett, 118 (2017).

[290] T. Speck, Stochastic thermodynamics for active matter, Epl-Europhys Lett, 114 (2016).

[291] J.R. Gomez-Solano, S. Samin, C. Lozano, P. Ruedas-Batuecas, R. van Roij, C. Bechinger, Tuning the motility and directionality of self-propelled colloids, Sci Rep-Uk, 7 (2017).

[292] T.A. de Pirey, G. Lozano, F. van Wijland, Active Hard Spheres in Infinitely Many Dimensions, Phys Rev Lett, 123 (2019).

[293] E. Mones, A. Czirok, T. Vicsek, Anomalous segregation dynamics of self-propelled particles, New J Phys, 17 (2015).

[294] Y. Bozorgi, P.T. Underhill, Role of linear viscoelasticity and rotational diffusivity on the collective behavior of active particles, J Rheol, 57 (2013) 511-533.

[295] L. Vennamneni, S. Nambiar, G. Subramanian, Shear-induced migration of microswimmers in pressure-driven channel flow, J Fluid Mech, 890 (2020).

[296] M. Atakhorrami, D. Mizuno, G.H. Koenderink, T.B. Liverpool, F.C. MacKintosh, C.F. Schmidt, Short-time inertial response of viscoelastic fluids measured with Brownian motion and with active probes, Phys Rev E, 77 (2008).

[297] D. Weihs, M.A. Teitell, T.G. Mason, Simulations of complex particle transport in heterogeneous active liquids, Microfluid Nanofluid, 3 (2007) 227-237.

[298] E.A. Medrano, B.J.H. van de Wiel, R.E. Uittenbogaard, L.M.D. Pires, H.J.H. Clercx, Simulations of the diurnal migration of Microcystis aeruginosa based on a scaling model for physical-biological interactions, Ecol Model, 337 (2016) 200-210.

[299] A.E. Koser, N.C. Keim, P.E. Arratia, Structure and dynamics of self-assembling colloidal monolayers in oscillating magnetic fields, Phys Rev E, 88 (2013).

[300] C. Kruger, C. Bahr, S. Herminghaus, C.C. Maass, Dimensionality matters in the collective behaviour of active emulsions, Eur Phys J E, 39 (2016).

[301] A. Dehkharghani, N. Waisbord, J. Dunkel, J.S. Guasto, Bacterial scattering in microfluidic crystal flows reveals giant active Taylor-Aris dispersion, P Natl Acad Sci USA, 116 (2019) 11119-11124.

[302] S. Nambiar, S. Phanikanth, P.R. Nott, G. Subramanian, Stress relaxation in a dilute bacterial suspension: the active-passive transition, J Fluid Mech, 870 (2019) 1072-1104.

[303] M.E. Cates, E. Tjhung, Theories of binary fluid mixtures: from phase-separation kinetics to active emulsions, J Fluid Mech, 836 (2017).

[304] E. Nazockdast, J.F. Morris, Active microrheology of colloidal suspensions: Simulation and microstructural theory, J Rheol, 60 (2016) 733-753.

[305] S. Paul, A. Kundu, A. Banerjee, Active microrheology to determine viscoelastic parameters of Stokes-Oldroyd B fluids using optical tweezers, J Phys Commun, 3 (2019).

[306] S. Paul, R. Kumar, A. Banerjee, Active microrheology using a two-particle system coupled by hydrodynamic interactions in optical tweezers, Optical Trapping and Optical Micromanipulation Xv, 10723 (2018).

[307] T. Neckernuss, L.K. Mertens, I. Martin, T. Paust, M. Beil, O. Marti, Active microrheology with optical tweezers: a versatile tool to investigate anisotropies in intermediate filament networks, J Phys D Appl Phys, 49 (2016).

[308] J.W. Swan, R.N. Zia, Active microrheology: Fixed-velocity versus fixed-force, Phys Fluids, 25 (2013).

[309] T.A. Waigh, Advances in the microrheology of complex fluids, Rep Prog Phys, 79 (2016).

[310] A. Cordoba, T. Stieger, M.G. Mazza, M. Schoen, J.J. de Pablo, Anisotropy and probe-medium interactions in the microrheology of nematic fluids, J Rheol, 60 (2016) 75-95.

[311] G. Gregoire, H. Chate, Y.H. Tu, Active and passive particles: Modeling beads in a bacterial bath, Phys Rev E, 64 (2001).

[312] F.Z. Mou, X.F. Li, Q. Xie, J.H. Zhang, K. Xiong, L.L. Xu, J.G. Guan, Active Micromotor Systems Built from Passive Particles with Biomimetic Predator-Prey Interactions, Acs Nano, 14 (2020) 406-414.

[313] A. Laskar, R.K. Manna, O.E. Shklyaev, A.C. Balazs, Modeling the biomimetic self-organization of active objects in fluids, Nano Today, 29 (2019).

[314] O. Granek, Y. Baek, Y. Kafri, A.P. Solon, Bodies in an interacting active fluid: far-field influence of a single body and interaction between two bodies, J Stat Mech-Theory E, 2020 (2020).

[315] M. Elismaili, S. Hamze, H. Xu, D. Gonzalez-Rodriguez, Activity-modulated phase transition in a two-dimensional mixture of active and passive colloids, Eur Phys J E, 43 (2020).

[316] B. Sprinkle, A. Donev, A.P.S. Bhalla, N. Patankar, Brownian dynamics of fully confined suspensions of rigid particles without Green's functions, J Chem Phys, 150 (2019).

[317] A. Daddi-Moussa-Ider, M. Lisicki, C. Hoell, H. Lowen, Swimming trajectories of a three-sphere microswimmer near a wall, J Chem Phys, 148 (2018).

[318] K. Dietrich, D. Renggli, M. Zanini, G. Volpe, I. Buttinoni, L. Isa, Two-dimensional nature of the active Brownian motion of catalytic microswimmers at solid and liquid interfaces, New J Phys, 19 (2017).

[319] A. Daddi-Moussa-Ider, C. Kurzthaler, C. Hoell, A. Zottl, M. Mirzakhanloo, M.R. Alam, A.M. Menzel, H. Lowen, S. Gekle, Frequency-dependent higher-order Stokes singularities near a planar elastic boundary: Implications for the hydrodynamics of an active microswimmer near an elastic interface, Phys Rev E, 100 (2019).

[320] L. Caprini, U.M.B. Marconi, Active particles under confinement and effective force generation among surfaces, Soft Matter, 14 (2018) 9044-9054.

[321] M. Theers, R.G. Winkler, Effects of thermal fluctuations and fluid compressibility on hydrodynamic synchronization of microrotors at finite oscillatory Reynolds number: a multiparticle collision dynamics simulation study, Soft Matter, 10 (2014) 5894-5904.

[322] M. De Pietro, M.A.T. van Hinsberg, L. Biferale, H.J.H. Clercx, P. Perlekar, F. Toschi, Clustering of vertically constrained passive particles in homogeneous isotropic turbulence, Phys Rev E, 91 (2015).

[323] N. Sarkar, A. Basu, Role of interfacial friction for flow instabilities in a thin polar-ordered active fluid layer, Phys Rev E, 92 (2015).

[324] A. Maitra, P. Srivastava, M.C. Marchetti, S. Ramaswamy, M. Lenz, Swimmer Suspensions on Substrates: Anomalous Stability and Long-Range Order, Phys Rev Lett, 124 (2020).

[325] H. Behmadi, Z. Fazli, A. Najafi, A 2D suspension of active agents: the role of fluid mediated interactions, J Phys-Condens Mat, 29 (2017).

[326] R.A. Lambert, F. Picano, W.P. Breugem, L. Brandt, Active suspensions in thin films: nutrient uptake and swimmer motion, J Fluid Mech, 733 (2013) 528-557.

[327] M. Moradi, A. Najafi, Effective viscosity of a two-dimensional suspension of interacting active particles, Phys Rev E, 96 (2017).

[328] L.H. Ning, P. Liu, Y.W. Zong, R. Liu, M.C. Yang, K. Chen, Universal Scaling Law for Colloidal Diffusion in Complex Media, Phys Rev Lett, 122 (2019).

[329] J.W. Wang, Anomalous Diffusion of Active Brownian Particles in Crystalline Phases, Iop C Ser Earth Env, 237 (2019).

[330] T. Debnath, Y.Y. Li, P.K. Ghosh, F. Marchesoni, Active microswimmers in a finite two dimensional trap: The role of hydrodynamic interaction, J Chem Phys, 150 (2019).

[331] A.W. Zantop, H. Stark, Squirmer rods as elongated microswimmers: flow fields and confinement, Soft Matter, 16 (2020) 6400-6412.

[332] E. Kanso, A.C.H. Tsang, Pursuit and Synchronization in Hydrodynamic Dipoles, J Nonlinear Sci, 25 (2015) 1141-1152.

[333] E. Kanso, S. Michelin, Phoretic and hydrodynamic interactions of weakly confined autophoretic particles, J Chem Phys, 150 (2019).

[334] W. Xi, F. Kong, J.C. Yeo, L.T. Yu, S. Sonam, M. Dao, X.B. Gong, C.T. Lim, Soft tubular microfluidics for 2D and 3D applications, P Natl Acad Sci USA, 114 (2017) 10590-10595.

[335] V.K. Narla, D. Tripathi, G.P.R. Sekhar, Time-dependent analysis of electroosmotic fluid flow in a microchannel, J Eng Math, 114 (2019) 177-196.

[336] F. Gentile, M. Ferrari, P. Decuzzi, Transient Diffusion of Nanovectors in Permeable Capillaries, J Serb Soc Comput Me, 1 (2007) 1-19.

[337] R. Alonso-Matilla, B. Chakrabarti, D. Saintillan, Transport and dispersion of active particles in periodic porous media, Phys Rev Fluids, 4 (2019).

[338] G.B. Akguc, Stirring active particles to form life crystal using convective flow, Physica A, 513 (2019) 775-780.

[339] A. Creppy, F. Plouraboue, O. Praud, X. Druart, S. Cazin, H. Yu, P. Degond, Symmetry-breaking phase transitions in highly concentrated semen, J R Soc Interface, 13 (2016).

[340] P.S. Mahapatra, A. Kulkarni, S. Mathew, M.V. Panchagnula, S. Vedantam, Transitions between multiple dynamical states in a confined dense active-particle system, Phys Rev E, 95 (2017).

[341] E. BenJacob, I. Cohen, A. Czirok, T. Vicsek, D.L. Gutnick, Chemomodulation of cellular movement, collective formation of vortices by swarming bacteria, and colonial development, Physica A, 238 (1997) 181-197.

[342] M.K.D. Manshadi, M. Mohammadi, L.K. Monfared, A. Sanati-Nezhad, Manipulation of micro- and nanoparticles in viscoelastic fluid flows within microfluid systems, Biotechnol Bioeng, 117 (2020) 580-592.

[343] L. Caprini, F. Cecconi, A. Puglisi, A. Sarracino, Diffusion properties of self-propelled particles in cellular flows, Soft Matter, 16 (2020) 5431-5438.

[344] S. Yamanaka, A. Furukawa, H. Tanaka, Complex dynamical interplay between solid particles and flow in driven granular suspensions, Phys Rev E, 100 (2019).

[345] M.K. Petersen, J.B. Lechman, S.J. Plimpton, G.S. Grest, P.J. in't Veld, P.R. Schunk, Mesoscale hydrodynamics via stochastic rotation dynamics: Comparison with Lennard-Jones fluid, J Chem Phys, 132 (2010).

[346] M.R. Shabanniya, A. Naji, Active dipolar spheroids in shear flow and transverse field: Population splitting, cross-stream migration, and orientational pinning, J Chem Phys, 152 (2020).

[347] Q.L. Lei, M.P. Ciamarra, R. Ni, Nonequilibrium strongly hyperuniform fluids of circle active particles with large local density fluctuations, Sci Adv, 5 (2019).

[348] P. Chuphal, P. Varun, S. Thakur, Dynamics of diffusiophoretic vesicle under external shear flow, J Chem Phys, 151 (2019).

[349] A. Wysocki, H. Rieger, Capillary Action in Scalar Active Matter, Phys Rev Lett, 124 (2020).

[350] R. Tietze, S. Lyer, E. Schreiber, J. Mann, S. Durr, C. Alexiou, Local Cancer Therapy with Magnetic Nanoparticles, Else Kroner Fresen S, 2 (2011) 154-+.

[351] J.N. Hu, S.W. Huang, L. Zhu, W.J. Huang, Y.P. Zhao, K.L. Jin, Q.C. ZhuGe, Tissue Plasminogen Activator-Porous Magnetic Microrods for Targeted Thrombolytic Therapy after Ischemic Stroke, Acs Appl Mater Inter, 10 (2018) 32988-32997.

[352] E.O. Fridjonsson, J.D. Seymour, Colloid particle transport in a microcapillary: NMR study of particle and suspending fluid dynamics, Chem Eng Sci, 153 (2016) 165-173.

[353] L.E. Udrea, N.J.C. Strachan, V. Badescu, O. Rotariu, An in vitro study of magnetic particle targeting in small blood vessels, Phys Med Biol, 51 (2006) 4869-4881.

[354] Y. Alapan, B. Yigit, O. Beker, A.F. Demirors, M. Sitti, Shape-encoded dynamic assembly of mobile micromachines, Nat Mater, 18 (2019) 1244-+.

[355] R. Soheilian, H. Abdi, C.E. Maloney, R.M. Erb, Assembling particle clusters with incoherent 3D magnetic fields, J Colloid Interf Sci, 513 (2018) 400-408.

[356] S.A. Mallory, C. Valeriani, A. Cacciuto, An Active Approach to Colloidal Self-Assembly, Annu Rev Phys Chem, 69 (2018) 59-79.

[357] R. Singh, R. Adhikari, Generalized Stokes laws for active colloids and their applications, J Phys Commun, 2 (2018).

[358] I. Theurkauff, C. Cottin-Bizonne, J. Palacci, C. Ybert, L. Bocquet, Dynamic Clustering in Active Colloidal Suspensions with Chemical Signaling, Phys Rev Lett, 108 (2012).

[359] M. Theers, E. Westphal, K. Qi, R.G. Winkler, G. Gompper, Clustering of microswimmers: interplay of shape and hydrodynamics, Soft Matter, 14 (2018) 8590-8603.

[360] M.N. Popescu, W.E. Uspal, Z. Eskandari, M. Tasinkevych, S. Dietrich, Effective squirmer models for self-phoretic chemically active spherical colloids, Eur Phys J E, 41 (2018).

[361] M.N. Popescu, W.E. Uspal, A. Dominguez, S. Dietrich, Effective Interactions between Chemically Active Colloids and Interfaces, Accounts Chem Res, 51 (2018) 2991-2997.

[362] A. Zottl, H. Stark, Emergent behavior in active colloids, J Phys-Condens Mat, 28 (2016).

[363] J.B. Delfau, J. Molina, M. Sano, Collective behavior of strongly confined suspensions of squirmers, Epl-Europhys Lett, 114 (2016).

[364] S. Thutupalli, D. Geyer, R. Singh, R. Adhikari, H.A. Stone, Flow-induced phase separation of active particles is controlled by boundary conditions, P Natl Acad Sci USA, 115 (2018) 5403-5408.

[365] M. Theillard, R. Alonso-Matilla, D. Saintillan, Geometric control of active collective motion, Soft Matter, 13 (2017) 363-375.

[366] L.J. Lei, S. Wang, X.Y. Zhang, W.J. Lai, J.Y. Wu, Y.X. Gao, Phoretic self-assembly of active colloidal molecules*, Chinese Phys B, 30 (2021).

[367] R. Soto, R. Golestanian, Self-Assembly of Catalytically Active Colloidal Molecules: Tailoring Activity Through Surface Chemistry, Phys Rev Lett, 112 (2014).

[368] J. Zhang, J. Yan, S. Granick, Directed Self-Assembly Pathways of Active Colloidal Clusters, Angew Chem Int Edit, 55 (2016) 5166-5169.

[369] S.J. Ebbens, D.A. Gregory, Catalytic Janus Colloids: Controlling Trajectories of Chemical Microswimmers, Accounts Chem Res, 51 (2018) 1931-1939.

[370] Y. Wang, H. Lei, P.J. Atzberger, Fluctuating hydrodynamic methods for fluid-structure interactions in confined channel geometries, Appl Math Mech-Engl, 39 (2018) 125-152.

[371] W.N. Yang, J. Li, Z.P. Xu, J. Yang, Y. Liu, L.H. Liu, A Eu-MOF/EDTA-NiAl-CLDH fluorescent micromotor for sensing and removal of Fe3+ from water, J Mater Chem C, 7 (2019) 10297-10308.

[372] M. Ren, W.L. Guo, H.S. Guo, X.H. Ren, Microfluidic Fabrication of Bubble-Propelled Micromotors for Wastewater Treatment, Acs Appl Mater Inter, 11 (2019) 22761-22767.

[373] W.J. Liu, H.B. Ge, X. Chen, X.L. Lu, Z.W. Gu, J.X. Li, J. Wang, Fish-Scale-Like Intercalated Metal Oxide-Based Micromotors as Efficient Water Remediation Agents, Acs Appl Mater Inter, 11 (2019) 16164-16173.

[374] J. Liu, J. Li, G. Wang, W.N. Yang, J. Yang, Y. Liu, Bioinspired zeolitic imidazolate framework (ZIF-8) magnetic micromotors for highly efficient removal of organic pollutants from water, J Colloid Interf Sci, 555 (2019) 234-244.

[375] J. Hwang, H.M. Yang, K.W. Lee, Y.I. Jung, K.J. Lee, C.W. Park, A remotely steerable Janus micromotor adsorbent for the active remediation of Cs-contaminated water, J Hazard Mater, 369 (2019) 416-422.

[376] X. He, R. Buchel, R. Figi, Y.C. Zhang, Y. Bahk, J. Ma, J. Wang, High-performance carbon/MnO2 micromotors and their applications for pollutant removal, Chemosphere, 219 (2019) 427-435.

[377] C.Y. Liang, C. Zhan, F.Y. Zeng, D.D. Xu, Y. Wang, W.W. Zhao, J.H. Zhang, J.H. Guo, H.H. Feng, X. Ma, Bilayer Tubular Micromotors for Simultaneous Environmental Monitoring and Remediation, Acs Appl Mater Inter, 10 (2018) 35099-35107.

[378] A.K. Singh, T. Bhuyan, S. Maity, T.K. Mandal, D. Bandyopadhyay, Magnetically Actuated Carbon Soot Nanoparticle-Based Catalytic CARBOts Coated with Ni/Pt Nanofilms for Water Detoxification and Oil-Spill Recovery, Acs Appl Nano Mater, 3 (2020) 3459-3470.

[379] Z.H. Zhan, F.N. Wei, J.H. Zheng, C. Yin, W.G. Yang, L.G. Yao, S.S. Tang, D. Liu, Visible light driven recyclable micromotors for "on-the-fly" water remediation, Mater Lett, 258 (2020).

[380] T. Hou, S.S. Yu, M.F. Zhou, M. Wu, J. Liu, X.L. Zheng, J.X. Li, J. Wang, X.L. Wang, Effective removal of inorganic and organic heavy metal pollutants with poly(amino acid)-based micromotors, Nanoscale, 12 (2020) 5227-5232.

[381] J.J. Wang, R.F. Dong, Q.X. Yang, H.Y. Wu, Z.J. Bi, Q.Y. Liang, Q.L. Wang, C. Wang, Y.F. Mei, Y.P. Cai, One body, two hands: photocatalytic function- and Fenton effect-integrated light-driven micromotors for pollutant degradation, Nanoscale, 11 (2019) 16592-16598.

[382] D.M. Zhang, D. Wang, J.A. Li, X.Y. Xu, H. Zhang, R.M. Duan, B. Song, D.F. Zhang, B. Dong, One-step synthesis of PCL/Mg Janus micromotor for precious metal ion sensing, removal and recycling, J Mater Sci, 54 (2019) 7322-7332.

[383] B.R. Zhang, G.S. Huang, L. Wang, T.B. Wang, L. Liu, Z.F. Di, X.Y. Liu, Y.F. Mei, Rolled-Up Monolayer Graphene Tubular Micromotors: Enhanced Performance and Antibacterial Property, Chem-Asian J, 14 (2019) 2479-2484.

[384] A. Molinero-Fernandez, M.A. Lopez, A. Escarpa, Electrochemical Microfluidic Micromotors-Based Immunoassay for C-Reactive Protein Determination in Preterm Neonatal Samples with Sepsis Suspicion, Anal Chem, 92 (2020) 5048-5054.

[385] Z.G. Wu, L. Li, Y.R. Yang, P. Hu, Y. Li, S.Y.O. Yang, L.V. Wang, W. Gao, A microrobotic system guided by photoacoustic computed tomography for targeted navigation in intestines in vivo, Sci Robot, 4 (2019).

[386] S. Park, G. Yossifon, Micromotor-Based Biosensing Using Directed Transport of Functionalized Beads, Acs Sensors, 5 (2020) 936-942.

[387] E. Karshalev, Y. Zhang, B.E.F. de Avila, M. Beltran-Gastelum, Y.J. Chen, R. Mundaca-Uribe, F.Y. Zhang, B. Nguyen, Y. Tong, R.H. Fang, L.F. Zhang, J. Wang,

Micromotors for Active Delivery of Minerals toward the Treatment of Iron Deficiency Anemia, Nano Lett, 19 (2019) 7816-7826.

[388] R. Cheng, W.J. Huang, L.J. Huang, B. Yang, L.D. Mao, K.L. Jin, Q.C. ZhuGe, Y.P. Zhao, Acceleration of Tissue Plasminogen Activator-Mediated Thrombolysis by Magnetically Powered Nanomotors, Acs Nano, 8 (2014) 7746-7754.

[389] M.A. Lopez-Ramirez, F. Soto, C. Wang, R. Rueda, S. Shukla, C. Silva-Lopez, D. Kupor, D.A. McBride, J.K. Pokorski, A. Nourhani, N.F. Steinmetz, N.J. Shah, J. Wang, Built-In Active Microneedle Patch with Enhanced Autonomous Drug Delivery, Adv Mater, 32 (2020).

[390] A. Aziz, M. Medina-Sanchez, N. Koukourakis, J.W. Wang, R. Kuschmierz, H. Radner, J.W. Czarske, O.G. Schmidt, Real-Time IR Tracking of Single Reflective Micromotors through Scattering Tissues, Adv Funct Mater, 29 (2019).

[391] X.Y. Pan, Q.Y. Wang, S.B. Li, X.J. Wang, X.J. Han, Bowl-like Micromotors Using Red Blood Cell Membrane as Template, Chemistryselect, 4 (2019) 10296-10298.

[392] T. Araki, S. Fukai, Controlled motion of Janus particles in periodically phase-separating binary fluids, Soft Matter, 11 (2015) 3470-3479.

[393] B. Delmotte, E.E. Keaveny, F. Plouraboue, E. Climent, Large-scale simulation of steady and time-dependent active suspensions with the force-coupling method, J Comput Phys, 302 (2015) 524-547.

[394] Y.Q. Wang, C. Huang, C.F. Zhou, C. Xu, S.J. Qiang, J.C. Li, Directional transport of active particles in the two-dimensional asymmetric ratchet potential field, Int J Mod Phys B, 34 (2020).

[395] S. Saad, G. Natale, Diffusiophoresis of active colloids in viscoelastic media, Soft Matter, 15 (2019) 9909-9919.

[396] N.R.S. Hu, M.M. Sun, X.K. Lin, C.Y. Gao, B. Zhang, C. Zheng, H. Xie, Q. He, Self-Propelled Rolled-Up Polyelectrolyte Multilayer Microrockets, Adv Funct Mater, 28 (2018).

[397] L. Kong, N.F. Rosli, H.L. Chia, J.G. Guan, M. Pumera, Self-Propelled Autonomous Mg/Pt Janus Micromotor Interaction with Human Cells, B Chem Soc Jpn, 92 (2019) 1754-1758.

[398] K. Kyoya, D. Matsunaga, Y. Imai, T. Omori, T. Ishikawa, Shape matters: Near-field fluid mechanics dominate the collective motions of ellipsoidal squirmers, Phys Rev E, 92 (2015).

[399] W.E. Uspal, M.N. Popescu, M. Tasinkevych, S. Dietrich, Shape-dependent guidance of active Janus particles by chemically patterned surfaces, New J Phys, 20 (2018).

[400] A.M. Brooks, S. Sabrina, K.J.M. Bishop, Shape-directed dynamics of active colloids powered by induced-charge electrophoresis, P Natl Acad Sci USA, 115 (2018) E1090-E1099.

[401] R.D. Baker, T. Montenegro-Johnson, A.D. Sediako, M.J. Thomson, A. Sen, E. Lauga, I.S. Aranson, Shape-programmed 3D printed swimming microtori for the transport of passive and active agents, Nat Commun, 10 (2019).

[402] D.R. Cairns, M.S. Shafran, K.A. Sierros, W.W. Huebsch, A.J. Kessrnan, Stimulus-responsive fluidic dispersions of rod shaped liquid crystal polymer colloids, Mater Lett, 64 (2010) 1133-1136.

[403] P. de Buyl, Mesoscopic simulations of anisotropic chemically powered nanomotors, Phys Rev E, 100 (2019).

[404] T. Vourc'h, J. Leopoldes, H. Peerhossaini, Light Control of the Diffusion Coefficient of Active Fluids, J Fluid Eng-T Asme, 142 (2020).

[405] T. Vourc'h, J. Leopoldes, H. Peerhossaini, Phototactic Behaviour of Active Fluids: Effects of Light Perturbation on Diffusion Coefficient of Bacterial Suspensions, Asme Jsme Ksme Joint, DOI (2019).

[406] A. Codutti, K. Bente, D. Faivre, S. Klumpp, Chemotaxis in external fields: Simulations for active magnetic biological matter, Plos Comput Biol, 15 (2019).

[407] T. Chakraborty, S. Chakraborti, A. Das, P. Pradhan, Hydrodynamics, superfluidity, and giant number fluctuations in a model of self-propelled particles, Phys Rev E, 101 (2020).

[408] M. Bourgoin, R. Kervil, C. Cottin-Bizonne, F. Raynal, R. Volk, C. Ybert, Kolmogorovian Active Turbulence of a Sparse Assembly of Interacting Marangoni Surfers, Phys Rev X, 10 (2020).

[409] A. Bolitho, R. Singh, R. Adhikari, Periodic Orbits of Active Particles Induced by Hydrodynamic Monopoles, Phys Rev Lett, 124 (2020).

[410] S. Jahanshahi, C. Lozano, B. ten Hagen, C. Bechinger, H. Lowen, Colloidal Brazil nut effect in microswimmer mixtures induced by motility contrast, J Chem Phys, 150 (2019).

[411] J.G. Lee, A.M. Brooks, W.A. Shelton, K.J.M. Bishop, B. Bharti, Directed propulsion of spherical particles along three dimensional helical trajectories, Nat Commun, 10 (2019).

[412] A. Chamolly, E. Lauga, Stochastic dynamics of dissolving active particles, Eur Phys J E, 42 (2019).

[413] L. Berthier, E. Flenner, G. Szamel, Glassy dynamics in dense systems of active particles, J Chem Phys, 150 (2019).

[414] C.A.M. La Porta, S. Zapperi, Statistical Features of Collective Cell Migration, Adv Exp Med Biol, 1146 (2019) 67-78.

[415] R. Ran, Q. Brosseau, B.C. Blackwell, B. Qin, R.L. Winter, P.E. Arratia, Bacteria hinder large-scale transport and enhance small-scale mixing in time-periodic flows, 118 (2021) e2108548118.

[416] A. Malevanets, R. Kapral, Mesoscopic model for solvent dynamics, J Chem Phys, 110 (1999) 8605-8613.

[417] J.T. Padding, A.A. Louis, Interplay between hydrodynamic and Brownian fluctuations in sedimenting colloidal suspensions, Phys Rev E, 77 (2008).

[418] J.T. Padding, A.A. Louis, Hydrodynamic interactions and Brownian forces in colloidal suspensions: Coarse-graining over time and length scales, Phys Rev E, 74 (2006).

[419] M.Y. Lin, H.M. Lindsay, D.A. Weitz, R. Klein, R.C. Ball, P. Meakin, Universal Diffusion-Limited Colloid Aggregation, J Phys-Condens Mat, 2 (1990) 3093-3113.

[420] M. Bostrom, V. Deniz, G.V. Franks, B.W. Ninham, Extended DLVO theory: Electrostatic and non-electrostatic forces in oxide suspensions, Adv Colloid Interfac, 123 (2006) 5-15.

[421] M. Hecht, J. Harting, T. Ihle, H.J. Herrmann, Simulation of claylike colloids, Phys Rev E, 72 (2005).

[422] D.R. Foss, J.F. Brady, Structure, diffusion and rheology of Brownian suspensions by Stokesian Dynamics simulation, J Fluid Mech, 407 (2000) 167-200.

[423] P.R. Hoskins, D. Hardman, Three-dimensional imaging and computational modelling for estimation of wall stresses in arteries, Brit J Radiol, 82 (2009) S3-S17.

[424] S. Plimpton, Fast Parallel Algorithms for Short-Range Molecular-Dynamics, J Comput Phys, 117 (1995) 1-19.

[425] J.G. Amar, F. Family, P.M. Lam, Dynamic Scaling of the Island-Size Distribution and Percolation in a Model of Submonolayer Molecular-Beam Epitaxy, Phys Rev B, 50 (1994) 8781-8797.

[426] D.A. Weitz, J.S. Huang, M.Y. Lin, J. Sung, Dynamics of Diffusion-Limited Kinetic Aggregation, Phys Rev Lett, 53 (1984) 1657-1660.